Effects of Water Quality Changes on the Corrosion of Iron, Accumulation and Release of Inorganic Contaminants in Drinking Water Distribution Systems

Ching-Yu Peng

A dissertation submitted in partial fulfillment of the
requirements for the degree of

Doctor of Philosophy

University of Washington
2012

Reading Committee:
Gregory V. Korshin, Chair
John F. Ferguson
Michael C. Dodd

Program Authorized to Offer Degree:
Department of Civil and Environmental Engineering

University of Washington

Abstract

Effects of Water Quality Changes on the Corrosion of Iron,

Accumulation and Release of Inorganic Contaminants

in Drinking Water Distribution Systems

Ching-Yu Peng

Chair of Supervisory Committee:

Professor Gregory V. Korshin

Department of Civil and Environmental Engineering

Corrosion and accumulation/release of trace inorganic contaminants in corrosion scales and sediments found in drinking water distribution systems (DWDSs) has gained considerable attention over the past several years. Many trace inorganic contaminants (e.g., lead, arsenic, nickel, vanadium and uranium) can accumulate on the surface of or be occluded within corrosion scales formed in DWDSs. However, little data are available on the actual concentrations of these contaminants beyond system entry-points. The accumulation of trace inorganic contaminants in DWDS solids can have consequences

for the health of exposed populations if these contaminants are released from the scales thus resulting in their high levels at consumers' tap.

This research ascertained the occurrence of inorganic contaminants in real drinking water systems. Corrosion scales and deposits from twenty drinking water utilities in the United States were characterized to determine the elemental, structural composition and the levels of inorganic contaminants in them. The modes of binding and mobility of these elements in the solids were also studied via sequential extractions. Effects of varying water quality conditions, including blending of desalinated water with surface water, NOM, and varying levels of anions (chloride and sulfate) on corrosion and accumulation/release of trace inorganic contaminants were thoroughly examined.

Among the trace inorganic contaminants found in the scales, barium had the highest concentrations, followed by, in the decreasing order, lead, nickel, vanadium, arsenic, chromium, uranium, cadmium, antimony, selenium, and thallium. Speciation via sequential extractions demonstrated that arsenic, chromium and vanadium are the most stable elements, while nickel and manganese are much more mobile than all the other inorganic contaminants examined in this study. NOM had a more pronounced effect on corrosion, metal release and retention of inorganic contaminants than the blending ratio or anions.

TABLE OF CONTENTS

LIST OF FIGURES

Figure Number **Page**

LIST OF TABLES

Table Number **Page**

ACKNOWLEDGEMENTS

I thank Dr. Paul B Liao for providing the Paul B. Liao Endowed Regental Fellowship for three years. I also thank the Water Research Foundation and U.S. National Science Foundation for funding my research.

I would like to express my sincere appreciation to my advisor Professor Gregory Korshin for his vast reserve of patience and knowledge. Many thanks to my committee members, Professor John Ferguson, Professor Mark Benjamin, Professor Michael Dodd, Dr. Steve Reiber, and Professor James Murray for their valuable comments and suggestions.

I would also like to thank my colleagues in the lab. Venkat Nanaboina, Haizhou Liu, Deb Dryer, Yuan Kao, Archana Kashinathan and Zhenxiao Cai. Thank you all for your help and support.

This dissertation is able to complete with the enormous encouragement of my parents, my brother and tremendous support from my husband I-Chieh. Without them, I cannot complete this degree. The honor that I receive should go to them.

DEDICATION

To my family.

Kuan-Lu Peng and Yueh-Chu Liao

I-Cheng Peng

I-Chieh Chien

Tzu-Hsun Stephensen Chien

Chapter 1 Introduction

Corrosion and accumulation/release of trace inorganic contaminants in corrosion scales and sediments found in drinking water distribution systems (DWDSs) has gained considerable attention over the past several years. Prior studies have demonstrated that when these inorganic contaminants are present at concentrations below their respective maximum contaminant levels (MCLs) or even at essentially non-detect levels in water sources, they are capable of accumulating to measurable levels on and within deposits that exist in DWDSs. For instance, Reiber and Dostal (2000); Lytle et al. (2004) determined that corrosion solids formed in treated water having arsenic levels < 10 μg/L had arsenic concentrations of up to several hundred μg/g. Lead pipe scales have also been reported to accumulate significant levels of As, Cd, Cr, Hg, and V (Schock, 2008; Gerke et al., 2009; Kim and Herrera, 2010).

The particular concern of inorganic contaminants accumulation is not the presence of these elements in the distribution systems *per se*, but rather the potential of their release or remobilization into the water column. The accumulated contaminants released from the scales can result in their high levels at consumer's tap (Fisher et al., 2000; Lytle et al., 2010). Therefore, the determination of mobility and availability of trace inorganic contaminants in DWDS solids needs to be ascertained.

Composition of DWDSs solids and water quality parameters, including pH, ORP, NOM, and corrosion inhibitors affect the fate and transport of inorganic contaminants in the udistribution systems. Thus, the characterization of physico-chemical properties of DWDSs solids and determination of effects of varying water qualities on them can

provide valuable insight on factors that influence and control the accumulation and release of inorganic contaminants in the DWDSs.

Therefore, the following specific research objectives were addressed:

Objective 1: Ascertain levels of inorganic contaminants typical for drinking water system scales and deposits

To determine the occurrence of inorganic contaminants in real drinking water systems, multiple samples of corrosion scales and deposits from twenty drinking water utilities in the United States were collected. Their elemental, structural composition and the levels of inorganic contaminants in them were thoroughly characterized.

Objective 2: Examine the speciation of inorganic contaminants in corrosion scales

The speciation of the accumulated inorganic contaminants was examined to determine the modes of binding and mobility of these elements in the solids. The speciation experiments involved sequential extractions to fractionate inorganic species bound to solids into operationally defined fractions that encompass states ranging from mobile species to those tightly bound by stable crystalline oxides of iron. In addition to sequential extractions, separate experiments were carried to determine concentrations of the target elements in soluble and particulate fractions (passing nominal pore sizes 5, 2, 1, and 0.4 μm) released to the ambient water.

Objective 3: Explore the accumulation and release of inorganic contaminants at varying water quality conditions

Varying water quality conditions, including blending of desalinated water with surface water, NOM, and varying levels of anions (chloride and sulfate) are believed to strongly influence the properties of corrosion scales. This affects the accumulation and release of

inorganic contaminants. Jar tests were employed to examine these effects of various water quality parameters on inorganic contaminants accumulation and release from iron, copper, and lead/tin coupons.

Objective 4: Ascertain effects of NOM and anions on iron corrosion

The hypothesis that NOM has the dominant effect on iron corrosion, accumulation and release of inorganic contaminants was tested in jar tests that quantified the effects of NOM and anions (chloride and sulfate) on iron corrosion. Altered NOM (Suwannee River NOM ozonated with different ratio of O_3/DOC) was used to explore the influence of different types of NOM on iron corrosion.

Chapter 2 Literature Review

2.1 Inorganic contaminants

Several elements and metalloids are of particular interest for drinking water quality regulations and, as a result, for this study because of their potential for physical accumulation in scales and deposits in drinking water distribution systems (DWDS). Inorganic contaminants of particular importance include sixteen elements (Mg, Al, P, Ca, V, Cr, Mn, Fe, Ni, Cu, Zn, As, Cd, Ba, Pb, and U) that are both major constituents of corrosion solids and frequently occurring inorganic contaminants retained by them. Seven of these elements are primary regulated inorganic contaminants (As, Ba, Cd, Cr, Cu, Pb, and U); four of them are secondary regulated inorganic contaminants, including Al, Fe, Mn and Zn. Table 2.1.1 and Table 2.1.2 summarize target levels for these elements as defined under the National Primary Drinking Water Regulations (NPDWRs) and National Secondary Drinking Water Regulations (NSDWRs) (U.S. EPA, 2009a). Vanadium (V) is also relevant to this study because of their listing on the Contaminant Candidate List 3 (CCL3) (U.S. EPA, 2009b).

Though currently unregulated, two additional inorganic compounds of high interest include phosphorus (P) and nickel (Ni). Regarding phosphorus, the majority of source waters used for potable supply contain less than 0.3 mg/L as PO_4. However, many drinking water utilities purposefully apply phosphorus-based chemicals (e.g. polyphosphate, orthophosphate or ortho/poly blend) during treatment for corrosion control, resulting in finished water phosphate levels in the range of 0.5 to 3 mg/L as PO_4. These phosphorus species are well known to form precipitates with other metals, such as aluminum, calcium and iron. The phosphate-based solids may serve as sinks for a number

of metals, which will affect their accumulation and release (Copeland et al., 2007). Nickel is of interest to this research because it has been regulated in the past due to its adverse health effects. The original Maximum Contaminant Level (MCL) for nickel was 0.1 mg/L. The current WHO guideline for nickel is 70 µg/L (Guidelines for Drinking-Water Quality, 2008). Besides phosphorus and nickel, magnesium (Mg) and calcium (Ca) are also of interest due to their abundance in the source water and relative prevalence in distribution system scales and deposits.

Table 2.1.1 Summary of regulations for, toxic effects and sources of selected primary regulated inorganic contaminants

Contaminant	Primary MCL (MCLG)[(a)]	Potential acute and sub-chronic health effects	Potential chronic health effects	Sources of contaminant in drinking water
Arsenic (As)	0.010 mg/L (0.000 mg/L)	Nausea, vomiting, epigastric and abdominal pain, diarrhea.	Skin damage, circulatory distress. Increased risk of cancer.	Erosion of natural deposits; runoff from orchards, runoff from glass & electronics production wastes; leaching from cement linings
Barium (Ba)	2 mg/L (2 mg/L)	Vomiting, diarrhea, muscular weakness, hypertension.	Hypertension.	Discharge of drilling wastes; discharge from metal refineries; erosion of natural deposits; leaching from cement linings
Cadmium (Cd)	0.005 mg/L (0.005 mg/L)	Nausea, vomiting, diarrhea, muscle cramps, liver damage, shock, renal failure.	Kidney damage, renal dysfunction, anemia, hypertension.	Corrosion of galvanized pipes; erosion of natural deposits; discharge from metal refineries; runoff from waste batteries and paints
Chromium (Cr)	0.1 mg/L (0.1 mg/L)	Skin irritation, ulceration.	Damage to liver, kidney circulation, and nerve tissue. Dermatitis.	Discharge from steel and pulp mills; erosion of natural deposits; leaching from cement linings
Copper (Cu)	1.3 mg/L[(b)] (1.3 mg/L)	Stomach and intestinal distress, liver and kidney damage, and anemia.	Kidney, liver, and nervous system damage.	Corrosion of household plumbing systems; erosion of natural deposits
Lead (Pb)	0.015 mg/L[(b)] (0 mg/L)	Nervous, cardiovascular, kidney and reproductive damage. Impaired mental development in children.	Nervous, cardiovascular, kidney and reproductive damage. Impaired mental development in children.	Corrosion of household plumbing systems; erosion of natural deposits
Uranium (U)	30 μg/L	Increased risk of cancer.	Increased risk of cancer,	Erosion of natural deposits

	(0 µg/L)		and kidney damage.	

(a) Maximum Contaminant Level and Maximum Contaminant Level Goal (USEPA, 2009).

(b) Action Level under the Lead and Copper Rule.

Table 2.1.2 Summary of regulations for, toxic effects and sources of selected secondary regulated inorganic contaminants

Compound	Secondary MCL[(a)]	Potential acute and sub-chronic health effects	Potential chronic health effects	Sources of contaminant in drinking water
Aluminum (Al)	0.05 to 0.2 mg/L	None found.	None found.	Erosion of natural deposits; post-precipitation of aluminum-based coagulant residual or filter breakthrough; leaching from cement-mortar linings
Iron (Fe)	0.30 mg/L	None found.	None found.	Corrosion of household plumbing systems; erosion of natural deposits; post-precipitation of iron-based coagulant residual or filter breakthrough
Manganese (Mn)	0.05 mg/L	Mental disturbances, lethargy, tremors, increased muscle tonus.	Neurological impairment.	Erosion of natural deposits; discharge from manganese-iron alloys production and smelting processes
Zinc (Zn)	5 mg/L	Nausea, vomiting, diarrhea, abdominal cramps.	Anemia.	Corrosion of household plumbing systems; erosion of natural deposits; discharge from mining and steel production

(a) Maximum Contaminant Level (USEPA, 2009).

2.2 Contaminant sinks

Corrosion scales

Internal corrosion in drinking water distribution systems (DWDSs) refers to an electrochemical oxidation-reduction interaction between a metal surface, such as a pipe wall, and the water with which it is in contact. Corrosion scales are oxidized metal precipitates that form on the inner surface of metallic piping due to electrochemical oxidation-reduction reactions between the elemental metal and dissolved constituents in the water, most notably hydrogen ion, dissolved oxygen (DO), and chlorine residual.

The rates of generation of corrosion scales and their chemical composition, structures, as well as morphologies and solubility of predominant mineralogical phases constituting them are all affected by both the pipe materials (e.g., cast iron, steel or PVC) on which they are deposited and water chemistry parameters that include pH, temperature, DIC and alkalinity, concentrations of sulfate, chloride and natural organic matter (NOM), dissolved oxygen (DO) and disinfectant type and residual, presence of corrosion inhibitors (e.g., phosphate), overall conductivity of water, and hydraulic patterns (Sarin et al., 2001; Korshin et al., 1996; Vazquez et al., 2006).

Iron and steel pipe have been used in water distribution systems for several centuries. The buildup of iron corrosion products inside the iron pipes has been observed in most water distribution pipes. Compounds usually found in iron corrosion scales include goethite (α-FeOOH), lepidocrocite (γ-FeOOH), magnetite (Fe_3O_4), siderite ($FeCO_3$), ferrous hydrous hydroxide ($Fe(OH)_2$), ferric hydroxide ($Fe(OH)_3$), ferrihydrite ($5Fe_2O_3 \cdot 9H_2O$), green rusts (e.g., $Fe_4^{II}Fe_2^{III}(OH)_{12}(CO_3)$), and calcium carbonate ($CaCO_3$) (Benjamin et al., 1996; Sarin et al., 2001; Sarin et al., 2004).

Iron corrosion scales have structured layers that include (1) an inner porous layer in contact with pipe surface, (2) a relatively dense shell-like outer layer that covers the porous layer, and (3) an outer surface layer that is loosely attached to the shell-like layer and is in contact with the water. The porous inner layer of a iron pipe scale is largely composed of ferrous iron, such as $Fe(OH)_2$, $FeCO_3$, FeS (pyrrhotite), and $Fe_3(PO_4)_2 \cdot 8H_2O$(vivianite). Green rusts, goethite, lepidocrocite, and magnetite were also identified as components in this layer. The predominant composition of the dense shell-like outer layers is magnetite and goethite. This dense, relatively hard structures separates the bulk water from the easily oxidizable Fe(II) compounds in the inner layer; thus tend to protect against iron release. The outer layer is loosely held and in contact with following water and so it is highly susceptible to water qualities and physical disturbances. The dominant mineral found in the outer layer is amorphous hydrous ferric oxide. Goethite, lepidocrocite, manganese dioxide, calcite, and gypsum have also been found here (Benjamin et al., 1996; Sarin et al., 2001; Sarin et al., 2004; Burlingame et al., 2006). Figure 2.2.1 shows a simplified schematic of structure and possible composition of corrosion scales found in iron/steel pipes.

The most common forms of copper corrosion scales are cuprite (Cu_2O), tenorite (CuO), hydrous cupric oxide ($Cu(OH)_2$), and malachite ($Cu_2CO_3(OH)_2$) (AwwaRF and TZW, 1996). The most common compounds found on a lead service pipe and lead-bearing alloys and soldiers are cerussite ($PbCO_3$) and Hydrocerussite ($Pb_3(CO_3)_2(OH)_2$). In the presence of moderate-to-high free chlorine, lead dioxide (PbO_2) can be formed on the scale surfaces. Lead dioxide is highly insoluble and tends to create a protective barrier on

the pipe wall against corrosion, thereby influencing lead solubility and release (Lytle and Shock, 2005; Vazquez et al., 2006).

Formation of corrosion scales via precipitation

Chemical precipitation produces a separable solid phase due to exceedance of a solubility product constant. Water quality conditions, such as pH, ORP, concentrations of cations (e.g., calcium or magnesium) and anions (e.g., carbonate, phosphate, and sulfate), affect the formation of chemical precipitates. Common chemical precipitates found in DWDSs, such as those involving iron, manganese, aluminum, and phosphate, have been shown to have a high affinity for concentrating regulated inorganic elements (Schock, 2005). Other precipitates capable of being produced in water distribution systems directly involve regulated elements, e.g., $BaSO_4$, CuO, PbO_2, UO_2, and $Cr(OH)_3$.

The formation of calcium carbonate ($CaCO_3$) is a typical and widely recognized example of chemical precipitation. It often occurs in groundwater supplies with high hardness and DIC. A thin layer of $CaCO_3$ is frequently deemed to be desirable, as it can act as a protective layer to reduce the chance of corrosion. When thick layers of $CaCO_3$ are deposited, scaling occurs. Excessive scaling is undesirable because of loss of carrying capacity in the system. The Langelier Saturation Index (LSI) is the most widely used index to estimate the tendency of a water to precipitate a protective layer of $CaCO_3$ on the pipe wall.

Other examples of chemical precipitates formed within distribution systems include oxides, oxyhydroxides, and hydroxides of iron, manganese, and aluminum (Sly *et al.*, 1990). Insoluble hydrous ferric oxide and manganese oxide precipitates usually occur in many groundwater supplies after oxidation processes. Without an effective solids

removal process downstream, these precipitates may be carried over to the distribution system. Residual of coagulants (such as iron- or aluminum-based salts) used in the drinking water treatment plants has also been found in the finished water. Snoeyink et al. (2003) reported the breakthrough of aluminum coagulant and post-precipitation in the distribution system.

By-products of cement corrosion (e.g., aluminum, calcium, barium) may precipitate with anions (e.g., phosphate, carbonate, and sulfate) in bulk water, yielding a variety of compounds. Snoeyink et al. (2003) reported the formation of hydrated aluminum phosphate (variscite, $AlPO_4 \cdot 2H_2O$) from aluminum leaching from cement lining and subsequent precipitation with orthophosphate.

Sediments

Sediments found in DWDS represent a class of loosely deposited particulate matter typically comprised of turbidity, sand, silt, and organic material. The definition of sediments is often expanded to include mobilized and re-deposited chemical scale and corrosion byproducts, a cell material and organic detritus released from biofilms (Friedman *et al.*, 2010). Regular sediment load entering the distribution system is from the incomplete removal of suspended solids at the treatment plants (Gauthier *et al*., 2003; Vreeburg *et al.*, 2008; Verberk *et al.*, 2009). The quantity, composition, and physiochemical properties of sediments are dependent on pipe material, water characteristics, routine hydraulics, and history/type of distribution system maintenance practices (e.g., flushing, pigging) (Friedman *et al.*, 2003).

Biofilms

Biofilms are present in many distribution systems and defined as a complex system formed by and comprising microbes, organic, and inorganic material accumulated amidst a microbially-produced organic polymer matrix attached to the inner surface of the distribution system (EPA, 2002b). Biofilms are capable of promoting both physical and chemical accumulation of inorganic elements through processes such as sorption, bacterially-mediated formation and precipitation reactions, and microbiologically-induced corrosion (MIC) (Teng et al., 2008; Park et al, 2008). As a result, factors (such as assimilable organic carbon, disinfectant residual or nutrients) which influence biofilm formation and stability can impact accumulation and release of inorganic compounds in the distribution system.

Several studies have documented the ability of biofilms present in DWDS to accumulate inorganic compounds, and particularly cations, via sorption (Hanjangsit, 1994; Flemming, 1995; Percival et al., 1997). Biofilm sorption sites may include cell walls, cellular membranes, cytoplasm, and extracellular polymeric substances (EPS), each of which have differing properties and sorption affinities. Cell walls, composing of carboxyl and phosphoryl groups, interact passively with cations and have been shown to be major sites for metal deposition. The mechanisms for binding of metals on cell walls are ion exchange reactions, precipitation and complexation (Flemming, 1995). Cytoplasm is also a potential site for accumulation of dissolved substances. Cadmium has been found to be accumulated intracellular by a large number of organisms (Flemming, 1995). EPS may contain anionic groups, such as carboxyl, phosphoryl, and sulphate groups, which represent a cation exchange potential. A wide variety of metal ions have been reported to be bound to EPS (Flemming, 1995; Flemming *et al*., 2007). Nelson et al. (1995) provide

an example in which both cells and EPS material attached to an iron substrate were responsible for immobilizing lead from water. Schock (2005) also observed that certain biofilms in natural aquatic environments can influence the transport and fate of heavy metals.

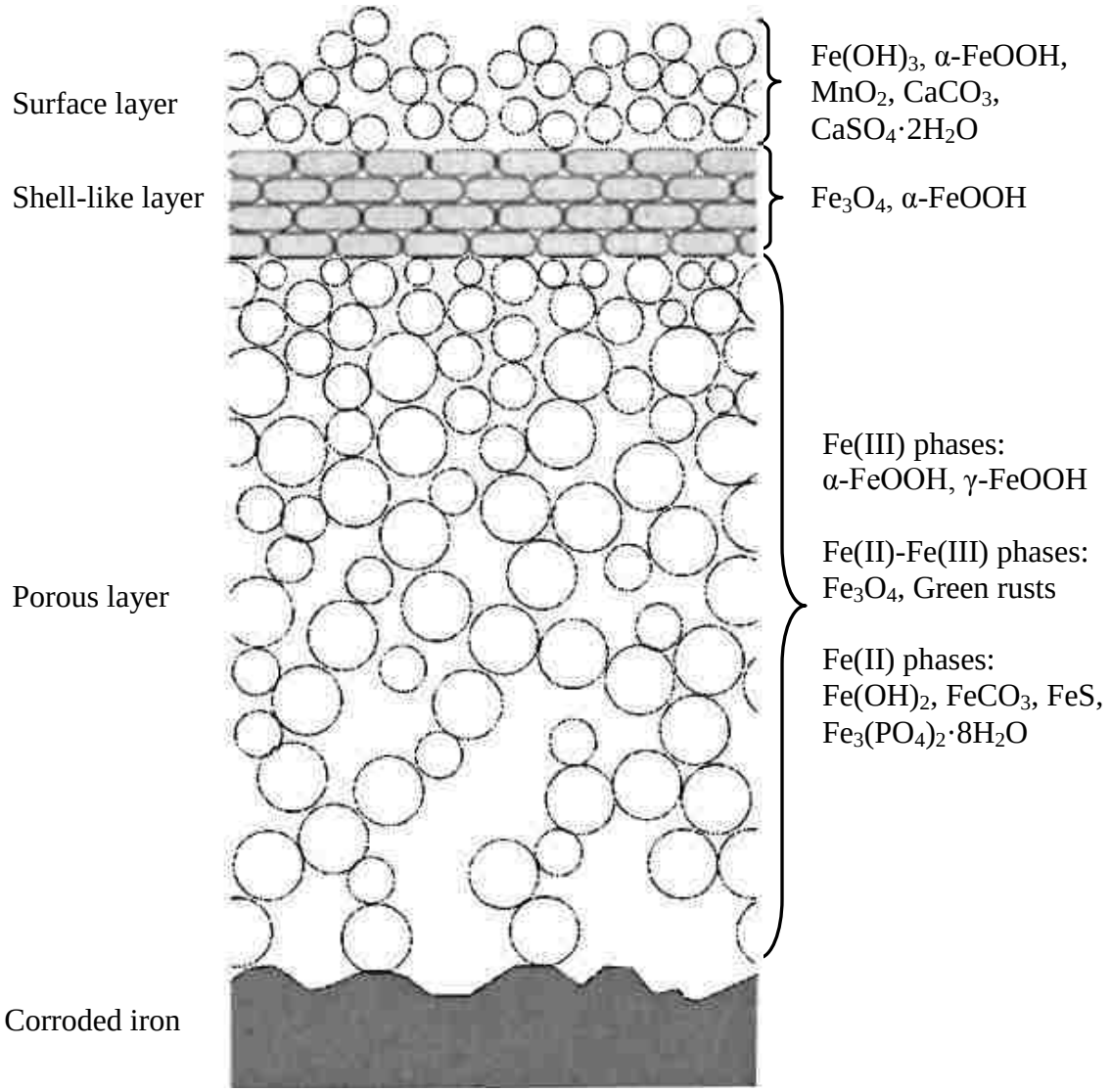

Figure 2.2.1 Schematic of scale structure and possible composition of corrosion scales found in iron/steel pipes (modified from Sarin et al., 2004)

2.3 Accumulation of inorganic contaminants

The accumulation of trace inorganic contaminants in DWDS solids can have consequences for the health of exposed populations if these contaminants are released from the scales thus resulting in their high levels at consumers' tap (Fisher et al., 2000; Lytle et al., 2010).

Various contaminant accumulation and release mechanisms that may occur in distribution system piping are depicted in Figure 2.3.1 (Hill et al., 2010). Figure 2.3.1 illustrates the concept of a water main as a reactor; contaminants can be accumulated via sorption, coprecipitation and sedimentation. These contaminants can also be released due to desorption, destabilization, transformation, and hydraulics. This concept assumes the existence of the non-conservative behavior of contaminants in the DWDSs; although current regulatory framework (Safe Drinking Water Act) for inorganic contaminants presumes that their behavior in distribution systems is physically and chemically conservative.

For this reason, current requirements for monitoring and determination of compliance with maximum contaminant levels (MCLs) apply only to system entry points. As a result, most drinking water utilities have no data on the concentrations of inorganic contaminants within their systems, except for first-draw lead and copper results obtained based on Lead and Copper Rule (Schock and Holm, 2003; Hill et al., 2010).

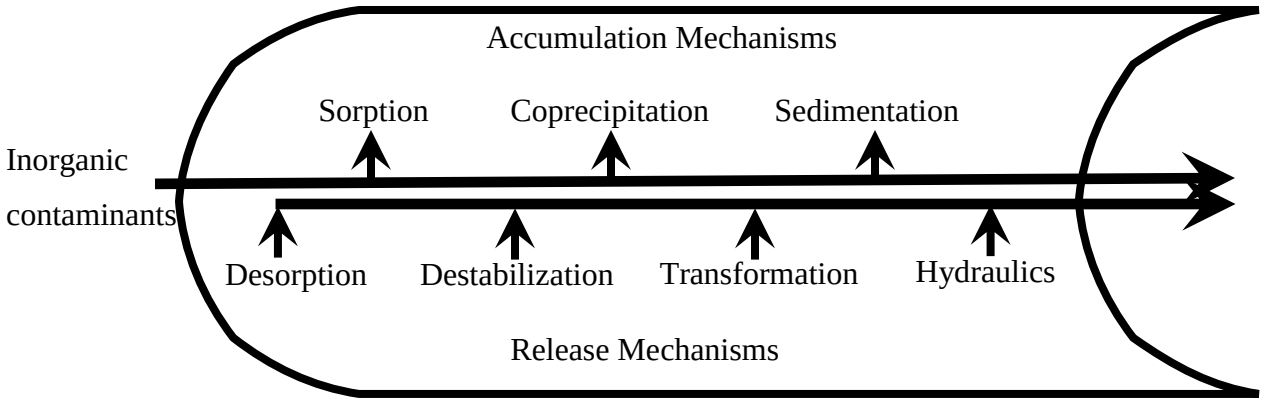

Figure 2.3.1 Contaminant accumulation and release mechanisms that may occur in distribution system piping (adopted from Hill et al., 2010).

Mechanisms of inorganic contaminants accumulation in DWDS include physical, chemical and biological processes. Many of accumulation mechanisms are reversible under certain conditions, which can lead to accumulated contaminants remobilize back into the water.

Mechanisms of inorganic contaminants accumulation

Physical Mechanisms

Physical accumulation may occur due to sedimentation under low-flow conditions. These conditions are often happened at remote areas of the system, dead-end segments, and storage reservoirs.

Chemical mechanisms of the retention of trace-level inorganic contaminants

Precipitation

As mentioned above, precipitation processes involving trace-level inorganic contaminants may occur depending on water quality conditions and deposit onto the

surface of piping, reservoirs, and plumbing systems. Chelating and sequestering agents, such as orthophosphate, NOM, silica, can complex with various inorganic contaminants (e.g. iron, copper, lead), resulting in their precipitation and deposition with the distribution system.

Sorption

Sorption involves the retention of a soluble contaminants onto (adsorption) or within (absorption) the surface of a preformed substrate. Sorption processes are equilibrium-based; therefore, they may be fully or partially reversible when water chemistry is changed. Coprecipitation involves adsorption and enmeshment of a contaminant within an actively precipitating substrate.

Adsorption/coprecipitation is considered to be the most significant mechanisms governing the accumulation of inorganic contaminants in DWDSs (Schock, 2005). Contaminants sorption onto substrates found in distribution systems is conceivably the major factor in trace metal partitioning and solubility control.

Biological Mechanisms

Biological mechanisms of contaminant accumulation are associated with sorption onto biofilm and bacterially-mediated formation and precipitation reactions.

Factors affecting accumulation

Factors with significant effect on contaminant accumulation are the composition of contaminant sinks and the chemistry of the bulk water, including pH and ORP.

Composition of contaminant sinks

Contaminant sinks comprise corrosion scales, precipitates, biofilm and sediment. Different compositions of contaminant sinks have various affinities for accumulating inorganic contaminants. The most common contaminant sinks within the distribution system include oxides, hydroxides, carbonates, hydrocarbonates, and silicates of iron, manganese and aluminum. Phosphate-based precipitates are also important sinks that occur in systems where orthophosphate/polyphosphate is used as corrosion inhibitor.

Due to the presence of iron-based materials, such as cast/ductile pipes, galvanized iron pipes and steel pipes in practically all distribution systems, iron mineral-associated sinks are significant to contaminants accumulation, especially because these solids (e.g., goethite, lepidocrocite, hematite, magnetite, and siderite) have strong affinities for various inorganic contaminants. Many researches have focused on arsenic immobilization on/within iron corrosion scales, given the fact that iron is a strong adsorbent for arsenic (Lytle et al., 2004; Reiber and Dostal, 2000). Other inorganic contaminants, including uranium and selenium, are also reported to be concentrated in the iron-based solids (Dodge et al., 2001; Su and Suarez, 2000).

Manganese sinks, including manganese oxides and oxyhydroxides, have been shown to be an important scavenger for trace metals such as lead, arsenate, barium and nickel (Dong et al., 2003; Ouvrard et al., 2002; Sugiyama et al., 1992). Hydrous manganese oxides (HMOs) are commonly found in deposits of DWDS, particularly for systems with measurable residual manganese in their treated water supply. Relative to iron oxides, HMOs usually have higher surface area and also a lower pH of zero surface charge which results in higher adsorption capacity (Trived et al., 2001; Tamura et al., 1996) as has been

demonstrated in comparative studies of nickel adsorption on HMO and iron hydroxides (Green-Pedersen et al., 1997).

Phosphate-based sinks, particularly those involving apatite, have been demonstrated to affect trace metal partitioning and solubility. Apatite minerals have high adsorptive affinity for lead, cadmium, copper, uranium and zinc (Gauglitz et al., 1992). Due to the remarkable binding affinity of apatite, it has been applied for in situ remediation of uranium from contaminated subsurface environments (Fuller et al., 2002).

Effects of pH

Solution pH can strongly influence surface charge and electrostatic interactions between inorganic contaminants and sinks thus affecting the extent of accumulation. The pH_{zpc} (pH of zero net surface charge) of iron minerals is typically between 7 to 8, while those for manganese- and aluminum-based oxides are lower, that is, between 5 to 7 (Schock, 2005; Valentine et al., 1990). This explains why, under neutral pH conditions, negatively-charged compounds such as arsenate or uranyl tend to adsorb to iron-based minerals, while, cations such as lead, nickel, copper, cadmium are more preferentially adsorbed to HMOs.

Oxidation-reduction potential

Oxidation-reduction potential (ORP) affects both the mineralogy, stability of iron- and manganese-based corrosion scales and chemical forms and properties of many inorganic contaminants, notably arsenic, chromium, selenium, uranium that exist in different oxidation states depending on ORP. Inorganic contaminants in different oxidation states exhibit different accumulation mechanisms and toxicology. In natural water, arsenate

(As(V)) adsorbs more efficiently to iron oxides than arsenite (As(III)). As(III) is also know to be more toxic and mobile species (Fendorf et al., 1997).

2.4 Release

Contaminant accumulation can be partially or fully reversible, depending on physical or chemical conditions in a specific DWDS. Release of accumulated contaminants can proceed via re-mobilization into the water as soluble species and/or release of particulates. Release mechanisms include physical (hydraulic disturbances) and chemical processes.

Mechanisms of inorganic contaminants release

Physical Mechanisms

Physical and hydraulic disturbances are capable of dislodging corrosion scales, chemical precipitates, biofilms, and sediments and entraining the solids in the bulk water. Accumulated inorganic elements associated on or within these sinks would also be mobilized. Previous studies have shown that inorganic contaminants release is associated with solids resuspension even when relatively small amounts of solids are mobilized (Reiber and Dostal, 2000; Lytle et al., 2010).

In general, physical disturbances may result from earthwork or construction near the active systems as well as hydrant flushing. Hydraulic disturbances within the distribution system may result from (1) changes in flow rate/velocity: due to peak demands, fire fighting activities, etc.; (2) flow reversals; (3) hydraulic pressure transients: sudden changes in velocity, pump start/stop cycles and etc.

Chemical Mechanisms

Dissolution

Corrosion scales, precipitates, sediments, and biofilms may become unstable if water quality conditions are perturbed. Parameters such as pH, ORP, alkalinity, DIC, and phosphate concentration generally govern the stable form of corrosion scales and precipitates. Other parameters (e.g., calcium, aluminum, and sulfate) are also significant with regard to the stability of chemical precipitates. Changes of these parameters may create disequilibrium and promote the dissolution of existing solids and release of accumulated inorganic contaminants.

Destabilization

Changes of major water chemistry parameters have the potential to completely destabilize existing chemical scales, leading to their physical release (as opposed to its chemical transformation). Such events can cause a dramatic increase in the concentration of solids-associated contaminants in drinking water. For instance, this has been observed in cases where a utility made substantial treatment changes related to disinfection (e.g., implementation of chlorination, conversion from free chlorine to chloramine), pH (e.g. implementation of caustic soda addition to raise pH), and has switched between sources of vastly different quality (e.g., surface water and groundwater).

Reiber *et al.* (2000) reported the first case of arsenic release from drinking water distribution system (DWDS) solids in Nebraska. The community had commenced the addition of chlorine to a previously non-chlorinated groundwater system. This resulted in a major red water (release of iron particulates) episode. During that time, extremely

elevated arsenic levels in the water samples were observed. Release of As-containing particles resulting from the breakdown of arsenic-containing iron corrosion solids was determined to be responsible for the high concentrations of arsenic of this event.

Desorption

The degree of re-partitioning of contaminants between a sink and the bulk water depends on the nature of contaminants and sinks involved, water chemistry and the degree of perturbation from initial equilibrium. The actual extent of re-equilibration may depend on the mechanism of sorption (e.g., inner- versus outer-sphere complexation), mass transfer limitations, and the available mass or surface area for desorption. However, co-precipitated and/or occluded contaminants may be more resistant to desorption and/or diffusion into bulk water (Friedman et al., 2010).

Copeland et al. (2007) demonstrated the impact of pH and orthophosphate on the desorption of arsenic from nine DWDS solids collected from utilities located in the Midwest. Contaminant-partitioning batch experiments were performed over the course of 168 hours (seven days) under a series of conditions intended to be representative potential real-world system operating conditions, i.e., pH levels of 7, 8, and 9 and orthophosphate concentrations of 0, 3, and 5 mg/L (i.e., 9 total test conditions per sample). They found that arsenic release tended to increase with increasing initial As concentration in the solid, increasing pH levels and orthophosphate concentrations. Given the minimal amount of iron released in the experiments and that no correlation between arsenic release and other water chemistry variables existed, they concluded that arsenic was released by desorption from the surfaces. The results suggest that arsenic adsorption onto iron-rich sinks is sensitive to pH perturbations and changes in the concentration of

competing constituents (e.g., phosphate), and that the extent of desorption is related to the magnitude of the chemical perturbation and the initial solids arsenic concentration.

Munk and Faure (2004) demonstrated small pH fluctuations could impact metals mobilization from sediments composed primarily of iron and aluminum oxides and hydroxides. The researchers observed that pH fluctuations on the order of 0.2 units considerably affected the release of previously adsorbed zinc, copper, nickel, molybdenum, and cadmium.

Frau et al (2008) reported the desorption of arsenate from three different ferrihydrite-bearing natural samples (mine tailings, streambed sediment and top soil). They found that arsenic was highly mobile when solids were exposed to orthophosphate- and carbonate-rich solutions because of competitive displacement and substitution. Effects of high aqueous carbonate concentrations on arsenic mobility and transport in the subsurface were studied by Radu et al. (2005). In synthetic iron oxide-coated sand column experiments, compared to phosphate, carbonate mobilized less adsorbed As(V) than was mobilized by phosphate, even with carbonate present in much higher concentrations than phosphate. The desorptive solutions (phosphate and sulfate) were also studied by O'Reilly et al (2001) to ascertain the kinetics and mechanisms of arsenate desorption on goethite. Sulfate was found to be a much less effective desorbent for adsorbed arsenic compared to phosphate.

Factors affecting chemical release

pH value

The pH value in a distribution system is a major factor determining the scale stability, particle surface charge, and chemical equilibrium conditions. Adjustment of pH value in

a system can contribute to scale instability, mineral dissolution and contaminant mobility within the system. Changes of pH can occur as a result of seasonal variations the source water quality and usage, and treatment changes such as enhancement of chemical treatments, control disinfection by-product (DBP) formation, and reduction of corrosion.

Oxidation-reduction potential

Oxidation-reduction potential (ORP) can influence not only the mineralogy, stability and physiochemical properties of scales, but also the chemical form and characteristics of inorganic contaminants. ORP variations due to changes in disinfection practices can have a large impact on the stability of scales and accumulated contaminants. Changes of disinfection implementation include changing disinfectants from free chlorine to chloramine and changing of disinfection residual.

Chloramine is a weaker disinfectants compared to chlorine. Utilities that switch disinfectants from chlorine to chloramine will reduce ORP values in the distribution system, which may result in existing scales beginning to weaken, dissolve, or change chemical form (e.g., Pb^{4+} to Pb^{2+}).

Corrosion inhibitors

The most common inhibitors used in the drinking water industry to improve corrosion resistance and scales stability are orthophosphates, polyphosphates, blended phosphates, and silicates. The addition of corrosion inhibitors, especially phosphates, may cause dramatic mineral phase transformation and/or desorption of contaminants via competition or displacement. The increase arsenic release in the presence of orthophosphate due to competitive effect was observed by Copeland et al. (2007).

2.5 Speciation of inorganic contaminants in corrosion solids

The preceding discussion indicates that, ultimately, the mobility and availability of contaminants accumulated in DWDS solids depends on their physico-chemical speciation that encompasses states ranging from mobile species that can be released via desorption to those tightly bound by stable crystalline oxides of iron and, in lesser extent, Ca and Mg carbonates, silica and manganese oxides predominating typical corrosion scales (Linge, 2008). Thus, the determination of mobility and other aspects of the speciation of trace level inorganic contaminants in DWDS solids require that the modes of binding of these elements in the solid matrix be ascertained.

That goal can be achieved via selective extractions that allow estimating contributions of the target elements bound by *a priori* defined types of solid phases. One sequential extraction procedure that has been extensively employed to speciate inorganic contaminants in soils and sediments was proposed by Tessier et al. (1979). It fractionates heavy metal species found in soils or sediments into five operationally defined fractions that correspond to exchangeable, carbonate-bound, iron and manganese oxide-bound, organically bound, and residual metal (Table 2.5.1). The Tessier's scheme was later modified to separate the fraction comprising species bound by iron and manganese oxides into narrower-defined fractions such as metal-organic complex-bound, easily-reducible metal oxide-bound, amorphous mineral colloid-bound, and crystalline iron oxide-bound species (Shuman, 1985; Krishnamurti et al., 1995). The sequential extraction scheme proposed by Krishnamurti et al. (1995) is shown in Table 2.5.2. One gram of solid samples (dry weight) was typically used in the schemes proposed by Tessier et al. (1979)

and Krishnamurti et al. (1995). Solid/liquid separation carried out in these schemes at each successive extraction step was achieved by centrifuging.

As was discussed above, iron and manganese minerals compounds, notably ferrihydrite, goethite, lepidocrocite, magnetite, hydrous manganese oxides, are commonly found in the corrosion scales and deposits of DWDSs (Benjamin et al., 1996; Sarin et al., 2001; Peng et al., 2010). Although the composition and properties of DWDS corrosion solids and deposits may be different from those of soils and sediments for which the Tessier's and related schemes have been developed, it is reasonable to assume that the sequential extraction can be a powerful fractionation method to investigate the speciation of heavy metals accumulated in DWDS solids.

Table 2.5.1 Operating conditions required in the Tessier sequential extraction procedure (Tessier et al., 1979)

Step	Fractions	Reagent	Experimental conditions
1	Exchangeable	8 ml of 1 M $MgCl_2$ at pH 7	1 h at 25ºC
2	Bound to carbonates	8 ml of 1 M CH_3COONa at pH 5 with CH_3COOH	5 h at 25ºC
3	Bound to Fe-Mn oxides	20 ml of 0.04 M $NH_2OH{\cdot}HCl$ in 25% CH_3COOH (pH~2)	6 h at 96±3ºC
4	Bound to organic matter	5 ml of 30% H_2O_2 at pH 2, 3 ml of 0.02 M HNO_3	2 h at 85ºC
		3 ml of 30% H_2O_2 at pH 2,	3 h at 85ºC
		Cool, 5 ml 3.2 M CH_3COOH	30 min at 25ºC
5	Residual	Digestion with HF and $HClO_4$	

Table 2.5.2 Sequential extraction scheme proposed by Krishnamurti et al. (1995)

Step	Fractions	Reagent	Reaction time and temperature
1	Exchangeable	10 ml of 1 M $Mg(NO_3)_2$ at pH 7	4 h at 25ºC
2	Carbonate-bound	25 ml of 1 M CH_3CO_2Na at pH 5	6 h at 25ºC
3	Metal-organic complex-bound	30 ml of 0.1 M $Na_4P_2O_7 \cdot 10\ H_2O$ at pH 10	20 h at 25ºC
4	Easily reducible metal oxide-bound	20 ml of 0.1 M $NH_2OH \cdot HCl$ in 0.01 M HNO_3	30 min at 25ºC
5	Organic-bound	5 ml of 30% H_2O_2 at pH 2, 3 ml of 0.02 M HNO_3	2 h at 85ºC
		3 ml of 30% H_2O_2 at pH 2,	2 h at 85ºC
		Cool, 10 ml $Mg(NO_3)_2$ in 20% HNO_3	30 min at 25ºC
6	Amorphous mineral colloid-bound	10 ml of 0.2 M $(NH_4)_2C_2O_4$ (adjusted to pH 3 with 0.2 M $H_2C_2O_4$)	4 h at 25ºC (dark)
7	Crystalline iron oxide-bound	25 ml of 0.2 M $(NH_4)_2C_2O_4$ (adjusted to pH 3 with 0.2 M $H_2C_2O_4$) in 0.1 M ascorbic acid	30 min at 95ºC
8	Residual	Digestion with HF and $HClO_4$	

Chapter 3 Materials and Methods

3.1 Characterization of elemental and structural composition of corrosion scales and deposits formed in drinking water distribution systems

3.1.1 Sampling sites and measurements

All drinking water utilities from which the samples of corrosions scales were collected were located in the United States. The selection of these utilities and detailed information on harvesting and handling to the samples is presented in the report by Friedman et al., 2010. Table 3.1.1 provides a summary of the sampling sites and their selected relevant characteristics. .

The samples examined in this study included (1) pipe specimens, either obtained from a recent "live" extraction or from a storage area (referred to as "boneyard" specimens); (2) hydraulically-mobile deposit material collected during hydrant flushing events; and (3) distribution system water samples. A limited set of distribution system water samples was collected at a site near the location where the solid sample was obtained. General water quality parameters (pH, temperature, alkalinity, disinfectant residual, and turbidity) were measured at the same time and location as water sample collection.

The harvested samples were initially sent to the Environmental Engineering and Science Laboratory (EES) of the University of Iowa for digestion and other processing. Some digestions were also performed in our laboratory, as described in the sections that follow. Water samples were shipped to our lab. Upon receipt, they were filtered through a 33-mm

Millex®-HA syringe filter (Millipore Corporation, Bedford MA) with a 0.45-µm nominal pore size to remove particulate matter. The filtrate was acidified to reach a 1% nitric acid concentration and placed in 15 mL conical polypropylene test tubes. The samples were spiked with internal standards (^{45}Sc, ^{74}Ge, and ^{103}Rh) and stored at 4ºC until analyzed.

3.1.2 Solid Samples Collection

Of the 72 collected solid samples, 26 were hydrant flush solids and 46 were pipe specimens (including 34 live pipe extractions and 12 boneyard samples). The hydrant flush samples obtained during conventional flushing provided an opportunity to assess the composition of hydraulically-mobile solids released due to hydraulic disturbances. In contrast with hydrant flush solids, scale from pipe specimens can be operationally considered as hydraulically-inert material.

All collected solid material was dried at 103ºC for 24 hours and weighed to determine its dry mass. In the case of pipe specimens, a portion of mixed dried sample was crushed using a mortar and pestle, passed through a number 50 sieve (300-µm mesh) and homogenized. The crushed/sieved material was digested and analyzed to determine its elemental composition. For selected samples, subsets of both crushed and uncrushed material were used examined using X-Ray Diffraction (XRD) and Scanning Electron Microscopy (SEM) to determine their mineralogy and morphology.

Determination of the elemental composition was possible for 35 of 46 pipe specimens and 23 of 26 of hydrant flush solids. The determination of elemental sulfur and carbon content was carried out for the subsets of 48 and 36 samples, respectively.

Table 3.1.1 Summary of utility participants and solid samples examined in this study

Utility Identifier	Region	Service Population	Water Sources[a]	Primary Treatment and Post-Treatment Applications	Solid samples provided by the utility	Pipe material[b]
W	Midwest	7,000	GW	Electrodialysis reversal, chloramines, poly-PO_4	3 pipe specimen, 5 hydrant flush	Cast iron
CL	Midwest	28,000	GW	Fluoridation, PO_4 blend, free chlorine	5 pipe specimen, 2 hydrant flush	Cast iron
SA	West	60,000	GW, SW	Free chlorine, Fe/Mn removal, pH adjustment, fluoride	3 pipe specimen, 2 hydrant flush	1 PVC, 4 Cement-Lined Iron
CH	West	11,000	GW	Free chlorine	1 pipe specimen	steel
RW	West	6,300	GW	Free chlorine	2 pipe specimen	Galvanized Iron
IN	West	57,000	GW, SW	Free chlorine, Fe/Mn/As removal, fluoride, ortho-PO_4	4 pipe specimen	1 Cement-Lined Iron, 3 Ductile Iron
CC	West	1,900	GW	Free chlorine, Fe/Mn removal, pH adjustment, fluoride,	6 pipe specimen	4 Cast iron, 2 Cement-Lined Iron
DN	West	1,200,000	SW	Conventional treatment, chloramines	2 pipe specimen	Cast iron
CA	West	100,000	GW, SW	Free chlorine, Fe/Mn removal	2 pipe specimen	1 steel, 1 Cast iron
PC	West	8,000	GW, SW	Free chlorine, Fe/Mn/As removal	2 pipe specimen	Galvanized Iron
WDB	Northeast	1,200	GW	Free chlorine	1 pipe specimen	HDPE
WA	Northeast	6,000	GW	Free chlorine, pH adjustment	4 pipe specimen	Cast iron
B	West	493,000	SW, GW	Conventional treatment, chloramines	4 pipe specimen	2 Ductile Iron , 1 cast iron , 1 Cement-Lined Iron,
G	Midwest	5,000	GW	Free chlorine, cation exchange, pH adjustment, fluoride	2 hydrant flush	1 cast iron, 1 Cement-Lined Iron
AZ	West	245	GW	Free chlorine	1 pipe specimen	PVC
BC	West	28,000	GW	Free chlorine	2 pipe specimen	PVC
J	Midwest	145,000	GW	PO_4 blend, chloramines	10 hydrant flush	Cast iron
NC	Midwest	200	GW	Cation exchange, poly-PO_4, fluoride, free chlorine	1 hydrant flush	PVC
ST	Midwest	15,000	GW	Cation exchange, PO_4 blend, pH adj., fluoride, free chlorine	2 pipe specimen, 2 hydrant flush	2 Cast iron, 2 Cement-Lined Iron
K	Midwest	8,000	GW	Chloramines, HMO Filter Process, pH adjustment	2 pipe specimen, 2 hydrant flush	1 Ductile Iron , 3 cast iron

(a) GW = groundwater; SW = surface water.

(b) For hydrant flush samples, pipe material refers to the type of pipe used to distribute water in the flushing zone.

3.1.3 Analytical Procedures

All digestions of solid samples were performed at the EES using USEPA Method 3050B (Acid Digestion of Sediments, Sludges and Soils). For 58 samples that had adequate mass for processing, the fraction of sample mass that was digested by the above procedure ranged from 24 to 96%, with an average ± standard deviation of 78% ± 15% (Friedman et al., 2010). Aliquots of the digests were sent to the CEE to determine their elemental composition.

Ten of the solid samples were chosen for morphological and surface elemental composition using SEM and energy dispersive spectroscopy (EDS) technique. SEM/EDS measurements were performed with a JEOL-7000F high-resolution SEM instrument (JEOL Corporation, Japan). EDS data were acquired in two modes. The first mode allowed examining the entire surface of the sample, while the second mode corresponded to localized spots that were selected primarily on the basis of apparent morphological differences. Prior to SEM/EDS analysis, the requisite amount of the solid was placed on a 9.5-mm aluminum specimen mount (Ted Pella Inc., Redding CA) using double-coated 9-mm conductive carbon pads (Ted Pella Inc., Redding CA). The sample was vacuum sputter-coated to deposit a thin conductive flim of platinum or 60% gold and 40% palladium layer with an SPI sputter coater (Structure Probe Inc., West Chester PA).

XRD measurements were performed for the aforementioned ten selected samples to identify predominant mineralogical phases. Analysis of the first group of solid samples (consisting of CC-A, CC-D, CH-A, J-B, and J-E) were carried out using a Philips PW1830 X-ray diffractometer (Philips, Netherlands). Analysis of the second group of

solid samples (consisting of RW-A, RW-B, PC-A, PC-B and J-J) were carried out using a Siemens D5000 X-ray diffractometer (Siemens Corporation, New York NY). Ni-filtered Cu-Kα radiation (λ of 1.5406 Å) was used to perform crystallographic analysis in both cases. The range of 2θ values was 10º to 80º with a 0.05º step size. The scanning speed was 2º per second. XRD patterns were identified using Jade^{+} software (version 6). Diffraction data were compared against reference patterns from the 1995 version of International Center for Diffraction Data (ICDD).

3.1.4 Analytical Parameters and Methods

Inorganic elements of treated water and digested solid samples were analyzed by the method of inductively coupled plasma-mass spectroscopy (ICP-MS) in accord with Standard Method 3125. The following isotopes were targeted for analysis: ^{27}Al, ^{75}As, ^{138}Ba, ^{42}Ca, ^{111}Cd, ^{52}Cr, ^{56}Fe, ^{24}Mg, ^{55}Mn, ^{60}Ni, ^{31}P, ^{208}Pb, ^{123}Sb, ^{82}Se, ^{28}Si, ^{205}Tl, ^{238}U, ^{51}V, and ^{66}Zn. Appropriate corrections for interferences were made. Corrections were introduced for arsenic and lead to account for specific ion interferences. For ^{75}As, corrections for effects of ^{77}ArCl and ^{72}Se were made. For ^{208}Pb, corrections for effects of ^{206}Pb and ^{207}Pb were made.

Analyses were carried out with a PerkinElmer ELAN DRC-e ICP-MS instrument equipped with an AS 93 Plus autosampler (PerkinElmer Instruments, Shelton CT). Atomization was achieved using a MicroMist nebulizer with baffled cyclonic spray chamber (PerkinElmer Instruments, Shelton CT). Data processing and acquisition were carried out using ELAN instrument software (version 3.3). Excluding iron, all inorganic elements were analyzed using the standard mode (involving a dynamic bandpass tuning parameter of 0.25). Iron measurements were made in the Dynamic Reaction Cell mode to

remove interfering ions. This mode involved use of ammonia as a reaction gas (0.5 mL/min) and a dynamic bandpass tuning parameter of 0.50.

A certified reference material (CRM) (River Water Reference Material for Trace Metals SLRS-4) was purchased from the National Research Council of Canada (Ottawa, Canada) to evaluate ICP-MS performance. Results of ICP-MS analysis on this CRM are summarized in Table 3.1.2. On the average, the deviation from expected values was ±3.6% indicating a reasonable level of accuracy. Recoveries of known additions were also conducted. They ranged from 85% to 120%.

Table 3.1.2 Measurement summary for SLRS-4 Certified Reference Material (CRM)

Element	CRM certified concentration (µg/L)	CRM certified Std. Deviation (µg/L)	ICP-MS measured concentration (µg/L)	Observed Deviation
Aluminum	54.0	±4.0	56.2	4.1%
Arsenic	0.68	±0.06	0.66	-3.1%
Barium	12.2	±0.6	12.3	0.9%
Calcium	6,200	±200	5,918	-4.6%
Cadmium	0.01	±0.002	0.01	0%
Chromium	0.33	±0.02	0.35	4.8%
Iron	103	±5.0	102.4	-0.6%
Magnesium	1,600	±100	1,657	3.6%
Manganese	3.37	±0.18	3.36	-0.2%
Nickel	0.67	±0.08	0.68	0.7%
Lead	0.09	±0.007	0.08	-8.1%
Antimony	0.23	±0.04	0.21	-9.6%
Uranium	0.05	±0.003	0.05	0%
Vanadium	0.32	±0.03	0.32	0%
Zinc	0.93	±0.10	1.0	7.4%

3.2 Speciation of inorganic contaminants in corrosion scales and deposits in drinking water distribution systems

The determination of mobility and availability of trace level inorganic contaminants in DWDS solids were achieved via sequential extractions, separate filtration and structure-sensitive method of X-ray Adsorption Spectroscopy (XAS).

3.2.1 Solid samples characteristics

Three pipe specimens (CC-A, CC-B, and CC-D) and two hydrant flush samples (J-E and J-J) were selected for the experiments based on higher concentrations of trace inorganic contaminants in them. Four samples of the samples that had a sufficient mass were analyzed by X-ray Diffraction (XRD) measurement to identify their mineralogical phases. XRD analyses were described in more detail in previous section. Specific surface area was carried out using a Quantachrome NOVA 4200e instrument and calculated using multi-point BET method.

3.2.2 Sequential extraction procedures and operationally defined metal fractions

Speciation of the selected inorganic contaminants (As, Cr, V, U, Cd, Ni, Mn) in the solid samples was determined based on the sequential extraction scheme described by Krishnamurti et al. (1995). Important details of the scheme are summarized in Table 3.2.1. The following fractions that correspond to different operationally defined modes of binding of inorganic contaminants in the solid phases were established:

(1) ***Exchangeable metal***: heavy elements associated with exchangeable binding sites. This mode of binding is expected to result in relatively easy displacement of the bound metals by competing ions.

(2) ***Carbonate-bound metal***: heavy elements associated with sorption on or occlusion into carbonates, typically calcite ($CaCO_3$) and dolomite ($CaMg(CO_3)_2$). Elements coprecipitated with calcite can be dissolved by acidic sodium acetate.

(3) ***Metal-organic complexes***: heavy elements associated with humic species present in the solid matrix.

(4) ***Easily reducible metal oxide-bound metal***: heavy elements associated with easily reducible metal oxides such as manganese (III, IV) oxides. Hydroxylamine hydrochloride ($NH_2OH \cdot HCl$) is specific to Mn oxides, leaving crystalline iron oxides unaffected and dissolving minimal amounts of amorphous iron oxides.

(5) ***Organic-bound metal***: heavy elements associated with organic matter other than humic substances.

(6) ***Amorphous mineral colloid-bound metal***: heavy elements associated with amorphous iron oxides and poorly crystalline aluminosilicate mineral colloids. Acidic ammonium oxalate ($(NH_4)_2C_2O_4$) performed in dark is specific for dissolving amorphous minerals.

(7) ***Crystalline iron oxide-bound metal***: heavy elements associated with crystalline iron oxides.

(8) ***Mobilization-resistant metal***: heavy elements associated with mineral lattices resistant to the above successive sequential extractions (Krishnamurti and Naidu, 2002; Linge, 2008).

Sequential extractions were carried out in duplicate using one gram of each solid sample (except CC-B, in which case 0.4 gram was used). Requisite amounts of the solids were placed in 50 ml metal free polypropylene centrifuge tubes (VWR). After each extraction, the tubes containing solids were centrifuged for 10 minutes at 4000 rpm to separate the supernatant. The residual solids were rinsed with 10 ml of de-ionized distilled water, centrifuged again for 10 min at 4000 rpm, and the resulting supernatant collected for further analyses. All chemicals used in the sequential extraction procedure were all ACS grade. Their solutions were checked to determine the concentration of the target trace metals in them (Table 3.2.2).

Table 3.2.1 Sequential extraction scheme for speciation used in this study (Krishnamurti et al., 1995)

Step	Fractions	Reagent	Reaction time and temperature
1	Exchangeable	10 ml of 1 M $Mg(NO_3)_2$ at pH 7	4 h at 25ºC
2	Carbonate-bound	25 ml of 1 M CH_3CO_2Na at pH 5	6 h at 25ºC
3	Metal-organic complex-bound	30 ml of 0.1 M $Na_4P_2O_7 \cdot 10\ H_2O$ at pH 10	20 h at 25ºC
4	Easily reducible metal oxide-bound	20 ml of 0.1 M $NH_2OH \cdot HCl$ in 0.01 M HNO_3	30 min at 25ºC
5	Organic-bound	5 ml of 30% H_2O_2 at pH 2, 3 ml of 0.02 M HNO_3	2 h at 85ºC
		3 ml of 30% H_2O_2 at pH 2,	2 h at 85ºC
		Cool, 10 ml $Mg(NO_3)_2$ in 20% HNO_3	30 min at 25ºC
6	Amorphous mineral colloid-bound	10 ml of 0.2 M $(NH_4)_2C_2O_4$ (adjusted to pH 3 with 0.2 M $H_2C_2O_4$)	4 h at 25ºC (dark)
7	Crystalline iron oxide-bound	25 ml of 0.2 M $(NH_4)_2C_2O_4$ (adjusted to pH 3 with 0.2 M $H_2C_2O_4$) in 0.1 M ascorbic acid	30 min at 95ºC
8	Mobilization-resistant	Digestion with HNO_3 and 30% H_2O_2	

Table 3.2.2 Concentrations of the target trace metals in the chemicals used in the sequential extraction scheme.

Step	Chemicals	As (µg/L)	Cr (µg/L)	V (µg/L)	U (µg/L)	Cd (µg/L)	Ni (µg/L)	Mn (µg/L)
1	1 M $Mg(NO_3)_2$	0.171	1.275	0.078	0.003	0.057	28.534	109.89
2	1 M CH_3CO_2Na	0.129	43.992	11.583	0.011	0.012	0.64	1.96
3	0.1 M $Na_4P_2O_7 \cdot 10\ H_2O$	0.183	2.27	1.09	0.014	0.388	1.709	1177.74
4	0.1 M $NH_2OH \cdot HCl$	0.12	1.093	0.147	0.003	0.019	0.403	1.82
5	30% H_2O_2, 0.02 M HNO_3	0.24	9.303	0.138	0.003	0.177	138.14	185.84
	$Mg(NO_3)_2$ in 20% HNO_3							
6	0.2 M $(NH_4)_2C_2O_4$	0.12	4.32	4.124	0.003	0.209	2.33	31.75
7	0.2 M $(NH_4)_2C_2O_4$ in 0.1 M ascorbic acid	0.314	23.1	22.236	0.008	0.66	14.175	58.433
8	HNO_3 and 30% H_2O_2	0.41	3.007	0.493	0.005	0.408	0.425	0.012

3.2.3 Separation of soluble and particulate fractions of metal released from suspended corrosion solids

To determine concentration of the target elements in solids assigned to soluble and particulate fractions released from suspended corrosion solids, twenty milligrams of each sample were dispersed into 100 ml water with alkalinity 100 mg/L as $CaCO_3$ and pH 7.6 placed in 125 ml Nalgene metal free bottles. Samples were placed on a shaker and aliquots were taken for analyses after 30, 60 and 120 minutes of exposure. The samples were filtered through filters with nominal pore size of 5, 2, 1, and 0.4 μm (Whatman Nuclepore polycarbonate track-etched membranes). The filter units and syringes were prewashed with 1% HNO_3 and then rinsed with de-ionized distilled water. Sample aliquots of 15 ml were filtered directly into 15 ml metal free tubes. The first 5 ml of filtrate was discarded. Filtered samples were acidified to 1% HNO_3 with ultrapure HNO_3 and stored at 4ºC prior to analysis.

3.2.4 X-ray Absorption Spectroscopy

X-ray absorbance near edge structure (XANES) and extended X-ray absorption fine structure spectra of three arsenic model compounds and CC-D sample were carried out at beamline X19-A of the National Synchrotron Light Source (NSLS) at Brookhaven National Laboratory (BNL), Upton, NY. The X-ray energy was varied from 200 eV below to 1000 eV above the absorption K-edges of As (E_k = 11868 eV) using a double crystal Si(111) monochromator. Samples were ground and mounted on a piece of 3M scotch® tape via brushing; the tape was then folded several times until the intensity of the signal reached a suitable range for numerical analysis. The synthetic model compound

(adsorbed As(V)-Fe) was prepared in our lab. Adsorption of As(V) (sodium arsenate ,$Na_2HAsO_4 \cdot 7H_2O$) was achieved by reacting a suspension of 0.5 g/L dry 2-line ferrihydrite synthesized following the procedures described by Schwertmann and Cornell (1991) with 0.1 M As solution at pH 7.5 for one day. The suspension was centrifuged at 4000 rpm for 10 min to separate solid and liquid. The separated solid was then freeze dried for one day. Two model compounds (sodium arsenite $NaAsO_2$ and sodium arsenate ($Na_2HAsO_4 \cdot 7H_2O$) were measured in the transmission mode; while the adsorbed As(V)-Fe and CC-D were analyzed in the fluorescence mode. Fluorescence mode was carried out by using the Lytle detector with a Germanium filter and Soller-type slits to minimize the fluorescence background. To improve the signal-to noise ratio, at least 4 measurements were obtained and averaged for the diluted samples. Gold metal foil was always measured in the transmission mode simultaneously with all other samples and used as the reference for the alignment of energies.

Energy calibration was performed with Athena® software and achieved by assigning the first inflection point of the simultaneously measured Au foil to 11919 eV. The edge jump of pre- and post-edge regions was then normalized. The function was then transformed from energy unit (eV) to photoelectron wave vector (k) unit ($Å^{-1}$) to produce the EXAFS function ($\chi(k)$). The k^3-weighted $\chi(k)$ function was then Fourier transformed (FT) using a Hanning window to create the radical structure function (RSF) in R-space (Å). The experimental EXAFS data were then fitted with coordination number (N), interatomic distance (R), and the Debye-Waller parameter (σ^2) using Artemis® program. Linear least-squared fitting (LSF) was done on the XANES spectra after background subtraction and normalization with Athena® program.

3.2.5 Elemental Analysis

Concentrations of several elements in samples generated using sequential extractions and filtration experiments that utilized filters with varying sizes were determined by inductively coupled plasma-mass spectroscopy (ICP-MS) (PerkinElmer ELAN DRC-e ICP-MS). The elements quantified in these measurements included arsenic (As), chromium (Cr), vanadium (V), uranium (U), cadmium (Cd), nickel (Ni) and manganese (Mn). Quality control samples, including laboratory-fortified blanks and laboratory-fortified samples, were performed for every ten samples analyzed. Average elemental recoveries ranged from 85.2 to 92.8% for the laboratory-fortified samples.

A certified reference material (CRM) (Loamy Sand, CRM 024-050) was purchased from RTC (Laramie, Wyoming) to quality check the analytical method. Results obtained from ICP-MS analysis of certified reference material is summarized in Table 3.2.3.

Table 3.2.3 Measurement summary for CRM 024-050 Certified Reference Material (CRM)

Element	CRM certified value (µg/g)	CRM certified Std. Deviation (µg/g)	ICP-MS measured value (µg/g)
Arsenic	3.42	±1.14	3.558
Chromium	25.4	±10.5	29.879
Vanadium	20.8	±7.03	23.081
Uranium	-	-	1.319
Cadmium	2.15	±0.54	2.17
Nickel	15	±5.34	20.975
Manganese	199	±17.6	191.378

3.3 Examination of effects of desalinated water on iron Corrosion, accumulation and release of inorganic contaminants

Jar tests were employed to determine the effects of various water quality parameters on inorganic contaminants accumulation and release from iron, copper, and lead/tin coupons. This study was carried out in two batches of corrosion exposures. Batch 1 employed only iron coupons to ascertain effects of blending of surface water and desalinated water on iron corrosion and inorganic contaminants accumulation. Batch 2 experiments used iron, copper and lead/tin coupons. These experiments were designed to evaluate effects of water quality conditions on metal corrosion and accumulation and release of inorganic contaminants within/from corroded metals.

3.3.1 Impacts of blending of surface water and desalinated water on iron corrosion and retention of inorganic contaminants

3.3.1.1 Iron coupon preparation

Iron coupons (3.2 cm length) were cut from plain steel round rod (0.32 cm diameter; material: cold rolled mild steel) and notched in the middle of each coupon for tying with nylon lines. Coupons were first cleaned with HPLC-grade methanol and then rinsed with distilled DI water. After cleaning, coupon surfaces were activated by dipping them in 0.01M HCl for ten seconds, rinsing with distilled DI water and then air-drying for 1 day. In order to determine the weight loss, coupons for jar tests were weighed with a Sargent-Welch analytical balance before exposures.

3.3.1.2 Preparation of synthetic water

Jar experiments with iron coupons were carried out using synthetic water prepared to imitate the composition of the treated surface water and desalinated water produced by

Graham Hill water treatment plant and Seawater Desalination Pilot Plant in Santa Cruz, California, respectively (Liu et al., 2010). Synthetic waters in this thesis were prepared with ultra-pure DI water produced by a MilliQ-plus water purifier system (Millipore Corporation, Bedford, MA). The chemical composition of these synthetic waters is summarized in Table 3.3.1. Chemicals used in preparing synthetic waters were calcium chloride dehydrate (ACROS), magnesium chloride (J.T. Baker), sodium chloride (Sigma-Aldrich) and sodium sulfate anhydrous (J.T. Baker). For synthetic surface water, $5.85 \cdot 10^{-4}$ M $CaCl_2 \cdot H_2O$, $4.07 \cdot 10^{-4}$ M $MgCl_2$, $7.9 \cdot 10^{-4}$ M NaCl, and $8.25 \cdot 10^{-4}$ M Na_2SO_4 solutions were prepared. For synthetic desalinated water, $1.50 \cdot 10^{-5}$ M $CaCl_2 \cdot H_2O$, $1.48 \cdot 10^{-4}$ M $MgCl_2$, $4.43 \cdot 10^{-3}$ M NaCl, and $5.73 \cdot 10^{-5}$ M Na_2SO_4 solutions were prepared. To examine NOM effects on iron corrosion, Suwannee River Fulvic Acid (SRFA, purchased from the International Humic Substance Society) was used to represent the DOC concentrations in the synthetic water. DOC concentrations ranged from 0, 0.5, 1 to 2 mg/L in the test.

The blending ratio ranged from 0%, 20%, 50%, 80% to 100% desalinated water. The alkalinity and pH values were fixed at 120 mg/L as $CaCO_3$ and 7.5, respectively. A total of 20 water qualities were tested in batch 1. The detailed list of water qualities is given in Table 3.3.2. Fifteen ppb of nine inorganic contaminants, including V(V), Cr(III), Ni, Cu, Zn, As(V), Cd, Pb, and U (purchased from Ultra Scientific), were spiked into synthetic water.

Table 3.3.1 Chemical composition of synthetic waters prepared in batch 1 experiment (unit: mg/L)

Items	Surface water	Desalinated Water
Ca^{2+}	23.4	0.6
Mg^{2+}	9.9	3.6
Cl^-	28	157
SO_4^{2-}	79.2	5.5

Table 3.3.2 Detailed lists of water qualities used in batch 1 jar tests. The alkalinity and pH values were fixed at 120 mg/L as $CaCO_3$ and 7.5, respectively.

Jar number	Percentage of desalinated water in the blend (%)	[DOC] (mg/L)
1	0	0
2	0	0.5
3	0	1
4	0	2
5	20	0
6	20	0.5
7	20	1
8	20	2
9	50	0
10	50	0.5
11	50	1
12	50	2
13	80	0
14	80	0.5
15	80	1
16	80	2
17	100	0
18	100	0.5
19	100	1
20	100	2

3.3.1.3 Iron coupon jar tests

Three coupons tied with nylon lines were suspended from the jar's lid. Of these coupons, the top one was designated for morphological analyses; while the other two were designed for weigh loss measurements. Coupons hung in the center of each jar with about 3 cm distance from the walls. The lowest coupon was about 4 cm above the bottom of the

jar. The separation distance between two coupons was about 3 cm. Jar tests were conducted without continuous mixing and the jars were kept in dark to prevent algal growth.

From week three, samples were taken for soluble and total iron/inorganic contaminants concentration measurements at the end of each week-long exposure. Jars were gently shaken before taking samples. 15 ml of aliquot for total concentrations was taken with a 10 ml syringe at 5 cm below the water level. Another 15 ml of aliquot was filtered by a 0.45μm Millex filter to determine soluble concentrations. Samples were acidified with 1% ultra-pure nitric acid (purity: ≥65%) and stored in 4 ºC prior to analyses. ICP-MS analyses to determine concentration of iron and inorganic contaminants in the ambient water were performed in dynamic reaction cell (DRC) mode and standard mode.

Jar tests were conducted for eight weeks. Water was drained and exchanged with new water prepared as described above after each week-long exposure. The pH values were measured at the beginning and end of each week-long exposure.

Iron coupons were taken from jars and air-dried for one day at the end of exposure. Coupon weights were measured to determine the amount of corrosion products retained on their surfaces. The coupons were then immersed in 0.01 M phosphoric acid and then ultrasonically cleaned to remove the corrosion products from surfaces. The coupons were then rinsed with DI water, wiped with soft paper towels, air-dried for one day and then weighed to determine the weight loss after eight-week exposures. Morphologies and mineralogical phases of iron corrosion products from selected coupons were analyzed with a JEOL-7000F high-resolution SEM instrument (JEOL Corporation, Japan) and a Philips PW1830 X-ray diffractometer (Philips, Netherlands).

3.3.2 Separation of effects of chloride, sulfate and NOM on metal corrosion, accumulation and release of inorganic contaminants with/from corroded metals

Effects of anions (chloride or sulfate) and NOM on metal release, retention and release of inorganic contaminants were studied based on jar tests that employed iron, copper, lead/tin coupons and varying compositions of synthetic waters. In batch 2, inorganic contaminants were accumulated during the first eight weeks exposure. After eight weeks, selected coupons were switched to different water qualities to determine the effect of water parameters on release of accumulated inorganic contaminants.

3.3.2.1 Iron coupon preparation

Iron coupon preparation used in these experiments was the same as that described in previous section 3.3.1.1.

3.3.2.2 Copper and lead/tin coupon preparation

Copper or lead/tin coupons (10 cm length) were cut from copper wires (0.08 cm diameter) or lead/tin wires (0.16 cm diameter) and then twisted into spiral shape. Coupons were first cleaned with HPLC-grade methanol and then rinsed with distilled DI water. After cleaning, coupon surfaces were activated by dipping them in 0.01M HCl for ten seconds, rinsing with distilled DI water and then air-drying for 1 day.

3.3.2.3 Preparation of synthetic water

The chemical composition of synthetic water used in batch 2 is summarized in Table 3.3.3. Chemicals used in preparation of synthetic waters were the same as those described in section 3.3.1.2. Calcium standard (purchased from purchased from Ultra Scientific) were used to prepare jar number 1~4 and 11~14. Solutions with calcium concentrations

of $5 \cdot 10^{-4}$ M were prepared using $CaCl_2 \cdot H_2O$. Solutions with magnesium concentration of $4.11 \cdot 10^{-4}$ M was prepared from $MgCl_2$, Chloride concentrations ranging from $8.46 \cdot 10^{-4}$ to $7.05 \cdot 10^{-3}$ M were prepared from NaCl. Sulfate concentrations ranging from $4.17 \cdot 10^{-4}$ to $1.25 \cdot 10^{-3}$ M were prepared from Na_2SO_4. A total of 20 water qualities were tested in batch 2. Suwannee River Fulvic Acid (SRFA, purchased from the International Humic Substance Society) was used to represent the DOC concentrations in the synthetic water. Two DOC concentrations (0 and 1 mg/L) were tested. The alkalinity and pH values were fixed at 120 mg/L as $CaCO_3$ and 7.5, respectively. Five ppb of nine inorganic contaminants, including V, Cr, Ni, Cu, Zn, As, Cd, Pb, and U (purchased from Ultra Scientific), were spiked into synthetic water. In the case of copper or lead/tin exposures, copper or lead were not spike into synthetic water.

3.3.2.4 Iron coupon jar tests

Procedures of iron jar tests for the eight week exposures were largely the same as those described in section 3.3.1.3. After eight weeks, two coupons were removed from each jar to determine the weight loss after exposures. The other coupon was used in the release experiments. Coupons in jar number 1, 2, 3, 7, and 11 were chosen to switched to the opposite water compositions to test the effect of DOC, chloride and combined effect of DOC and chloride on the release of accumulated inorganic contaminants. The duration of release tests was eight weeks. During these tests, ambient water was drained and exchanged with new water prepared as described above without addition of inorganic contaminants after each week-long exposure. The pH and alkalinity were fixed at 7.5 and 120 mg/L as $CaCO_3$. The detail information of release experiment was listed in Table 3.3.4.

3.3.2.5 Copper and lead/tin jar tests

Two coupons per jar were suspended in 250 mL solution. Two coupons tied with nylon lines were suspended from the jar's lid. Coupons hung in the center of each jar with about 2 cm distance from the walls. The lowest coupon was about 1 cm above the bottom of the jar. The separate distance between two coupons was about 2cm. The jars were kept in dark to prevent biological activities.

The sampling procedure during exposures was as same as that in iron jar test. Since the corrosion rates of copper and lead/tin are much lower than iron, no weight loss measurement was conducted in copper and lead/tin jar tests. After eight weeks, coupons in jar number 1, 2, 3, 7, and 11 were chosen to be switched to the opposite water compositions to test the effect of DOC, chloride and combination of DOC and chloride on the release of accumulated inorganic contaminants. The detail information of release experiment was listed in Table 3.3.4.

Table 3.3.3 Chemical composition of synthetic waters prepared in batch 2 jar test. The alkalinity and pH values were fixed at 120 mg/L as $CaCO_3$ and 7.5, respectively.

Jar number	[DOC] (mg/L)	[Ca^{2+}] (mg/L)	[Mg^{2+}] (mg/L)	[Cl^-] (mg/L)	[SO_4^{2-}] (mg/L)
1	0	0	10	30	80
2	0	10	10	30	80
3	0	20	10	30	80
4	0	20	0	30	80
5	0	20	10	80	80
6	0	20	10	160	80
7	0	20	10	250	80
8	0	20	10	30	0
9	0	20	10	30	40
10	0	20	10	30	120
11	1	0	10	30	80
12	1	10	10	30	80
13	1	20	10	30	80
14	1	20	0	30	80
15	1	20	10	80	80
16	1	20	10	160	80
17	1	20	10	250	80
18	1	20	10	30	0
19	1	20	10	30	40
20	1	20	10	30	120

Table 3.3.4 Experimental conditions for release of inorganic contaminants

Coupon from jar number	Water composition	Effect
11 ([DOC]=1 mg/L)	1 ([DOC]=0 mg/L)	DOC
1 ([DOC]=0 mg/L)	11 ([DOC]=1 mg/L)	DOC
7 ([Cl^-]=250 mg/L)	3 ([Cl^-]=30 mg/L)	Chloride
3 ([Cl^-]=30 mg/L)	7 ([Cl^-]=250 mg/L)	Chloride
17 ([DOC]=1 mg/L, [Cl^-]=250 mg/L)	2 ([DOC]=0 mg/L, [Cl^-]=30 mg/L)	DOC and chloride
2 ([DOC]=0 mg/L, [Cl^-]=30 mg/L)	17 ([DOC]=1 mg/L, [Cl^-]=250 mg/L)	DOC and chloride

3.4 Assessment of Effects of NOM and Anions on Iron Corrosion

Jar tests were employed in this study to determine the effects of NOM and anions (chloride and sulfate) on iron corrosion in more detail. Altered NOM (Suwannee River NOM ozonated with different ratio of O_3/DOC) was used to explore the influence of different types of NOM on iron corrosion.

3.4.1 Iron coupon preparation

Iron coupons (2 cm length) were cut from iron stocks (0.32 cm diameter) and notched in the middle of each coupon for tying with nylon lines. The cleaning procedures were the same as those described in section 3.3.1.1.

3.4.2 Preparation of synthetic water

The chemical composition of synthetic water used in this study is summarized in Table 3.4.1. Chemicals used in preparing synthetic waters were sodium bicarbonate, sodium

chloride (Sigma-Aldrich) and anhydrous sodium sulfate (J.T. Baker). A total of 77 water qualities were tested. Suwannee River NOM (SRNOM, purchased from the International Humic Substance Society) was used to represent the DOC concentrations in the synthetic water. Three DOC concentrations (0, 1 and 2 mg/L) were tested. The alkalinity and pH values were fixed at 120 mg/L as $CaCO_3$ and 7.5, respectively.

Altered NOM was prepared by ozonation of Suwannee River NOM (SRNOM). The O_3/DOC mass ratio ranged from 0, 1 and 2. Ozonation of NOM was performed with an ozone generator (IN USA AC-2025). Ozone concentrations were determined using the standard indigo method. To prepare ozonated NOM, initial experiments were carried using a 5 mg/L (as DOC) SRNOM to which O_3/DOC mass ratios 1 or 2 were applied. The contact time was 30 min during which the ozone disappeared completely. UV absorbance of the initial and final solutions were measured to establish the correlation between changes of NOM absorbance vs. O_3/DOC mass ratios. Following that. a 300 mg/L SRNOM stock solution was prepared and continuously reacted with ozone to achieve a decreased of the UV absorbance equivalent to that established in experiments with a low DOC concentrations (5 mg/L) ozonated using O_3/DOC mass ratios of 1 or 2.

Altered NOM was characterized by high performance size exclusion chromatography (HPSEC). The HPSEC analysis employed a DIONEX Ultimate 3000 HPLC system and Ultimate 3000 diode array detector to acquire absorbance data at 200-500 nm. NOM molecules were separated with an Agilent PL aquagel-OH 30 column (300 mm * 7.5 mm, 8 μm) at flow rate of 0.5 mL/min. Ammonium bicarbonate (NH_4HCO_3) 0.01 M was used as eluent. A sample of 100 μL was injected in the column and the analysis time was 20 min.

3.4.3 Iron coupon jar tests

Three coupons tied with nylon lines were suspended into 1 L plastic jar from the jar's lid. In this study, only 600 mL of synthetic water was filled in each jar. Coupons hung in the center of each jar with about 3 cm distance from the walls. The lowest coupon was about 2 cm above the bottom of the jar. The separate distance between two coupons was about 2 cm. The jars were kept in dark.

Procedures of iron jar tests for the eight week exposures were the same as those described in preceding section 3.3.1.3. After eight weeks, two coupons were removed from each jar to determine the weight loss after exposures.

Table 3.4.1 Chemical composition of synthetic waters in iron jar test. The alkalinity and pH values were fixed at 120 mg/L as $CaCO_3$ and 7.5, respectively.

Jar number	[DOC] (mg/L)	O_3/DOC ratio	[Cl^-] (mg/L)	[SO_4^{2-}] (mg/L)	Effect
1	0	0	0	0	DOC
2	1	0	0	0	
3	2	0	0	0	
4	1	1	0	0	Altered DOC
5	1	2	0	0	
6	2	1	0	0	
7	2	2	0	0	
8	0	0	40	0	Chloride
9	0	0	80	0	
10	0	0	120	0	
11	0	0	160	0	
12	0	0	200	0	
13	1	0	40	0	
14	1	0	80	0	
15	1	0	120	0	
16	1	0	160	0	
17	1	0	200	0	
18	2	0	40	0	
19	2	0	80	0	
20	2	0	120	0	
21	2	0	160	0	
22	2	0	200	0	
23	1	1	40	0	Cl^- + altered DOC
24	1	1	80	0	
25	1	1	120	0	
26	1	1	160	0	
27	1	1	200	0	
28	1	2	40	0	
29	1	2	80	0	
30	1	2	120	0	
31	1	2	160	0	
32	1	2	200	0	
33	2	1	40	0	
34	2	1	80	0	
35	2	1	120	0	
36	2	1	160	0	
37	2	1	200	0	
38	2	2	40	0	
39	2	2	80	0	
40	2	2	120	0	
41	2	2	160	0	
42	2	2	200	0	

43	0	0	0	40	Sulfate
44	0	0	0	80	
45	0	0	0	120	
46	0	0	0	160	
47	0	0	0	200	
48	1	0	0	40	
49	1	0	0	80	
50	1	0	0	120	
51	1	0	0	160	
52	1	0	0	200	
53	2	0	0	40	
54	2	0	0	80	
55	2	0	0	120	
56	2	0	0	160	
57	2	0	0	200	
58	1	1	0	40	SO_4^{2-} + altered DOC
59	1	1	0	80	
60	1	1	0	120	
61	1	1	0	160	
62	1	1	0	200	
63	1	2	0	40	
64	1	2	0	80	
65	1	2	0	120	
66	1	2	0	160	
67	1	2	0	200	
68	2	1	0	40	
69	2	1	0	80	
70	2	1	0	120	
71	2	1	0	160	
72	2	1	0	200	
73	2	2	0	40	
74	2	2	0	80	
75	2	2	0	120	
76	2	2	0	160	
77	2	2	0	200	

Chapter 4 Characterization of elemental and structural composition of corrosion scales and deposits formed in drinking water distribution systems

Many trace inorganic contaminants (e.g., lead, arsenic, nickel, vanadium and uranium) can accumulate on the surface of or be occluded within corrosion scales formed in drinking water distribution systems (DWDSs). However, few data are available on the actual concentrations of these contaminants beyond system entry-points. This study was conducted to determine the occurrence levels and patterns of 10 common matrix elements and 11 trace inorganic contaminants in DWDSs. While the amount of information concerning the properties of corrosion scales, deposits and colloidal particles in DWDSs is remarkable (Tuovinen et al., 1980; Benjamin et al., 1996; Sarin et al., 2001; Teng et al., 2008; Gerke et al., 2008; Borch et al., 2008; Barkatt et al., 2009), there is a need to provide a more complete characterization of their physico-chemical properties. This information can provide valuable insight on factors that influence and control the accumulation and co-occurrence of regulated trace inorganic contaminants. Thus, structural compositions of extracted pipe solids and hydraulically-mobile deposits originating from representative DWDSs were also investigated.

4.1 Treated water quality

Treated water conditions were ascertained through a combination of "snapshot" site-specific distribution system sampling (at locations where solid samples were obtained) and utility-provided records of entry-point and system monitoring results (Friedman et al., 2010). The compilation of distribution system water quality observations for each utility and sample site is provided in Table 4.1 and Table 4.2. It should be noted that the water quality conditions reported here reflect only the data obtained from either the water sampling performed specifically for this study or utility-provided water quality data representing entry-point sampling.

Of the 20 utility participants, 17 utility participants had Fe concentrations at or above 0.06 mg/L (i.e., 20% of the secondary MCL) in entry-point and/or distribution system water samples. The median iron concentration in the treated water at sampling locations was 0.25 mg/L. A total of 11 utility participants reported and/or were found to have manganese present at concentrations exceeding 0.01 mg/L (i.e., 20% of the secondary MCL) in entry-point and/or distribution system water samples; however, the median Mn concentration in treated water at sampling locations was only 0.5 μg/L. Six utilities had dedicated iron and/or manganese removal processes (e.g., greensand filtration, permanganate-enhanced direct filtration, hydrous manganese oxide (HMO) filtration process) at problem sources. Five utilities used polyphosphate (either alone or as part of an ortho/poly blend) to sequester the soluble, reduced forms of these metals and/or to prevent excessive calcite precipitation.

All utility participants, except in cases mentioned below, were in compliance with applicable inorganic primary drinking water regulations at the time of their participation.

Water samples from utilities SA and WDB had a lead concentration above the U.S. EPA lead action level (AL) of 15 µg/L. The highest lead level measured was 73 µg/L in the water sampled from utility SA. Utility WDB reported an average uranium concentration above the U.S. EPA uranium maximum contaminant level (MCL) of 30 µg/L, although this MCL was not in effect at the time. It should be noted that the water qualities reported here reflect only the data obtained from either the water sampling conducted specifically for this study or utility-provided water quality reports representing entry-point sampling.

4.2 Morphological examination of corrosion scales

The morphological properties of selected samples of corrosion scales were examined using SEM/EDS and XRD. The examined samples typically lacked morphologically significant features (Figure 4.1). EDS analysis indicated that most frequently detected elements found on the surfaces were Fe, O, C, Si, S and Ca.

XRD showed that goethite (α-FeOOH), magnetite (Fe_3O_4) and siderite ($FeCO_3$) were major phases present in the samples (Table 4.3). This observation was in accordance with the findings of Sarin et al., 2001 and Barkatt et al., 2009. Calcite $CaCO_3$ was identified in the hydrant flush samples, which may be indicative of its precipitation from the bulk distributed water. Quartz SiO_2 was also frequently found. Its presence may be attributed to carryover from the source water or as treatment breakthrough. Hydroxyapatite $Ca_5(PO_4)_3(OH)$ was observed in cases where the utility applied orthophosphate or phosphate blend to control corrosion. It should be noted that while the possibility of the presence of some artifacts caused by sample processing (partial conversion of Fe(II) to Fe(III) caused by drying, Sarin et al., 2001) cannot be ruled out, XRD characterization of

Table 4.1 Distribution system water quality - general water quality parameters and common matrix elements

Utility Identifier	Associated Samples	Data Source	pH	Temp (°C)	Alkalinity (mg/L $CaCO_3$)	Disinfectant Residual (mg/L)		Al (µg/L)	Ca (mg/L)	Fe (mg/L)	Mg (mg/L)	Mn (µg/L)	Si (mg/L)	S (mg/L)	P[(b)] (mg/L)	Zn (µg/L)
W	A-H	Sample	7.7	24	147	0.60	Comb.	61	65	0.27	22	0.04	4	161	0.45	3.1
CL	A, B	Sample	8.2	18	238	0.68	Free	0.5	52	0.14	24	0.06	4	19	0.40	2.4
CL	C	Sample	8.5	20	244	0.83	Free	0.2	52	0.15	29	0.03	3	11	0.57	28.1
CL	D, E	Survey	NA[(a)]	NA	NA	NA	Free	NA	NA	NA	NA	NA	NA	NA	NA	NA
CL	F	Sample	8.3	19	233	0.42	Free	1.1	55	0.15	28	0.4	4	15	0.58	< 0.06
CL	G	Sample	7.9	19	235	0.68	Free	0.7	60	0.18	25	0.1	4	33	0.51	11.1
SA	A	Sample	8.1	19	65	0.02	Free	5.1	19	0.05	4	<0.01	14	3	0.25	23.0
SA	B, C	Sample	7.4	17	95	0.04	Free	0.3	10	0.03	6	0.1	15	5	0.06	9.8
SA	D	Sample	8.0	16	48	0.01	Free	1.7	9	0.04	4	1.2	5	8	0.07	< 0.06
SA	E	Sample	8.1	18	68	0.07	Free	1.0	10	0.06	3	0.3	15	2	0.3	< 0.06
CH	A	Sample	8.0	19	64	0.12	Free	2.1	23	0.22	5	0.3	3	7	0.01	3.6
RW	A, B	Sample	7.1	15	76	0.51	Free	8.4	17	0.24	7	0.5	12	4	0.12	3.9
IN	A-D	Sample	7.4	20	204	0.65	Free	4.4	64	0.28	30	6.6	3	24	0.13	2.3
CC	A-F	Sample	7.6	14	177	0.81	Free	<0.14	45	0.28	14	3.9	10	25	0.46	1.6
DN	A-B	Survey	7.8	12	49	1.35	Comb.	30	26	< 0.05	NA	< 6.0	NA	NA	NA	< 5.0
CA	A-B	Sample	7.3	18	135	1.90	Free	0.1	44	0.27	15	0.2	9	30	0.37	158
PC	A-B	Sample	7.6	2	136	0.3	Free	59	106	12.1	28	0.02	5	69	0.04	97.3
WDB	A-B	Survey	7.6	NA	NA	NA	Free	NA	19	< 0.03	NA	50.0	NA	NA	NA	10.0
WA	A-D	Sample	7.2	NA	NA	< 0.1	Free	507	12	0.03	3	11.1	7	12	0.01	6.0
B	A, B, D	Sample	8.1	23	119	2.14	Comb.	145	27	1.4	5	0.1	6	20	<0.002	1.0
B	C	Sample	7.8	18	115	1.84	Comb.	134	29	2.0	9	0.8	6	27	0.09	22.3
G	A	Sample	7.9	22	277	0.6	Free	22	2	<0.001	1	0.2	3	2	0.01	<0.06
G	B	Sample	NA	NA	276	NA	Free	3.1	2	<0.001	1	0.1	3	2	0.01	<0.06
AZ	A	Sample	7.3	31	267	0.3	Free	<0.14	310	0.96	93	29.9	10	462	0.02	4.4
BC	A, B	Sample	7.2	37	150	0.2	Free	<0.14	155	0.45	40	0.1	13	144	0.01	47.2
J	A-D, G-J	Survey	7.6	NA	289	NA	Comb.	NA	91	1.22	38	55.4	NA	NA	NA	18
J	E, F	Survey	7.6	NA	280	NA	Comb.	NA	59	0.21	20	7.8	4.1	NA	NA	< 20
NC	A	Sample	7.2	20	278	0.13	Free	<0.14	60	0.16	33	30.0	3	12	0.31	<0.06
ST	A	Sample	7.4	28	265	0.71	Free	0.6	26	0.07	16	<0.01	4	9	0.12	<0.06
ST	B	Sample	7.4	24	236	0.97	Free	0.4	52	0.15	35	<0.01	4	9	0.01	<0.06
ST	C	Sample	7.5	21	232	1.04	Free	<0.14	43	0.11	34	<0.01	5	9	0.01	<0.06
ST	D	Sample	7.4	26	261	0.58	Free	0.5	50	0.14	33	1.9	4	9	0.06	<0.06
K	A-D	Survey	8.0	NA	268	3.50	Comb.	NA	63	0.02	28	9.0	6.9	NA	NA	NA

[(a)]NA = no data available. [(b)]Phosphorus concentrations may have higher concentrations than the actual values due to significant matrix effects.
Source: Friedman et al, 2010. ©2010 Water Research Foundation. Reprinted with permission.

Table 4.2 Distribution system water quality – trace inorganic elements

Utility Identifier	Associated Samples	Data Source	Ba (mg/L)	Pb (µg/L)	Ni (µg/L)	V (µg/L)	As (µg/L)	Cr (µg/L)	U (µg/L)	Cd (µg/L)	Sb (µg/L)	Se (µg/L)	Tl (µg/L)
W	A-H	Sample	0.02	<0.003	3.65	0.23	0.19	0.58	0.13	<0.003	<0.006	0.43	0.004
CL	A, B	Sample	0.05	0.03	1.66	0.64	0.35	0.18	0.26	0.005	<0.006	0.33	<0.003
CL	C	Sample	0.09	0.02	0.17	0.65	1.70	0.38	0.17	0.020	0.011	0.23	0.003
CL	D, E	Survey	NA[(a)]	NA	NA	NA	NA	NA	NA	NA	NA	NA	NA
CL	F	Sample	0.08	0.04	0.28	0.72	1.40	0.58	0.19	0.005	0.035	0.34	0.004
CL	G	Sample	0.06	0.03	1.88	0.68	0.53	0.18	0.31	0.005	0.010	0.79	<0.003
SA	A	Sample	0.01	0.02	0.36	0.89	5.18	<0.05	0.02	0.003	0.022	0.12	0.004
SA	B, C	Sample	0.003	0.79	0.48	1.35	0.75	1.00	0.04	0.013	0.028	0.23	0.003
SA	D	Sample	0.005	73.0	0.37	2.02	4.95	0.49	0.39	0.008	0.535	0.14	0.020
SA	E	Sample	0.002	0.09	0.34	0.65	4.66	0.73	0.01	0.007	0.025	<0.009	0.008
CH	A	Sample	0.02	0.13	0.23	0.95	0.61	0.25	0.47	0.012	0.122	0.18	0.004
RW	A, B	Sample	0.005	0.01	<0.05	3.42	2.20	0.39	0.08	0.007	0.049	0.35	0.020
IN	A-D	Sample	0.11	0.03	1.09	<0.08	1.45	1.05	0.45	0.023	0.087	0.45	0.003
CC	A-F	Sample	0.07	0.06	0.36	<0.08	0.50	0.57	1.25	0.004	0.012	0.64	0.003
DN	A-B	Survey	0.04	<1.0	<0.8	<1.0	<1.0	<2.0	<0.30	<1.0	<0.5	<3.0	NA
CA	A-B	Sample	0.05	0.03	1.35	<0.08	0.12	0.70	0.42	0.31	0.015	0.83	<0.003
PC	A-B	Sample	0.07	0.06	0.91	0.23	4.24	1.11	3.25	0.306	4.21	1.72	18.1
WDB	A-B	Survey	<0.5	25.0	NA	NA	0.70	1.10	110	<0.5	<0.5	<1.0	<0.5
WA	A-D	Sample	0.03	0.08	0.19	0.12	<0.12	0.64	0.01	<0.003	<0.006	0.24	0.007
B	A, B, D	Sample	0.07	0.06	0.24	0.69	1.43	0.58	0.90	0.024	0.065	0.81	0.013
B	C	Sample	0.08	0.07	0.39	1.65	1.61	0.60	1.72	0.036	0.129	1.03	0.010
G	A	Sample	0.57	0.07	0.36	0.88	0.70	0.62	0.01	<0.003	<0.006	0.23	0.003
G	B	Sample	0.59	0.03	0.07	1.01	1.60	0.77	0.01	<0.003	<0.006	0.27	0.004
AZ	A	Sample	0.03	0.17	4.38	1.21	0.89	4.53	8.30	0.019	0.051	1.09	<0.003
BC	A, B	Sample	0.05	0.78	1.45	1.21	3.60	4.24	3.29	0.023	0.072	8.32	<0.003
J	A-D, G-J	Survey	0.06	0.02	0.12	0.08	2.0	0.54	0.12	<2.0	NA	4.5	NA
J	E, F	Survey	0.07	0.02	1.2	0.08	2.0	1.00	0.24	<2.0	NA	9.1	NA
NC	A	Sample	0.03	0.04	0.35	0.85	1.10	0.91	0.01	<0.003	0.010	0.19	0.003
ST	A	Sample	0.06	0.05	0.68	0.64	0.35	3.31	0.16	0.005	0.015	0.63	<0.003
ST	B	Sample	0.11	0.02	1.03	0.62	0.13	2.69	0.15	0.014	0.007	0.12	<0.003
ST	C	Sample	0.10	0.02	0.86	0.44	0.06	2.43	0.14	<0.003	0.006	0.13	<0.003
ST	D	Sample	0.10	0.03	1.49	0.91	0.20	0.36	0.21	0.04	0.107	0.2	0.009
K	A-D	Survey	0.03	<1.0	<50	NA	<10	<10	NA	<1.0	<2.0	<10	<1.0

[(a)]NA = no data available.

Source: Friedman et al, 2010. ©2010 Water Research Foundation. Reprinted with permission.

the samples used in this study provides an important insight into the nature of prevalent solid phases formed in drinking water distribution systems (Borch et al., 2008; Gerke et al., 2008).

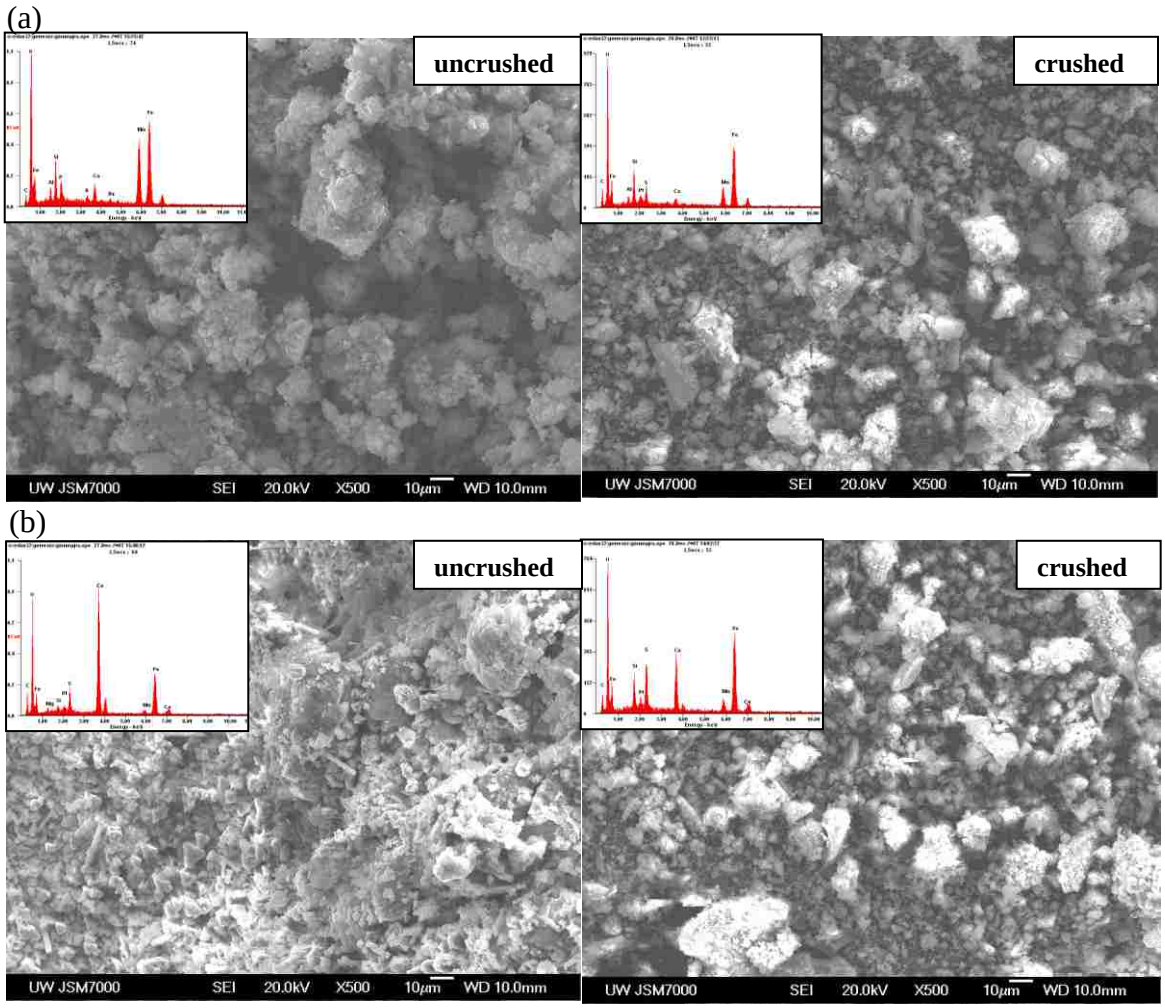

Figure 4.1 SEM morphology (mag. X500) spectra of uncrushed and crushed samples of (a) CC-A (b) J-B. Insets show EDS spectra of the entire surface of samples.

Table 4.3 Crystal phase identification of pipe deposits

Pipe specimen sample		
Sample ID	Pipe material	X-ray diffraction results
CC-A	cast iron	magnetite, quartz
CC-D	cast iron	siderite, quartz, hydroxyapatite
CH-A	steel	goethite, magnetite, quartz
PC-A	galvanized iron	goethite, magnetite, siderite, troilite
PC-B	galvanized iron	goethite, siderite
RW-A	galvanized iron	magnetite, troilite
RW-B	galvanized iron	magnetite, troilite
Hydrant flush samples		
Sample ID	Pipe material	X-ray diffraction results
J-B	cast iron	goethite, siderite, calcite, hydroxyapatite
J-E	cast iron	calcite, dolomite, quartz
J-J	cast iron	goethite, magnetite, ferrihydrite, calcite, quartz

4.3 Deposit composition-common matrix elements

The elemental composition of DWDS samples is discussed below in the context of the occurrence of the common matrix elements, notably iron, sulfur, total organic carbon (TOC), calcium, inorganic carbon (TIC), phosphorus, manganese, magnesium, aluminum and zinc. This combination of major matrix components was determined based on the approach developed in our recently completed study undertaken under the auspices of Water Research Federation (Friedman et al., 2010). The data for silicon (Si) will not be

considered since that element was not necessarily dissolved during the digestion procedure employed in this work.

Since statistical analysis of the data showed that the concentrations of these elements were not normally distributed (Friedman et al., 2010), the results at selected percentiles (e.g., median) are emphasized over average values and standard deviations. Table 4.4 provides a statistical summary of the concentrations of common elements constituting the solids. In most cases, the reporting units are micrograms of element per gram of deposit (µg/g), or parts-per-million. When the median result for a given element exceeds 10,000 µg/g, the results are presented as weight percent (wt%). For reference, 10,000 µg/g is equivalent to 1.0 wt%.

61% and 83% of samples processed in this study were pipe specimens and hydrant flush solids, respectively, formed on unlined cast iron. Thus, the data reported here are more representative of drinking water distribution systems in which unlined cast iron pipes predominate over other pipe materials.

Table 4.4 Statistical summary of elemental occurrence in deposit samples

Common Element	No. of Samples	Frequency	Average Result	Standard Deviation	Minimum Result	10th Percentile	Median Result	90th Percentile	Maximum Result
Al (µg/g)	58	58	1630	3150	32	120	620	3400	20300
Ca (µg/g)	58	56	29300	56500	<0.33	420	7700	87500	252700
Fe (wt%)	58	58	28.5	11.8	0.1	11.8	31.7	40.6	46.8
Mg (µg/g)	58	58	3190	6860	49	110	640	6950	37900
Mn (µg/g)	58	58	7320	31200	100	290	790	7000	232500
S (wt%)	48	48	1.4	1.7	0.05	0.15	1.1	2.8	10.9
Si (µg/g)	58	48	167	234	<0.22	<0.22	90	390	1330
P (µg/g)	58	58	2250	2520	100	450	1400	4300	12600
Zn (µg/g)	58	58	1370	3980	3.2	24	230	1900	19700
TIC (µg/g)	36	36	13300	23200	0.01	50	2500	45800	108500
TOC (µg/g)	36	36	19000	34100	0.01	4140	9800	32600	206700

4.3.1 Iron

Iron (Fe) was the most concentrated inorganic constituent in practically all samples. Thirty three of the 35 pipe specimens that contained enough mass for processing were composed of unlined iron or steel, and 19 of 23 hydrant flush samples that contained enough mass were obtained from unlined iron pipes. The median Fe concentration was 31.7 wt% and the 10^{th} and 90^{th} percentile Fe concentration were 11.8 wt% and 40.6 wt%, respectively. This was in agreement with the XRD data confirming the prominence of goethite α-FeOOH, magnetite Fe_3O_4, siderite $FeCO_3$ and in some cases troilite FeS. Figure 4.2(a) illustrates the cumulative iron occurrence profiles for all deposit samples and the different sample types (pipe specimens or hydrant flush solids). The Fe percentile

profiles for pipe specimens and hydrant flush solids were similar, with median Fe concentrations of 32.7 wt% and 28.4 wt%, respectively.

4.3.2 Sulfur

Sulfur (S) was the second-most prevalent inorganic constituent in the solids, with a median concentration of 11,100 μg/g (1.1 wt%). The 10^{th} and 90^{th} percentile S concentrations were 0.15 wt% and 2.8 wt%, respectively. Sulfur occurrence in the scales is likely to be due to the formation of troilite, a common under-layer component of iron corrosion scale (Benjamin et al., 1996). The XRD pattern for several samples (e.g., J-E, PC-A, RW-B) confirmed its presence. Figure 4.3(a) illustrates the cumulative sulfur occurrence profiles for all sample types. The profiles for pipe specimens and hydrant flush solids are very similar. The median S concentrations for pipe specimens and hydrant flush solids are 1.0 wt% and 1.1 wt%, respectively.

4.3.3 Organic carbon

The median concentration of organic carbon (TOC) was 9,800 μg/g (0.98 wt%), while its 10^{th} and 90^{th} percentiles were 0.4 wt% and 3.3 wt%, respectively. It was the third most common component of the corrosion scales. The occurrence of organic carbon may be a result of autochthonous process (biofilm growth) and sorption of NOM present in source waters. Figure 4.3(b) illustrates the cumulative organic carbon occurrence profiles for all sample types. TOC levels in hydrant flush solids were consistently higher that those in the pipe specimens, with median TOC concentrations of 1.7 wt% and 0.7 wt%, respectively. The observed dissimilarity between these two sample types could be ascribed to various factors. For instance, hydrant flush solids can be hypothesized to

retain more sorbed/occluded NOM or have higher rate of microbiological processes in them. It can be also hypothesized that some loss of labile organic carbon may have occurred in boneyard samples that were exposed to air for prolonged periods of time.

4.4.4 Calcium

Calcium (Ca) was the fourth most common element, with a median concentration of 7,700 μg/g (0.8 wt%). The 10^{th} and 90^{th} percentile Ca concentrations were 420 μg/g and 8.8 wt%, respectively. Calcium occurrence in deposits is likely to take place via the deposition of calcite, dolomite $CaMg(CO_3)_2$, and hydroxyapatite $Ca_5(PO_4)_3OH$. Each of these minerals was identified in XRD analyses. Hydroxyapatite was observed only in the samples from utilities that applied phosphate as part of their treatment process. While calcite was found in samples associated with "hard" waters, soluble Ca^{2+} and its complexes can associate with metal-oxide substrates due to surface adsorption (Ali et al., 1996; Weng et al., 2005). This may explain calcium occurrence in cases where the water was under-saturated with respect to calcium-based mineral phases. Figure 4.2(b) illustrates the cumulative calcium occurrence profiles for all deposit samples and the different sample types. The profiles for pipe specimens and hydrant flush solids are similar, with the median Ca concentrations 0.9 wt% and 0.74 wt%, respectively.

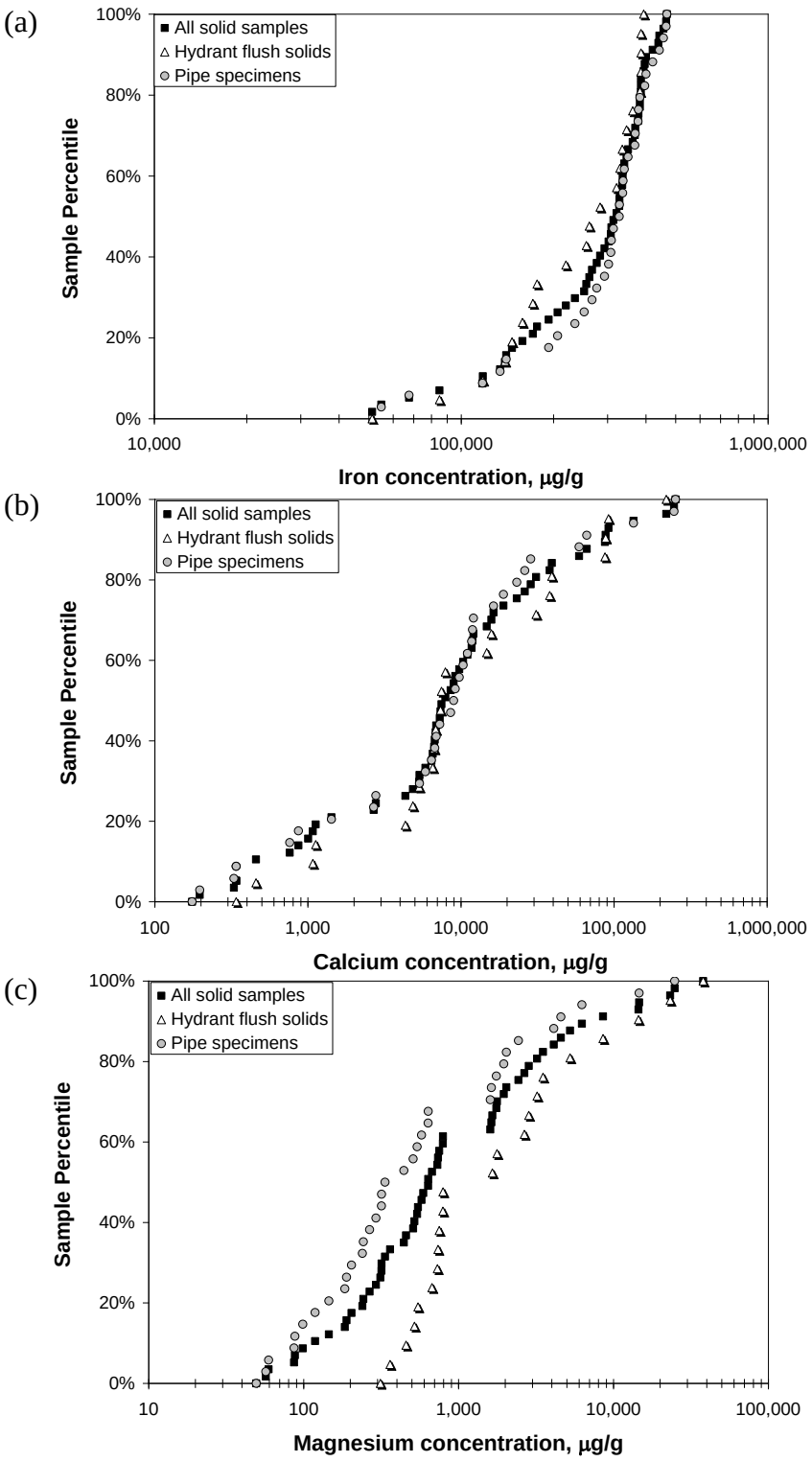

Figure 4.2 Cumulative occurrence profiles for (a) iron, (b) calcium, and (c) magnesium in corrosion scales and deposits.

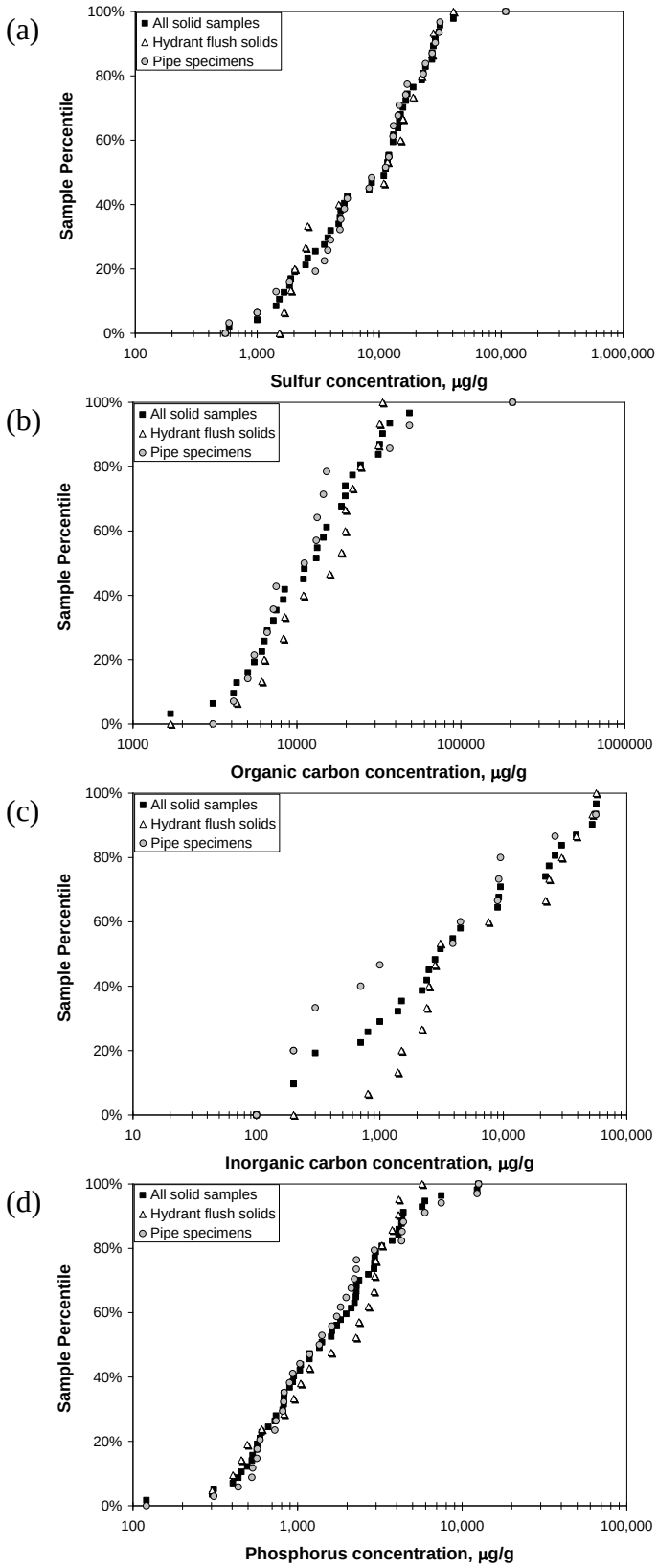

Figure 4.3 Cumulative occurrence profiles for (a) sulfur, (b) TOC, (c) TIC, and (d) phosphorus in corrosion scales and deposits.

4.3.5 Inorganic carbon

Inorganic carbon (TIC) was the fifth most prevalent element, with a median concentration of 2,500 µg/g. The 10^{th} and 90^{th} percentile TIC concentrations were 50 µg/g and 4.6 wt%, respectively. The occurrence of inorganic carbon in deposits is due to the presence of siderite, calcite, dolomite (Table 4.3) and surface adsorption/co-precipitation reactions involving bicarbonate and carbonate species. XRD patterns showed that the aforementioned mineral phases were present in several samples. Figure 4.3(c) illustrates the cumulative TIC occurrence profiles for all deposit samples and the different sample types. The Ca levels in hydrant flush solids were higher than those in pipe specimens across the entire range. The median TIC concentrations for pipe specimens and hydrant flush solids are 500 µg/g and 3,000 µg/g, respectively.

4.3.6 Phosphorus

Phosphorus (P) was the sixth most prevalent element, with a median concentration of 1,400 µg/g. The 10^{th} and 90^{th} percentile phosphorus concentrations were 450 µg/g and 4,300 µg/g (0.43 wt%), respectively. Phosphorus occurrence in the corrosion scale can be associated with the formation of hydroxyapatite $Ca_5(PO_4)_3OH$ (Table 4.3), adsorption of orthophosphate onto various mineral surfaces, and phosphorus uptake/accumulation in biofilm and cellular material.

The accumulation of phosphorus in the scales requires that it be present in the treated water. The total phosphorus concentration in water samples collected for this study ranged from non-detect (MQL of 0.001 mg/L) to 0.6 mg/L, with a median of 0.1 mg/L. Seven of the 20 utility participants reported adding phosphate-based chemicals in their treatment process. Several other utility participants have moderate levels of phosphorus

(of unknown speciation) originating in one or more of their sources of supply. Despite that, little correlation between phosphorus levels in water and solids was observed. Figure 4.3(d) illustrates the cumulative phosphorus occurrence. The profiles for pipe specimens and hydrant flush solids are similar. The median phosphorus concentrations for pipe specimens and hydrant flush solids are 1,360 μg/g and 1,600 μg/g, respectively.

4.3.7 Manganese

Manganese (Mn) was the seventh most abundant element found in the samples, with a median concentration of 790 μg/g. The 10^{th} and 90^{th} percentile Mn concentrations were 290 μg/g and 7,000 μg/g (0.7 wt%), respectively. Manganese occurrence in deposits is likely to be due to the formation and deposition of manganese oxyhydroxide solids starting from the manganese found in the treated water. Figure 4.4(a) illustrates the cumulative manganese occurrence profiles for all deposit samples and the different sample types. The results for pipe specimens were higher in manganese than hydrant flush solids. The median manganese concentrations for pipe specimens and hydrant flush solids are 940 μg/g and 610 μg/g, respectively.

4.3.8 Magnesium

Magnesium (Mg) was the eighth most abundant element found in deposit samples, with a median concentration of 640 μg/g. The 10^{th} and 90^{th} percentile Mg concentrations were 110 μg/g and 6,950 μg/g (0.7 wt%), respectively. Magnesium occurrence in deposits is expected to be due to the formation and deposition of minerals such as dolomite (Table 4.3). Figure 4.2(c) illustrates the cumulative magnesium occurrence profiles. The results

for hydrant flush solids were higher than pipe specimens, with the median Mg concentrations 800 µg/g and 340 µg/g, respectively.

4.3.9 Aluminum

Aluminum (Al) was the ninth most common element found in deposit samples, with a median concentration of 620 µg/g. The 10th and 90th percentile aluminum concentrations were 120 µg/g and 3,400 µg/g, respectively. Aluminum presence in deposits can be due to the deposition of alumina Al_2O_3, gibbsite $Al(OH)_3$, precipitation of amorphous aluminum hydroxide, and formation of aluminosilicates. Surface adsorption/co-precipitation reactions involving free Al^{3+} and its complexes may also account for its occurrence. Sources of aluminum may include the treated water, either due to natural occurrence in source water and/or the application and treatment "breakthrough" of aluminum-based coagulants. Figure 4.4(b) illustrates the cumulative aluminum occurrence profiles for all samples. The profiles for pipe specimens and hydrant flush solids are dissimilar, with the Al levels in pipe specimens being higher across the entire range. The median Al concentrations for pipe specimens and hydrant flush solids are 640 µg/g and 555 µg/g, respectively.

4.3.10 Zinc

Zinc (Zn) was the tenth most abundant element found in deposit samples, with a median concentration of 230 µg/g. The 10th and 90th percentile zinc concentrations were 24 µg/g and 1,900 µg/g, respectively. Sources of zinc may include the treated water, either due to natural occurrence in source water, applications of zinc orthophosphate and "inner" sources such as its presence as in galvanized pipe and as a component in copper-based

alloys. Internal corrosion of galvanized iron piping appears to be the primary source of zinc in many samples. Indeed, comparison between cast iron and galvanized iron specimens showed that Zn concentration were much higher in the latter case, with median Zn concentrations being 185 μg/g and 8422.5 μg/g. Figure 4.4(c) illustrates the cumulative Zn occurrence profiles for all deposit samples and the different sample types. The profiles for pipe specimens and hydrant flush solids are dissimilar, with the results for pipe specimens being higher across the entire range. The median zinc concentrations for pipe specimens and hydrant flush solids are 290 μg/g and 110 μg/g, respectively.

4.4 Occurrence of trace inorganic elements

The occurrence of eleven trace inorganic contaminants (i.e., barium, lead, nickel, vanadium, arsenic, chromium, uranium, antimony, cadmium, selenium, and thallium) in DWDS solids is discussed below. Because statistical analysis of the data showed that the concentrations of the target elements were not normally distributed (Friedman et al, 2010), the results at selected percentiles (e.g., median) are emphasized over average values and standard deviations. Major aspects of the occurrence for each target element are presented in Table 4.5.

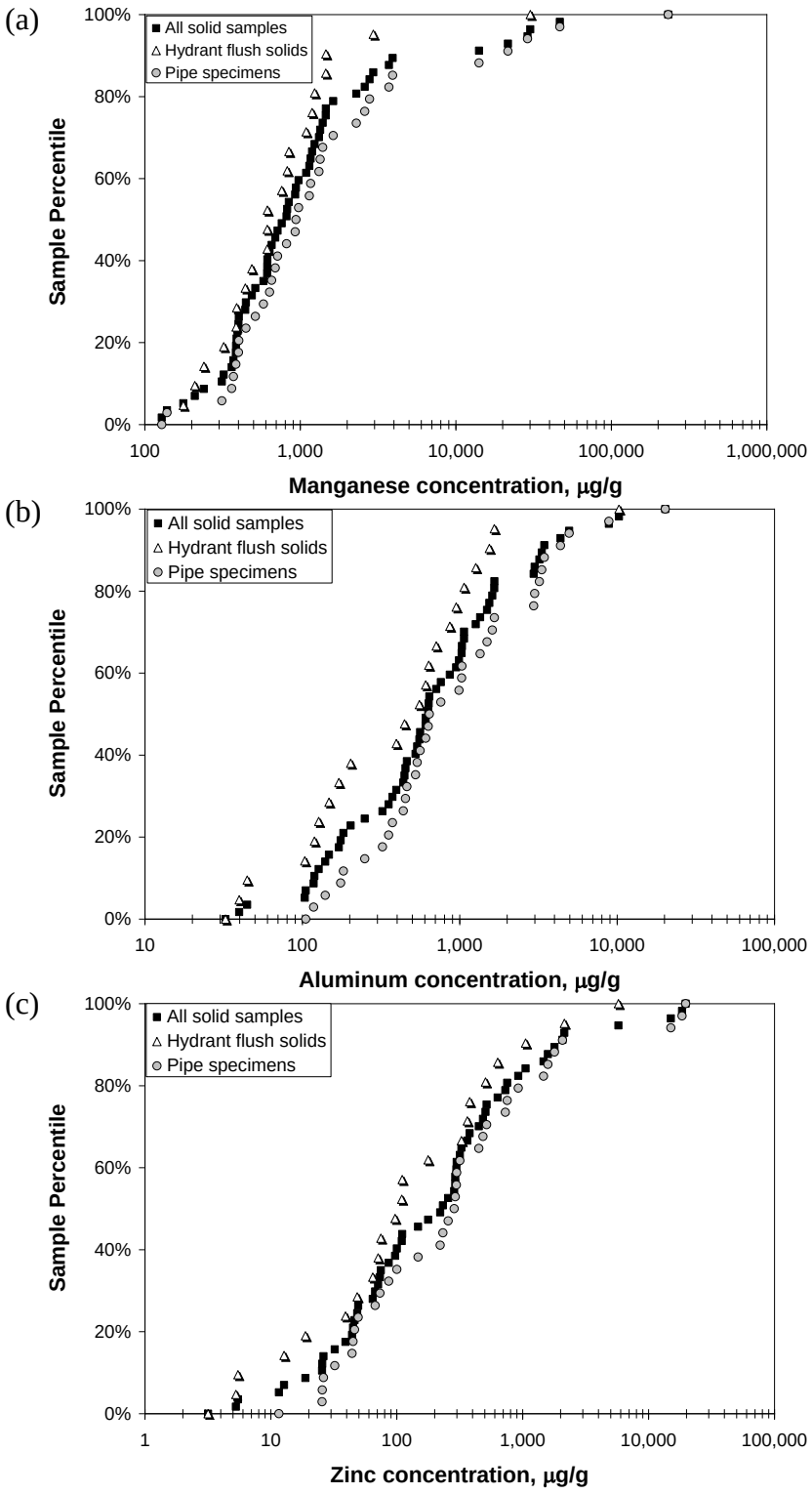

Figure 4.4 Cumulative occurrence profiles for (a) manganese, (b) aluminum, and (c) zinc in corrosion scales and deposits.

4.4.1 Barium

Barium was the most prominent trace element found in deposit samples, with a median concentration of 94 µg/g. The 10^{th} and 90^{th} percentile Ba concentrations were 33 µg/g and 450 µg/g, respectively. Figure 4.5(a) illustrates the cumulative barium occurrence profiles for each sample type. The profiles for pipe specimens and hydrant flush solids are very similar. The median Ba concentrations for pipe specimens and hydrant flush solids are 88 µg/g and 104 µg/g, respectively. However, care must be taken when comparing concentrations observed in pipe specimen vs. hydrant solids since the sample pools were not paired. As described in Friedman et al, 2010, not all participating utilities provided both pipe solids and hydrant solids, and those that did provide both types of solids did not necessarily collect them from the same stretch of pipe.

The correlation between barium occurrence in DWDS solids and its water column concentrations was poor. On the other hand, a notable correlation between barium and manganese concentrations in DWDS solids was observed (R^2=0.64). The presence of this correlation is in accord with the data of prior research showing that manganese oxides tend to interact with barium considerably stronger than iron oxides (Sugiyama et al, 1992; Murray 1975). This can indicate that manganese oxides formed in corrosion scales may effectively adsorb barium and the co-occurrence of Mn and Ba may play a critical role in barium retention.

4.4.2 Lead

Lead was the second most prominent trace element found in DWDS solids, with a median concentration of 20 µg/g. The 10^{th} and 90^{th} percentile Pb concentrations were 2.5 µg/g and 850 µg/g, respectively. Figure 4.5(b) illustrates the cumulative lead occurrence

profiles for each sample type. The profiles for pipe specimens and hydrant flush solids are highly dissimilar, with the Pb levels found in hydrant flush solids being higher across the entire range. The median Pb concentrations for pipe specimens and hydrant flush solids are 8 µg/g and 47 µg/g, respectively.

There was no correlation between lead levels in solid samples versus its water concentrations. A high correlation (R^2= 0.9) of lead versus zinc content in solids originating from the four galvanized iron pipes indicated that the pipe material may be a source of lead. 58% of the samples in the "high" lead group (68^{th} to 100^{th} percentile) were hydrant flush solids. This implies that particulate release events may be associated with highly prominent lead loads. A similar observation was made recently by McFadden et al, 2009. Other pipe components, such as lead-containing solders, can also contribute the accumulation of lead.

Table 4.5 Statistical summary of occurrence of trace inorganic contaminants in deposit samples

Trace Element	No. of Samples	Frequency	Average Result	Standard Deviation	Minimum Result	10th Percentile	Median Result	90th Percentile	Maximum Result
Ba (µg/g)	58	58	219	398	11.5	33	94	450	2,400
Pb (µg/g)	58	58	366	1,190	0.84	2.5	20	850	7,200
Ni (µg/g)	58	58	69	117	0.11	2.4	15	260	484
V (µg/g)	58	56	38	81	<0.007	0.54	14	61	451
As (µg/g)	58	58	81	185	0.01	0.67	13	209	940
Cr (µg/g)	58	58	31	52	0.53	1.4	7.3	118	251
U (µg/g)	58	58	5.1	15	0.03	0.14	1	16	113
Sb (µg/g)	58	58	0.55	1.2	0.02	0.05	0.14	0.86	6.5
Cd (µg/g)	58	58	2.0	5.8	0.005	0.06	0.26	2.8	34
Se (µg/g)	58	55	0.45	1.2	<0.0009	0.01	0.1	1.1	8.4
Tl (µg/g)	58	58	3.0	15	0.002	0.01	0.06	0.51	84

Source: Friedman et al, 2010. ©2010 Water Research Foundation. Reprinted with permission.

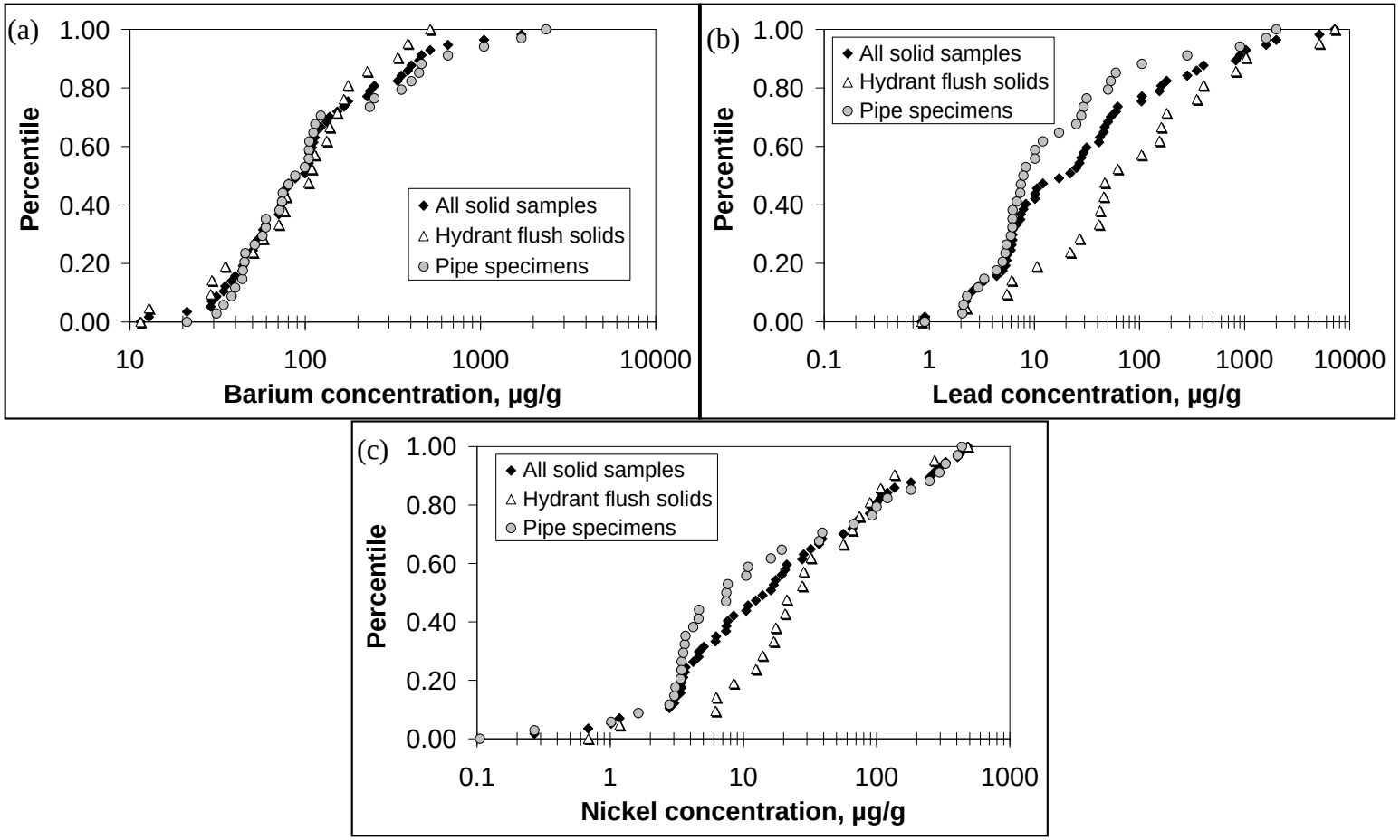

Figure 4.5 Cumulative occurrence profiles for (a) barium, (b) lead, and (c) nickel in deposit samples.
Source: Friedman et al, 2010. ©2010 Water Research Foundation. Reprinted with permission.

4.4.3 Nickel

Nickel was the third highest concentration trace element found in deposit samples, with a median concentration of 15 μg/g and 10^{th} and 90^{th} percentile concentrations of 2.4 μg/g and 260 μg/g, respectively. The cumulative nickel occurrence profiles for pipe specimens and hydrant flush solids were dissimilar, with the Ni levels in hydrant flush solids being higher across the entire range (Figure 4.5(c)). The median Ni concentrations for pipe specimens and hydrant flush solids were 7.5 μg/g and 21 μg/g, respectively.

As with Ba and Pb, no correlation existed between Ni levels in solid samples and its water concentrations. Manganese compounds have previously been shown to effectively adsorb nickel (Trived et al, 2001; Green-Pedersen et al, 1997). Of note is that all galvanized iron pipe specimens obtained in this study fell in the "high" nickel groups (68^{th} to 100^{th} percentile). This is possibly indicative of the role of the zinc coating as an "inner" source of nickel in DWDS. The zinc coating on galvanized pipe may contain lead, copper, cadmium, chromium, and other impurities (Hill, 2010). These impurities originated from pipe materials can serve as an "inner" source of these inorganic contaminants in DWDSs.

4.4.4 Vanadium

Vanadium had a median concentration of 14 μg/g, with 10^{th} and 90^{th} percentile concentrations were 0.5 μg/g and 61 μg/g, respectively. The cumulative vanadium profiles for pipe specimens and hydrant flush solids were highly dissimilar (Figure 4.6 (a)), with V concentration in pipe specimens being higher across the entire range. The median V concentrations for pipe specimens and hydrant flush solids are 27 μg/g and 5 μg/g, respectively.

The correlation between vanadium levels in DWDS solids and its concentrations in the processed water samples was significant (R^2=0.6). This may be interpreted to indicate that vanadium accumulation in corrosion solids proceeds via adsorption reactions possibly involving the vanadate anion prevalent in the pH range typical for DWDS environments (Roccaro et al, 2007). The affinity of iron solids (hematite and magnetite) and manganese oxides for vanadium is well-established (Terzano et al, 2007; Blackmore et al, 1996).

4.4.5 Arsenic

Arsenic was the fifth highest among the targeted contaminants in DWDS solids, with a 13 μg/g median and 10th and 90th percentiles of 0.7 μg/g and 206 μg/g, respectively. Like in the case of vanadium, the profiles for pipe specimens and hydrant flush solids were dissimilar, with the results for pipe specimens being much higher (Figure 4.6(b)). The median As concentrations for pipe specimens and hydrant flush solids are 22 μg/g and 6 μg/g, respectively. The correlation of arsenic occurrence in DWDS solids versus As concentrations in associated water samples was poor (R^2=0.3, Figure 4.7(a)). Of note is that the two hydrant flush solids (SA-E and SA-D) with the highest arsenic levels in the associated water samples (4.6 and 5 μg/L) had relatively low arsenic occurrence in deposits.

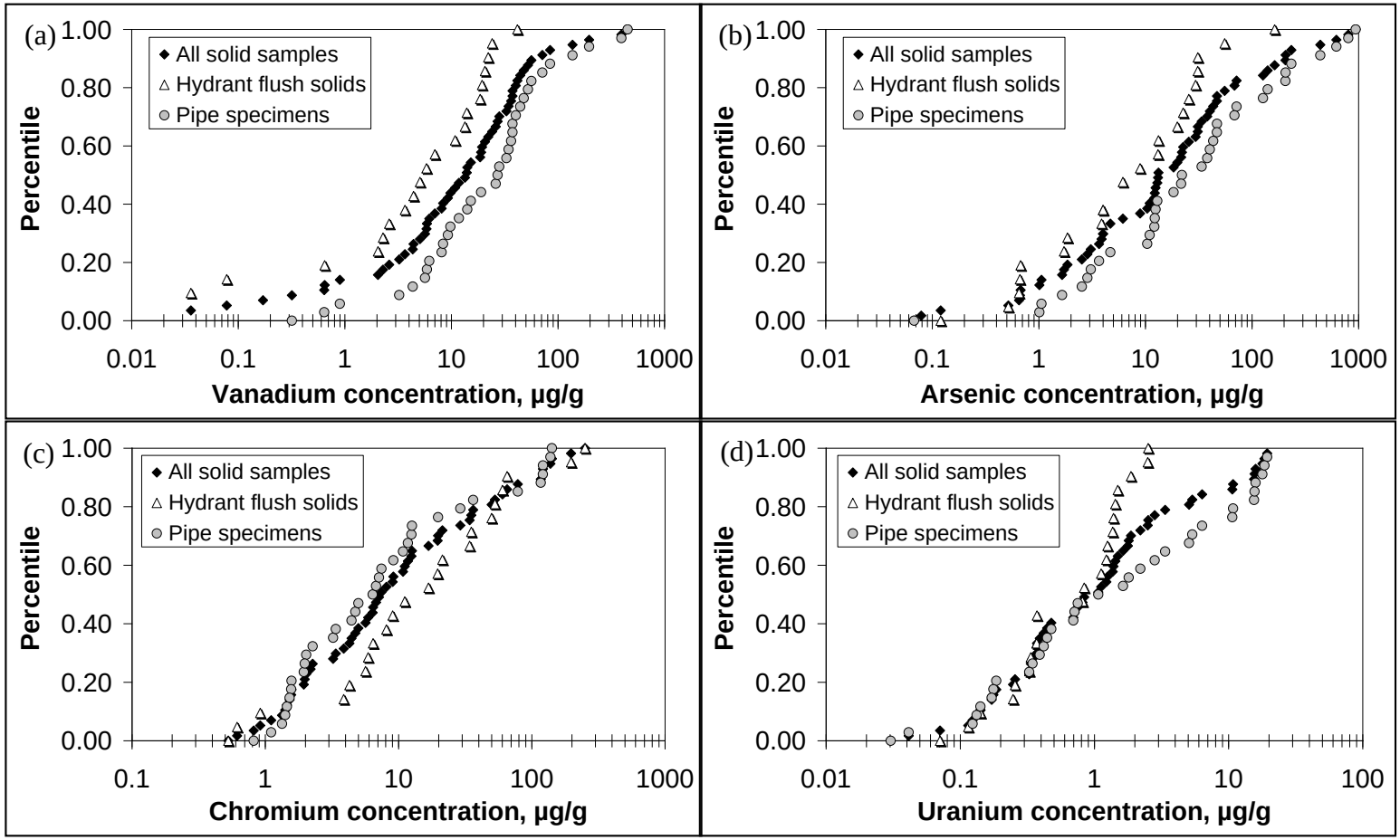

Figure 4.6 Cumulative occurrence profiles for (a) vanadium, (b) arsenic, (c) chromium, and (d) uranium in deposit samples. Source: Friedman et al, 2010. ©2010 Water Research Foundation. Reprinted with permission.

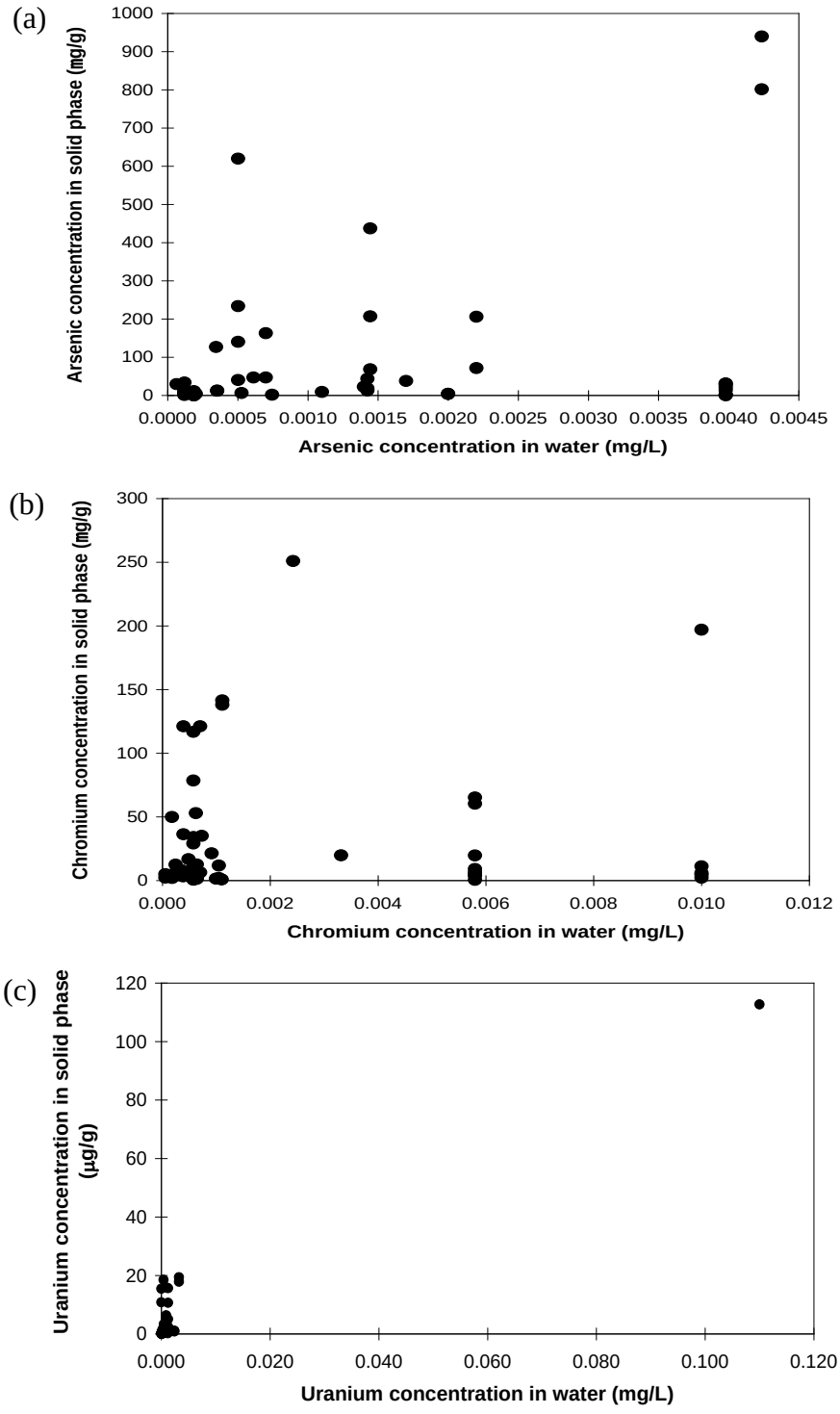

Figure 4.7 Relationship between (a) arsenic, (b) chromium, and (c) uranium concentration in deposit and water samples.

4.4.6 Chromium

Chromium had a median concentration of 7.3 μg/g, while its 10^{th} and 90^{th} percentile concentrations were 1.4 μg/g and 118 μg/g, respectively. Figure 4.6(c) illustrates the cumulative chromium occurrence profiles for all sample types. The profiles for pipe specimens and hydrant flush solids are dissimilar, with the results for hydrant flush solids being consistently higher. The median Cr concentrations for pipe specimens and hydrant flush solids are 6.4 μg/g and 11 μg/g, respectively.

While chromium occurrence in DWDS solids was poorly correlated with its concentrations in the associated water samples (R^2=0.3, Figure 4.7(b)), all four galvanized iron pipe specimens examined in this study fell in the "high" chromium groups (68^{th} to 100^{th} percentile) indicating that chromium impurities in the zinc coating may have been an "inner" source of chromium. 53% of the samples in the "high" chromium group are hydrant flush solids, implying that particulate release events may be associated with increased chromium loadings.

4.4.7 Uranium

Uranium had a median concentration of 0.95 μg/g in DWDS solids. Its 10^{th} and 90^{th} percentile concentrations were 0.14 μg/g and 15.5 μg/g, respectively. The profiles for pipe specimens and hydrant flush solids were similar below the median level, while the results for pipe specimens are higher above the 50^{th} percentile (Figure 4.6(d)).

Uranium levels in DWDS solids and its concentrations in the associated water samples appeared to be well correlated (R^2=0.9, Figure 4.7(c)). However, this relationship was heavily affected by one extreme sample (WDB-A). When that point was excluded, the R^2

value decreased to 0.50. This still suggests that uranium concentrations in water are likely to play a major role in determining its accumulation in corrosion scales and deposits.

4.4.8 Cadmium, antimony, selenium, and thallium

Cd, Sb, Se and Tl were found in all solids but their levels were much lower compared with those for elements described above. For instance, cadmium had a median concentration of 0.26 μg/g, with 10^{th} and 90^{th} percentiles at 0.06 μg/g and 2.8 μg/g, respectively (Figure 4.8(a)). Median concentrations for antimony, selenium and thallium were progressively smaller in the deposit samples (0.14, 0.10 and 0.06 μg/g). The 10^{th} and 90^{th} percentile concentrations and other data for these elements are given in Table 4.5 and Figure 4.8.

As was the case with several other metals (Pb, Ni, V and Cr), relatively elevated levels of Cd and Tl were found in galvanized pipe samples. Strong correlations also existed between cadmium occurrence in DWDS solids and zinc or manganese solid phases concentrations (R^2=0.82 or 0.60, respectively). For thallium, a strong correlation existed between its levels in DWDS solids and its water phase concentrations (R^2=0.99), although this is affected by two samples of galvanized iron pipe scales originating from utility PC. That utility had a thallium higher level in the treated water (0.0005 to 0.002 mg/L, as reported by the utility) and also relatively high levels of co-occurring manganese (0.26 to 0.28 wt%) in the solid phase.

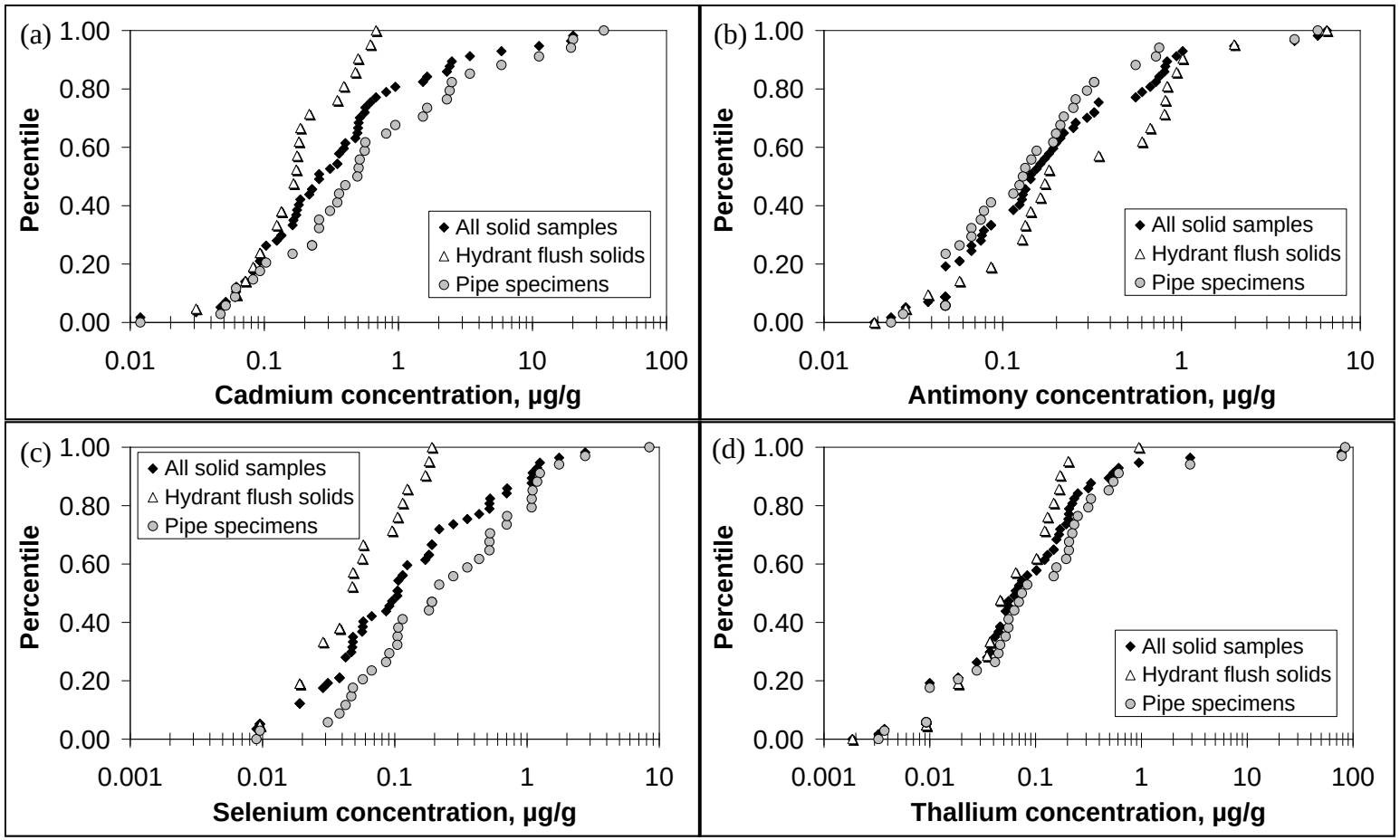

Figure 4.8 Cumulative occurrence profiles for (a) cadmium, (b) antimony, (c) selenium, and (d) Thallium in deposit samples. Source: Friedman et al, 2010. ©2010 Water Research Foundation. Reprinted with permission

4.4.9 Contaminant release

The results of our study demonstrate that significant quantities of trace inorganic contaminants can, and have, accumulated with distribution system piping materials. However, accumulation in and of itself is not necessarily a threat to public health, provided that the accumulated material is not released into the bulk water at levels that could be considered a danger to public health. Unfortunately, the processes that contribute to contaminant accumulation can be partially or fully reversible under certain chemical and hydraulic conditions (Hill et al, 2010). Our recent study that evaluated the speciation of selected inorganic contaminants in the corrosion scales using sequential extractions showed that arsenic, chromium and vanadium are mostly associated with crystalline iron oxides and tend to be mobilization-resistant. However, nickel and manganese are associated with organic carbon present in the scales and exhibited a higher mobility (Peng and Korshin, 2011).

Solid resuspension due to physical or hydraulic disturbances can result in accumulated contaminants release back into drinking water. Other release mechanisms such as dissolution or desorption can also contribute to consumer exposure to elevated levels of inorganic contaminants (Hill et al, 2010). While dissolution and desorption events may go unnoticed by the utility or consumer, physical/hydraulic release and destabilization episodes are more likely to result in easily observable "discolored" water events. The findings of this study indicate that utility personnel may need to re-evaluate their protocol for responding to customer complaints associated with discoloration or turbid water (Hill et al, 2010). Indeed, while physical/hydraulic release of Fe or Mn solids may give rise to

the apparent color, rarely have regulated trace inorganic contaminants been considered to be present, let alone analyzed for in such events (Hill et al, 2010).

4.5 Conclusions

Characteristics of corrosion scales formed in drinking water distribution systems predominated by unlined cast iron pipes and deposits mobilized during hydrant flushing events were determined using SEM/EDS, XRD and ICP/MS. XRD data showed that goethite (α-FeOOH), magnetite (Fe_3O_4) and siderite ($FeCO_3$) were the primary crystalline phases identified in most of the samples.

Among the major constituent elements of the scales, iron was most prevalent by a considerable margin, followed, in the order of decreasing prevalence, by sulfur, organic carbon, calcium, inorganic carbon, phosphorus, manganese, magnesium, aluminum and zinc. The nature of relatively abundant organic carbon found in the scales remains to be determined. The cumulative occurrence profiles of iron, sulfur, calcium and phosphorus for pipe specimens and hydrant flush solids were similar. For TOC, TIC and magnesium, the cumulative occurrence profiles showed that hydrant flush solids have consistently higher levels of these components compared with pipe specimens. On the other hand, the cumulative occurrence profiles for manganese, aluminum and zinc indicated that pipe specimens tended to have higher concentrations of these elements than hydrant flush solids. Comparison of relative occurrences of these elements indicates that hydraulic disturbances may have relatively less impact on the release of manganese, aluminum and zinc. However, observations concerning differences of concentrations of selected elements in pipe specimens and hydrant flush solids need to be confirmed in further exploration of hydraulically immobile and mobile solids originating from the same

systems. Zinc concentrations in the scales formed on galvanized iron was much higher than those formed on cast iron, with internal corrosion suspected of being the major sources of zinc in the former case.

Among the trace inorganic contaminants found in the scales, barium had the highest concentrations, followed by, in the decreasing order, lead, nickel, vanadium, arsenic, chromium, uranium, cadmium, antimony, selenium, and thallium. Hydrant flush solids tended to have higher levels of lead, nickel, chromium, and antimony compared with pipe specimens. The opposite was true for vanadium, arsenic, cadmium, selenium, and thallium. (Limitations associated with strict comparison of inorganic concentrations in pipe solids vs. hydrant solids are discussed in more detail in Friedman et al, 2010). Poor correlations between levels of trace inorganic elements in solids and those in water suggest that water chemistry parameters (e.g., pH, alkalinity, and hardness), "inner" sources from pipe materials and other aspects defining mineralogical and sorptive properties of corrosion scales play significant roles in the retention and incorporation of inorganic contaminants.

Chapter 5 Speciation of trace inorganic contaminants in corrosion scales and deposits formed in drinking water distribution systems

The accumulation of trace inorganic contaminants in DWDS solids can have consequences for the health of exposed populations if these contaminants are released from the scales thus resulting in their high levels at consumers' tap (Fisher et al., 2000; Lytle et al., 2010). The mobility and availability of contaminants accumulated in DWDS solids depends on their physico-chemical speciation that encompasses states ranging from mobile species that can be released via desorption to those tightly bound by stable crystalline oxides of iron and, in lesser extent, Ca and Mg carbonates, silica and manganese oxides predominating typical corrosion scales (Linge, 2008). The determination of mobility and other aspects of the speciation of trace level inorganic contaminants in DWDS solids were achieved via sequential extractions that allow estimating contributions of the target elements bound by *a priori* defined types of solid phases. In addition to sequential extractions, separate experiments were carried to determine concentrations of the target elements in soluble and particulate fractions (passing nominal pore sizes 5, 2, 1, and 0.4 μm) released to the ambient water. Finally, the structure-sensitive method of X-ray Adsorption Spectroscopy (XAS) were used to examine the speciation of As bound by one representative DWDS corrosion solids sample.

5.1 Solid sample characteristics

Three pipe specimens (CC-A, CC-B, and CC-D) and two hydrant flush samples (J-E and J-J) were selected for the experiments based on higher concentrations of trace inorganic contaminants in them. These samples were obtained from the earlier study funded by Water Research Foundation (Friedman et al., 2010). Relevant characteristics and elemental compositions of the examined samples are shown in Table 5.1. Three pipe specimens (CC-A, CC-B, and CC-D) originated from the same drinking water distribution system but were taken from three different locations. The utility relies on groundwater from multiple wells. Ambient water chemistry was likely to vary between the wells thus potentially resulting in variations of DWDS solids' properties in the distribution system. Two hydrant flush samples (J-E and J-J) were provided by the utility that relies on groundwater from multiple wells and operates a larger water system than utility CC. Accordingly, water quality conditions of distribution system J are likely to vary spatially and temporally because of the different source waters and their blending in the system. Indeed, the compositions of sample J-E and J-J were very different. The hydraulically mobilized material in sample J-E had comparatively low levels of iron (14.6 wt%) and manganese (760 μg/g), but a relatively high levels of total carbon (6.1 wt%). By comparison, levels of Fe, total carbon and Mn in sample J-J were 33.5 wt%, 3.4 wt% and 1091 μg/g, respectively.

Table 5.1 Characteristics and elemental compositions of solid samples examined in this study

Sample ID	Sample type	Pipe material[a]	Fe (µg/g)	Mn (µg/g)	As (µg/g)	Cr (µg/g)	V (µg/g)	U (µg/g)	Cd (µg/g)	Ni (µg/g)	BET[b] (m^2/g)	Mineralogy[c]
CC-A	Pipe specimen	Cast iron	235,000	46,692	40.2	7.13	196	5.08	11.2	121	97.42	Magnetite, quartz
CC-B	Pipe specimen	Cast iron	117,000	28,957	234	29.1	71.3	1.8	3.4	92.5	NM[d]	NM
CC-D	Pipe specimen	Cast iron	252,000	21,654	140	78.5	37.4	15.6	2.51	296	20.08	Siderite, quartz, hydroxyapatite
J-E	Hydrant flush	Cast iron	146,000	760	3.88	197	22.2	1.12	0.18	136	23.4	Calcite, dolomite, quartz
J-J	Hydrant flush	Cast iron	335,000	1,091	30.9	65.2	13.9	1.25	0.48	107	50.82	Goethite, magnetite, ferrihydrite, calcite, quartz

[a] For hydrant flush samples, pipe material refers to the type of pipe used to distribute water in the flushing zone.

[b] Crushed samples were used to analyze the BET surface area.

[c] Mineralogy was based on X-ray Diffraction (XRD) measurement.

[d] NM: Inadequate mass for testing

5.2 Speciation of inorganic contaminants via sequential extraction

The extraction efficiencies were determined by summing up the amounts extracted at each extraction step normalized by the total amount of a specific element. Duplicate samples were analyzed and extraction efficiencies from duplicate samples were averaged. Average extraction efficiencies for several elements examined in this study are presented in Table 5.2. They ranged from 95-114% with standard deviations shown in Table 5.2. The percent distribution of inorganic contaminants species extracted from individual solids can be found in Figure 5.1. The data presented in Figure 5.1 were the average values of the duplicate samples; the duplicates had an average standard deviation of ±5%. Very similar distributions of inorganic contaminants were found in samples CC-A and CC-D. However, the data for sample CC-B differed from them. Since these specimens originated from the utility that relies on groundwater from multiple wells, ambient water chemistry may vary between the wells thus potentially resulting in variations of DWDS solids' properties in the distribution system. The distributions of inorganic contaminants found in samples J-E and J-J were also different, especially for elements associated with the organic bound fraction. Although pipe specimens and hydrant flush samples examined in this study were not from the same distribution system, intrinsic differences in the generation of these two types of samples warrant their comparison that can reveal potentially important differences in retention and release of inorganic contaminants from these substrates. Average percent distributions of inorganic contaminants species shown in Figure 5.1 (a) to (e) are present in Figure 5.2. The following discussion of chemical fractionation data will focus on the data summarized in Figure 5.2. A summary of average values and standard deviations of contributions of different fractions of heavy

metals established using the sequential extraction scheme (Figure 5.2) is provided in the Table 5.3.

Table 5.2 Average extraction efficiencies and corresponding standard deviations (SD) of five corrosion solids and deposits examined in this study

	Average (%)	**SD (%)**
Arsenic (As)	107.2	13.6
Chromium (Cr)	113.5	14.6
Vanadium (V)	99.6	17.9
Uranium (U)	106.1	15.2
Cadmium (Cd)	94.8	28.3
Nickel (Ni)	107.1	31.2
Manganese (Mn)	103.2	24.5

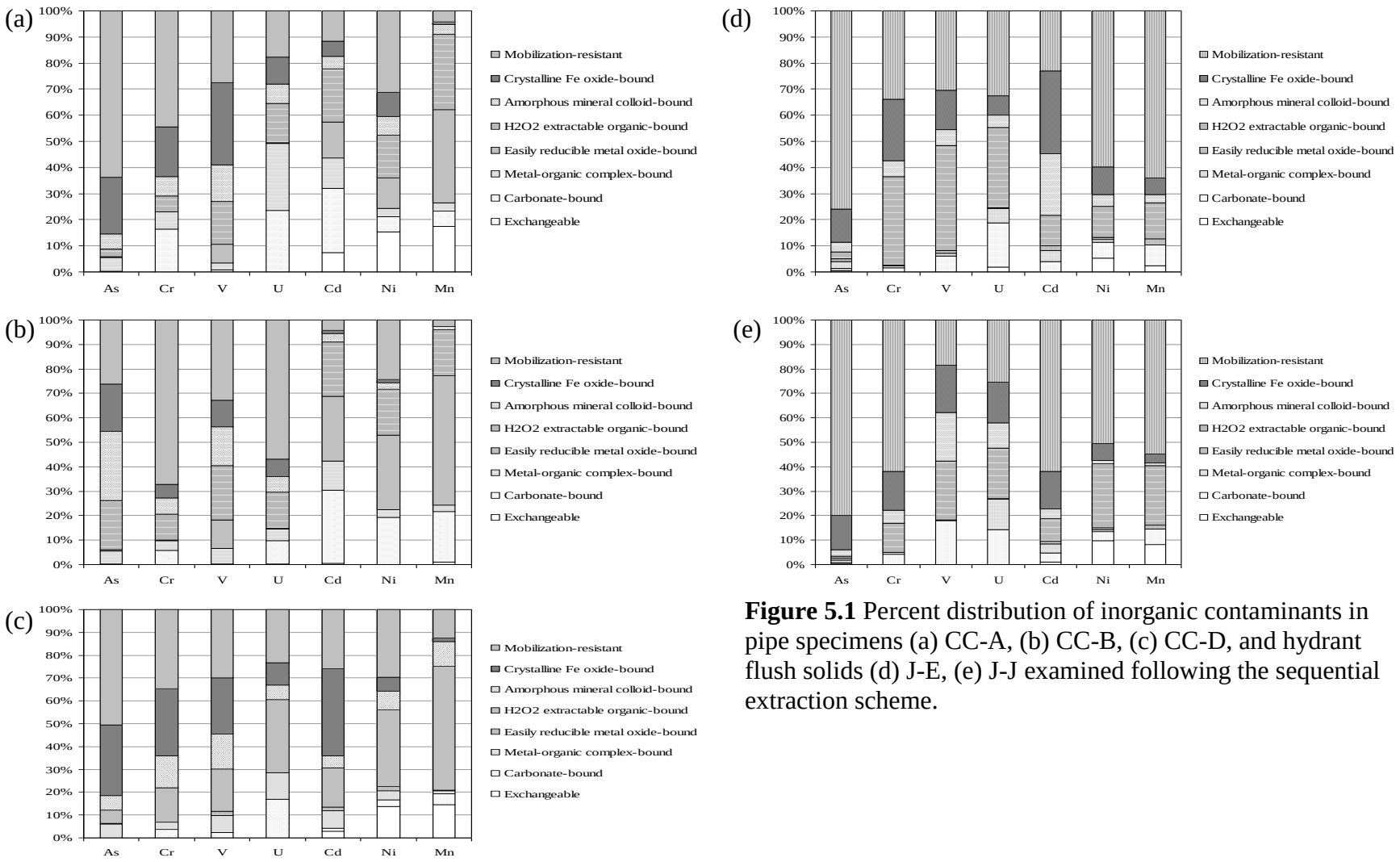

Figure 5.1 Percent distribution of inorganic contaminants in pipe specimens (a) CC-A, (b) CC-B, (c) CC-D, and hydrant flush solids (d) J-E, (e) J-J examined following the sequential extraction scheme.

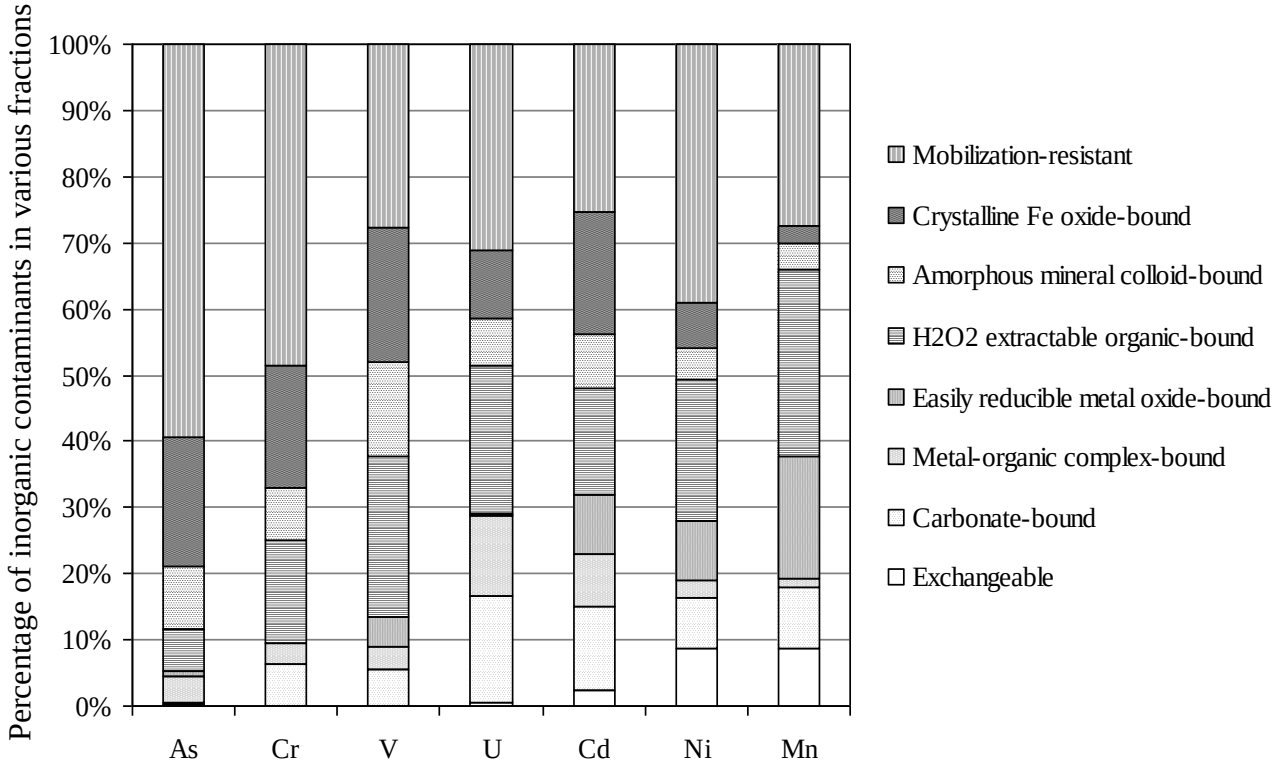

Figure 5.2 Average percent distributions of inorganic contaminants species in the corrosion solids and deposits examined in this study following the sequential extraction scheme.

Table 5.3 Average values and standard deviations of contributions of different fractions of heavy metals to total solids-associated elemental masses, as established using the sequential extraction scheme. (Average±S.D., unit:%)

Fractions	As	Cr	V	U	Cd	Ni	Mn
Exchangeable	0.2±0.3	0.0±0.0	0.04±0.03	0.4±0.8	2.4±3.1	8.8±6.3	8.7±7.3
Carbonate-bound	0.3±0.3	6.4±5.8	5.4±7.4	16.2±5.0	12.6±13.4	7.6±6.7	9.1±6.6
Metal-organic complex-bound	4.0±2.1	3.1±2.5	3.6±3.3	12.0±8.4	7.9±3.9	2.5±1.5	1.4±1.4
Easily reducible metal oxide-bound	0.6±0.4	0.05±0.08	4.3±4.8	0.2±0.1	9.0±11.2	9.1±12.7	18.6±24.3
Organic-bound	6.5±7.8	15.6±10.8	24.3±9.3	22.6±8.3	16.1±5.6	21.3±5.6	28.1±15.8
Amorphous mineral colloid-bound	9.3±10.7	7.9±3.5	14.3±5.1	7.0±1.9	8.2±8.6	4.8±2.8	3.9±4.0
Crystalline iron oxide-bound	19.8±7.3	18.6±8.9	20.3±8.1	10.3±3.8	18.5±16.0	6.7±3.5	2.6±2.5
Mobilization-resistant	59.3±21.7	48.4±15.4	27.8±5.6	31.2±15.4	25.3±22.2	39.1±15.2	27.6±29.4

5.2.1 Arsenic

Chemical fractionation data (Figure 5.2) showed that on the average, the distribution of As in five corrosion solids was dominated by the mobilization-resistant fraction (59.3%) that is deemed to correspond to a very low mobility of the retained contaminant. The fraction of arsenic associated with crystalline iron oxides was next in importance (19.8%), with contributions of amorphous mineral colloid-bound, organic-bound, metal-organic complex-bound fractions becoming progressively smaller (9.3%, 6.5% and 4%, respectively). Arsenic fractions assumed to have highest potential mobility had lowest, almost negligible contributions to the total arsenic, with the arsenic bound to easily reducible metal oxides, carbonate-bound and exchangeable sites having concentrations of 0.6%, 0.3% and 0.2%, respectively.

These results demonstrate that arsenic in the corrosion solids was dominated by the mobilization-resistant and crystalline iron oxide fractions contributing together to ca. 80% of the total. This may also indicate that As in these solids is mostly occluded in the stable mineral structures and, as a result, it is not likely to be easily mobilized. This is not surprising as As(V) is well known to have strong retention on mineral surfaces, especially iron minerals (Wilkie and Hering, 1996; Dixit and Hering, 2003). This also shows that the level of soluble arsenic release associated with possible chemical or physical perturbation affecting corrosion solids is expected by largely negligible.

This conclusion was confirmed by the data obtained when these samples were suspended in water having pH 7.6 and alkalinity 100 mg/L as $CaCO_3$, respectively. The average concentrations of inorganic contaminants released into ambient water from the five examined solids and belonging to different size fractions are shown in Table 5.4. Average

cumulative concentrations (in log scale) of released inorganic contaminants of individual solids in different size fractions are provided in Figure 5.3.

For arsenic, 2.8% and 8.7%, respectively, of the total As was released from suspended pipe specimens and hydrant flush solids and passing through a 5 μm filter (Figure 5.4). The average As levels released from suspended pipe specimens and hydrant flush solids into water were 0.44 μg/L and 0.14 μg/L, respectively.

Table 5.4 Average concentrations (μg/L) of inorganic contaminants released from suspension of corrosion solids and deposits

	Dissolved (< 0.45 μm)		**Particulate (0.45~1 μm)**		**Particulate (1~2 μm)**		**Particulate (2~5 μm)**	
	PS	**HF**	**PS**	**HF**	**PS**	**HF**	**PS**	**HF**
As	0.170	0.132	0.039	0	0.067	0.001	0.163	0.002
U	0.019	0.006	0.001	0.001	0.003	0.001	0.019	0.004
Cd	0.051	0.024	0.002	0.004	0.005	0.004	0.037	0.022
Ni	3.487	0.837	0.114	0.116	0.122	0.162	0.194	0.868
Mn	377.132	7.294	14.038	0.111	15.594	0.515	39.542	1.947

PS: pipe specimen. Three pipe specimens include CC-A, CC-B and CC-D.

HF: hydrant flush solid. Two hydrant flush solids include J-E and J-J.

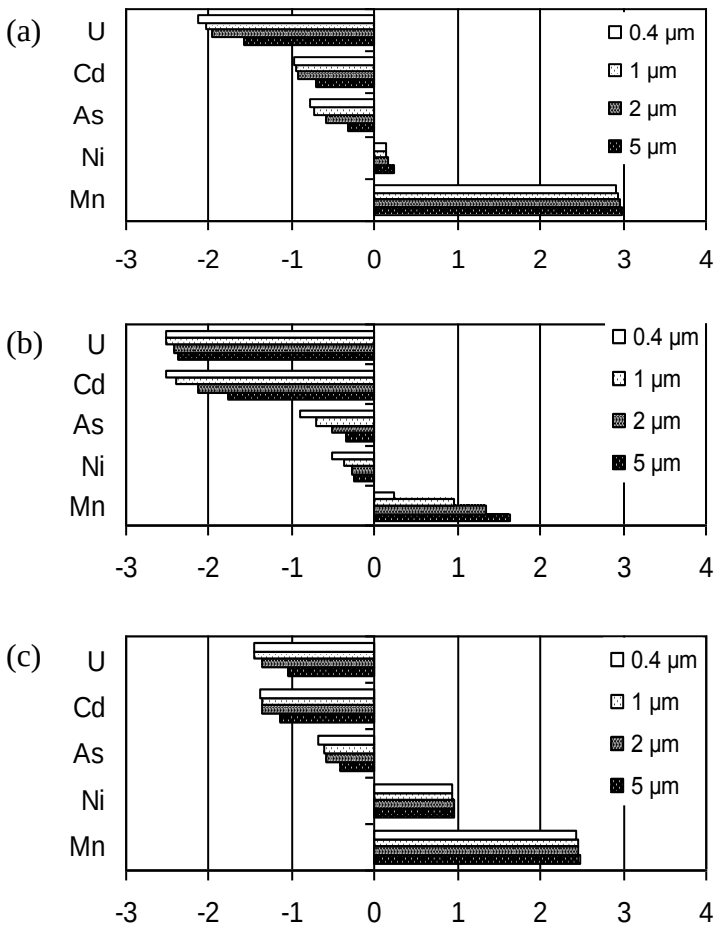

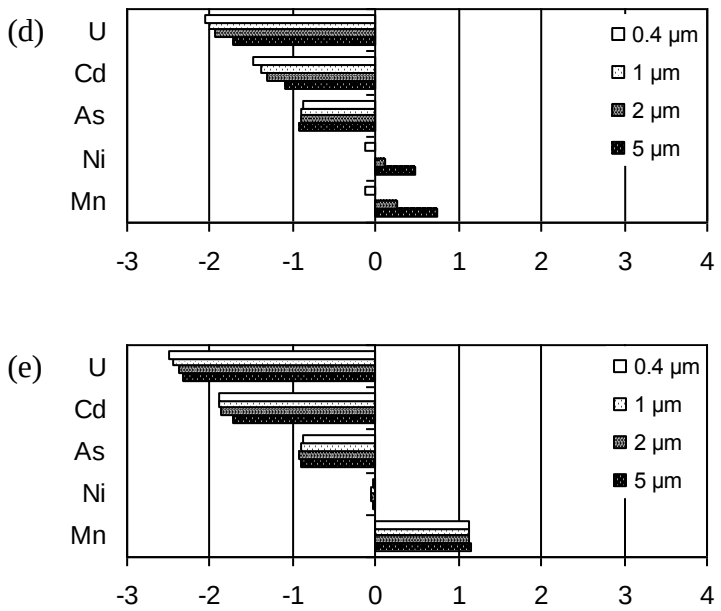

Figure 5.3 Cumulative concentrations of inorganic contaminants released from suspended corrosion solids (200 mg/L) at pH 7.6, alkalinity 100 mg/L passing filters with varying nominal pore sizes.(a) CC-A, (b) CC-B, (c) CC-D, (d) J-E, and (e) J-J solid samples.

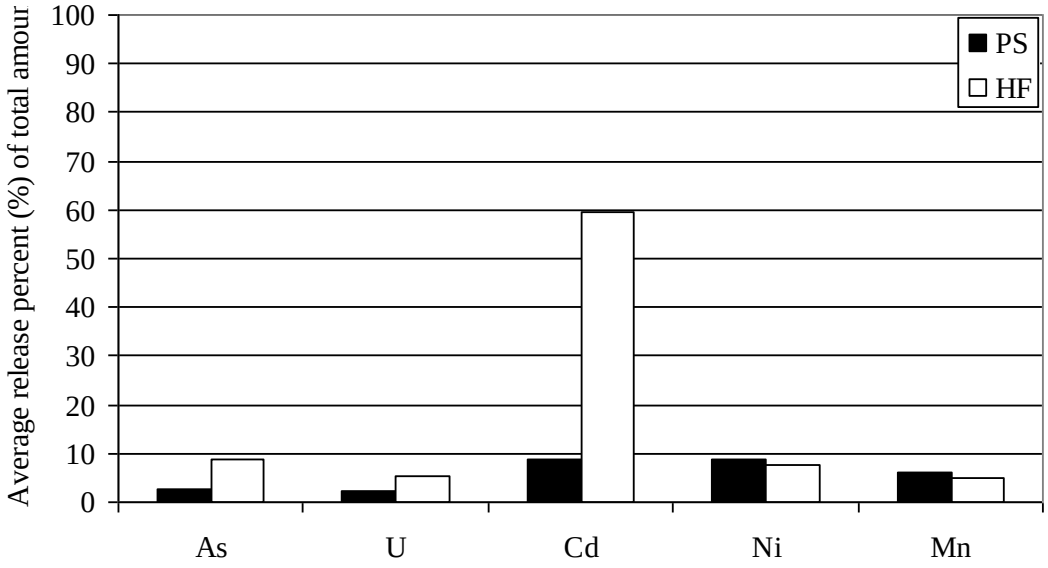

Figure 5.4 Average release percent (%) of inorganic contaminants released from suspended corrosion solids and deposits. (PS: pipe specimen, including CC-A, CC-B and CC-D. HF: hydrant flush solid, including J-E and J-J.)

Most of the arsenic released in the resuspension experiments from three pipe specimens was in the operationally defined soluble dissolved metal fraction (<0.4 μm) followed by the fraction assigned to particles with sizes between 2 to 5 μm. These two major size fractions contributed to ca. 80% of the total As passing a 5 μm filter while the 1~2 μm and 0.4~1 μm fractions constituted the rest, as shown in Figure 5.5.

The speciation of arsenic released from suspended samples exhibited a different distribution pattern for pipe specimens and hydrant flush solids. In all cases, actual concentrations of arsenic were very low. In the case of solids retained on the surface of corroding pipe, the average released As concentrations in dissolved fraction (<0.4 μm) and those corresponding to three ranges of varying particles sizes (2~5 μm, 1~2 μm and

0.4~1 μm) were 39%, 37%, 15% and 9%, respectively. In contrast, for hydrant flush solids, almost all (98%) released arsenic concentrations existed in the dissolved fraction.

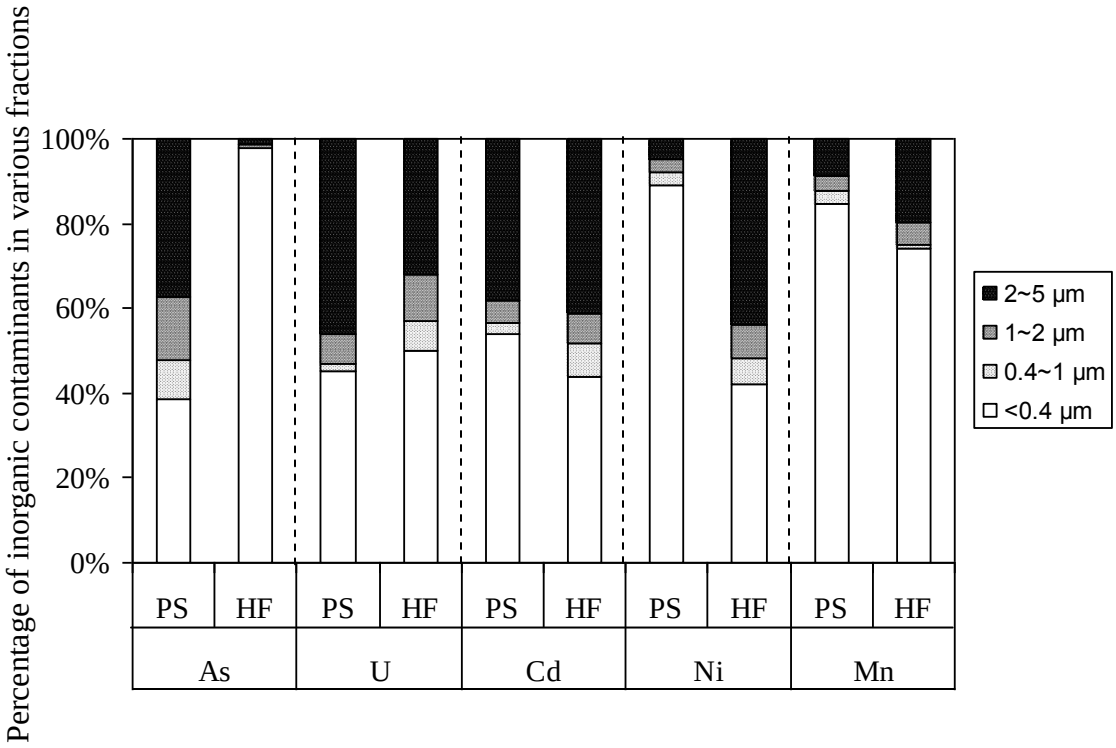

Figure 5.5 Average contributions of inorganic contaminants released from suspended corrosion solids and deposits and associated with different size fractions. (PS: pipe specimen, including CC-A, CC-B and CC-D. HF: hydrant flush solid, including J-E and J-J.)

X-ray Absorption Spectroscopy (XAS) was employed to further explore the chemical nature of arsenic in sample CC-D that had the highest As concentration among all studied solids. The white-line position of As in its X-ray absorbance spectra is known to be sensitive to the oxidation state of this element, with the white line locations at 11871.5 and 11875 eV for As(III) and As(V), respectively (e.g., Manning et al., 2002; Cancès et al., 2008). Accordingly, we examined the normalized As K-edge XANES spectrum of sample CC-D and processed the data using linear combinations of XANES spectra of

model compounds with known oxidation states fitted by means of linear least-squared fitting (LSF). Results of this fitting are shown in Figure 5.6 (a). The LSF procedure indicated that the arsenic in sample CC-D is dominated by As(V) components (91%), especially by As(V) having Fe atoms in its chemical environment. Less than 9% of the total As present in sample CC-D appears to exist as As(III).

The local coordination environment of arsenic in corrosion solid CC-D was also examined by EXAFS spectroscopy. Fourier-transformed spectra of As in CC-D are shown in Figure 5.6 (b). Peak positions shown in that figure are uncorrected for phase shifts so that they are slightly shifted from the true interatomic distances. The experimental spectrum was fitted with a theoretical model to yield interatomic distance (R), coordination number (CN), and the Debye-Waller parameter (σ^2) based on the optimized fit. These calculations (their results are summarized in Table 5.5) showed that in the first As coordination shell, four oxygen atoms located at a 1.67 Å distance from the central As atom were present. This As-O distance was statistically identical to the average As-O distances in the model compounds, such as scorodite ($FeAsO_4 \cdot 4H_2O$) and sodium arsenate ($Na_2HAsO_4 \cdot 7H_2O$) (Waychunas et al., 1993), and arsenate adsorbed on or coprecipitated with goethite, lepidocrocite, hematite or ferrihydrite (Fendorf et al., 1997; Sherman and Randall, 2003). The second peak in the spectra shown in Figure 5.6 (b) appears to indicate the presence of two iron atoms located at distance of 3.3 Å from the central As atom. This As-Fe distance appears to correspond to As associated with the surfaces of iron oxides by double-corner sharing (Fendorf et al., 1997; Sherman and Randall, 2003; Cancès et al., 2005). These data confirm that As present in the examined sample is in primarily +5 oxidation state and it is at least partly associated with Fe-

containing matrixes. This is in accord with data of prior research showing that As(V) tends to sorb very strongly on and be bound by mineral surfaces, especially iron minerals; while As(III) is considerably more mobile (Manning et al., 2002; Meng et al., 2002).

5.2.2 Chromium and vanadium

Chromium and vanadium exhibited somewhat similar fractionation patterns (Figure 5.2). The majority of Cr in the examined solids was associated with the mobilization-resistant (48.4%), crystalline iron oxide-bound (18.6%) and organic-bound (15.6%) fractions. The proportions of V occurring in the mobilization-resistant, crystalline iron oxide-bound and organic-bound fractions were 27.8%, 20.3% and 24.3%, respectively. A very low percentage of Cr (0%) and V (0.04%) were found in the exchangeable fraction. These findings suggest that Cr and V in these solids are located primarily in the stable matrixes and appear to be relatively immobile. This result is in agreement with the results of prior research demonstrating that iron based oxides are highly effective sorbents that remove chromium and vanadium in a wide range of water conditions (Smith and Ghiassi, 2006; Naeem et al., 2007).

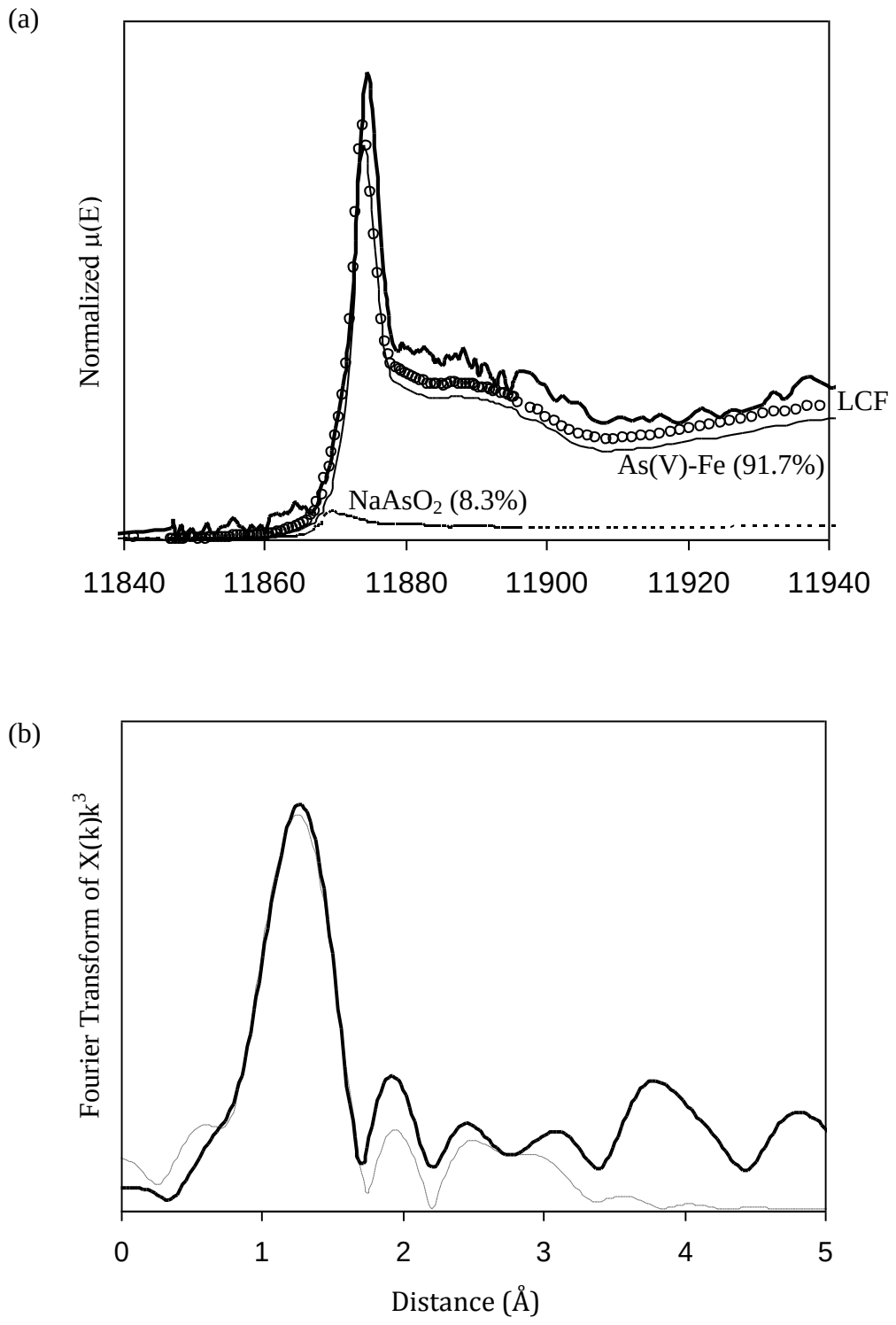

Figure 5.6 (a) Linear combination fitting of XANES and (b) Fourier transforms of the EXAFS for As in corrosion solid CC-D. The solid bold line in (a) represents the XANES data for corrosion solid CC-D. The dotted line in (a) corresponds to the linear combination fitting (LCF) of two model compounds (As(V)-Fe and $NaAsO_2$). The solid

and dashed lines in (a) correspond to the XANES data for As(V)-Fe and $NaAsO_2$ model compounds. The peak positions in (b) are uncorrected for phase shits. The dashed line in (b) is the model fits.

Table 5.5 EXAFS parameters defining local coordination environment of As in corrosion solid (CC-D)

Shell	Distance (Å)	Coordination number (CN)	Debye-Waller factor (σ^2)
As-O	1.67	4	0.001
As-Fe	3.30	2	0.002

This conclusion was supported by the data of determinations of soluble and particulate Cr and V concentrations released from suspended solids. In these experiments, the concentrations of Cr and V released were consistently below the method detection limits (Cr: 0.054 μg/L; V: 0.078 μg/L) and hence they were not included in Table 5.4, Figure 5.3, Figure 5.4 and Figure 5.5.

5.2.3 Uranium

Sequential extractions showed that in the case of uranium the mobilization-resistant (31.2%), organic-bound (22.6%), and carbonate-bound (16.2%) fractions had the highest contributions. The sum of the contributions of the mobilization-resistant and crystalline iron oxide-bound fractions accounted for 41.4% of the total U, which is less compared to all other elements examined in this study (except Mn).

The data also show that combined contributions of the organic-bound and metal-organic complex-bound fractions were 34.6% of the total uranium, while the contribution of the carbonate fraction was 16.2% (Figure 5.2). The associations of uranium with these fractions are in agreement with the strong complexation of the uranyl ion (UO_2^{2+})

prevalent in the aerobic environment with carbonate and natural organic matter (e.g., Zhou and Gu, 2005; Bednar et al., 2007; Stewart et al., 2010).

In experiments with suspended solids, 2.3% (0.042 µg/L) and 5.2% (0.012 µg/L) of U were released on the average from three pipe specimens and two hydrant flush solids, respectively (Figure 5.4). For the three pipe specimens, the average contributions of uranium associated with the 2-5 µm, 1-2 µm, 0.4-1 µm and <0.4 µm (soluble) fractions were 46.1%, 6.9%, 1.6% and 45.3%, respectively. The size fractions of uranium for the hydrant flush solids was similar, with 50% of released U found in the dissolved fraction (<0.4 µm), followed by 31.9%, 11.1% and 6.9% associated with the particular fraction of 2~5 µm, 1~2 µm and 0.4~1 µm, respectively (Figure 5.5).

5.2.4 Cadmium

Chemical fractionation data (Figure 5.2) showed that 25.3% of Cd in five corrosion solids was in the mobilization-resistant fraction. The next dominant fraction was cadmium associated with crystalline iron oxides (18.5%), followed by organic-bound (16.1%) and carbonate-bound (12.6%) metal. The remaining fractions had smaller contributions that decreased in the order: easily reducible metal oxides (9%)> amorphous mineral colloid (8.2%)> metal-organic complex (7.9%)> exchangeable cadmium (2.4%). Only 43.8% of Cd was retained in the stable mineral structures; while 31.9% of Cd, including exchangeable, carbonate, metal-organic complex and easily reducible metal oxides, was associated with potential mobile fractions.

The percentage of Cd released from the suspended solids was higher than that determined for As, V, Cr and U. Specifically, 8.8% (0.096 µg/L) and 59.7% (0.054 µg/L) of the total

Cd were released from three pipe specimens and two hydrant flush solids, respectively (Figure 5.4). The dominant fraction of Cd released from three pipe specimens (53.8%) and two hydrant flush samples (43.8%) was in dissolved (<0.4 μm) fraction. For three pipe specimens, the next predominant fraction was in particular fraction of 2~5 μm (38.3%), followed by particular fraction of 1~2 μm (5.4%) and particular fraction of 0.4~1 μm (2.6%). For two hydrant flush samples, the particular fraction of 2~5 μm (41.3%) was also the second important fraction, followed by particular fraction of 0.4~1 μm (7.8%) and particular fraction of 1~2 μm (7.1%) (Figure 5.5).

5.2.5 Nickel and manganese

Sequential extractions and filtration results demonstrated the existence of similar fractionation profiles for nickel and manganese, especially for pipe specimens (Figure 5.2 and Figure 5.4). This is possibly associated with a high affinity of hydrated manganese oxides to nickel and resulting co-accumulation of these two metals (Green-Pedersen et al., 1997; Trived and Axe, 2001; Trived et al., 2001).

In the case of nickel, the mobilization-resistant fraction contained the largest percentage (39.1%) of the metal. Organically bound nickel accounted for 21.3% of the total followed by other potentially mobile fractions including nickel associated with easily reducible metal-oxides (9.1%), followed by the exchangeable and carbonate-bound Ni (8.8 and 7.6%, respectively).

The organically-bound manganese was the predominant fraction (28.1%), followed by the mobilization-resistant fraction (27.6%). Nominally mobile fractions of manganese accounted for 36.4% of the total. These fractions included easily reducible metal-oxides

(18.6%), carbonate-bound (9.1%), and exchangeable (8.7%). The least important fractions are still amorphous mineral colloid-bound (3.9%), crystalline iron oxide-bound (2.6%), and metal-organic complex-bound (1.4%).

Filtration data obtained using suspended solids showed that on the average 8.8% (3.92 μg/L) and 7.7% (1.98 μg/L) of the total Ni present in these samples were released into water from three pipe specimens and two hydrant flush samples, respectively (Figure 5.4).. 89% of Ni released from the pipe specimens was in the dissolved (<0.4 μm) fraction while in case of hydrant flush samples only 42.2% of the released Ni passed through 0.4 μm filter. At the same time, a large part of released Ni (43.8%) from two hydrant flush samples is in particulate fraction of 2~5 μm.

On the other hand, 6.1% (446.3 μg/L) and 5% (9.87 μg/L) of total Mn were released into water from three pipe specimens and two hydrant flush samples, respectively (Figure 5.4). 84.5% and 73.9% of released Mn from three pipe specimens and two hydrant flush samples are in the dissolved (<0.4 μm) fraction. It needs to be recognized however, that manganese concentrations tend to be two or more magnitudes larger than those of nickel in the pipe specimens; although the release percentages of these two elements are very similar, manganese will have overwhelming concentrations compared to that of nickel.

5.3 Practical implications

The experimental data presented above demonstrate the existence of pronounced differences in the mobility of inorganic contaminants retained by DWDS corrosion scales and, when released, potentially affecting human health. The data show that the physico-chemical properties of As, Cr and V retained by DWDS corrosion scales accumulated are

similar. These three elements were found to be tightly bound by the solid matrixes and are expected to exhibit little mobility under most conditions typical for drinking water systems. However, because arsenic and, very likely, vanadium exist in anionic forms in these conditions, their mobility can hypothetically be increased via competition with and displacement by phosphate ions utilized for corrosion control (Jain and Loeppert, 2000; Copeland et al., 2007). Actual occurrence of such competition remains to be ascertained.

On the other hand, arsenic release may be associated with particulate matter, as was observed by Lytle et al. (2010) for a small drinking water system in which high arsenic levels were associated with iron oxide particles carried in the system by the source water. Our speciation data similarly indicate that because As present in corrosion solids is dominated by the mobilization-resistant and crystalline iron oxide-bound fractions, its release can occur primarily via particulates physically dislodged by hydraulic events or via colloidal mobilization of iron-based corrosion solids caused by changes of water chemistry. Conditions possibly associated with such phenomena in drinking water distribution systems need to be investigated in the future.

Similarly to our observations, high concentrations of vanadium (35 to 899 μg/g) in scales formed on surfaces of galvanized iron were reported by Gerke et al. (2010). In that study, the vanadium was determined to be present as discrete grains of the mineral vanadinite $Pb_5(V^{5+}O_4)_3Cl$ that were formed "up stream" from lead pipe present in the examined systems; Gerke et al. (2010) concluded that the vanadinite solid phase was mostly embedded in near-surface regions of iron corrosion by-products and, in the absence of physical dislodging or colloidal mobilization, it was not likely to increase V concentrations in the ambient water to dangerous levels. Our vanadium speciation data

are in agreement with the above observations as they confirm that, the vanadium in the tested samples was primarily associated with the mobilization-resistant and crystalline iron oxide-bound fractions and the concentration of vanadium released from iron-based corrosion solids were very low. Similar observation was made in this study for chromium but, in contrast with vanadium, the accumulation and release of Cr has not been sufficiently addressed in prior research.

In contrast with As, Cr and V, significant fractions of uranium and cadmium (ca. 16% and 13%, respectively) were associated with carbonate-type solids. Prior research (e.g., Rihs et al., 2004; Khaokaew et al., 2011) shows that calcite and other solid carbonate minerals can strongly sorb uranium and cadmium. Such minerals are common in corrosion scales and especially in hydrant flush samples where they can be dominant solid phases (Peng et al., 2010b). The retention of cadmium by these phases appears to be at least partially reversible as evidenced by the results that ca. 60% of the total cadmium was released from the resuspended hydrant flush samples. While actual levels of U and Cd in DWDS solids are very low and per se not likely to be of concern, this finding suggests that changes of drinking water alkalinity can be accompanied by changes of levels of these contaminants.

Nickel and manganese were determined to be the most mobile of all contaminants examined in our study. About 9% of the retained Ni and Mn were found to exist as the exchangeable fraction that is expected to be highly susceptible to variations of the ambient water quality. While estimation of health effects potentially associated with the release of nickel and manganese accumulated in DWDS solids goes beyond the scope of

this paper, this finding highlights the importance of manganese removal from drinking water and control of its status within drinking water distribution networks.

Notable contributions (more than 20%) of organic-bound fractions of vanadium, uranium, nickel and manganese may also indicate that biofilms and natural organic matter in the DWDSs play an important role in the accumulation of these inorganic contaminants. This is in agreement with prior findings showing that extracellular polymer substances (EPS) and biofilms *per se* can sorb inorganic contaminants (e.g., Flemming, 1995; Lalonde et al., 2007; Hitchcock et al., 2009). On the other hand, this finding indicates that changes of water chemistry causing destabilization of biofilms can be accompanied by release the sorbed contaminants. Further characterization of natural organic matter and biofilms found in DWDS solids is needed to provide more insight into the nature of binding of the examined and other inorganic contaminants.

5.4 Conclusions

Results of sequential extractions and measurements of soluble and particulate metal fractions released from suspended corrosion solids indicate that all examined trace-level heavy metals (As, Cr, V, U, Cd, Ni, and Mn) exhibit specific features of their fractionation and mobility. Arsenic, chromium and vanadium are primarily associated with the mobilization-resistant fraction that was unaffected by all eluents used in this study. At the same time, low percentages of As, Cr and V were associated with mobile fractions (exchangeable, carbonate-bound, metal-organic complex, and easily reducible metal oxide-bound). X-ray absorbance measurements demonstrated that the arsenic in the sample with the highest As concentration was dominated by As(V) bound by iron oxides.

Measurements of soluble and particulate metal concentrations demonstrated that only in the case of Ni and Mn released from solids suspended at pH 7.6 and alkalinity 100 mg/L the majority of the released metal was in the dissolved (<0.4 μm) fraction while the other elements were mostly associated particles with sizes between 0.4 to 5 μm. However, in the case of arsenic, the concentrations of release As were very low and almost all (98%) As released from the hydrant flush solids was in the dissolved fraction. The data of the resuspension and sequential extraction experiments were in close agreement and showed that Ni and Mn are much more mobile than all the other inorganic contaminants examined in this study.

Chapter 6 Examination of Effects of Desalinated Water on Iron Corrosion, Accumulation and Release of Inorganic Contaminants

6.1 Impacts of blending of surface water and desalinated water on iron corrosion and retention of inorganic contaminants

Effects of blending of surface water and desalinated water on soluble/total iron release, iron corrosion rate, and retention of inorganic contaminants were examined based on jar tests that used iron coupons and varying compositions of synthetic waters. Five blending ratios (0, 20, 50, 80, and 100% percentage of desalinated water) and four NOM concentrations (0, 0.5, 1, and 2 mg/L prepared from Suwannee River Fulvic Acid) were examined in this study. Specific details of these exposures are described in the Materials and Methods chapter of this thesis. The detailed list of anion compositions corresponding to blending ratios is shown in Table 6.1.

Table 6.1 Detailed lists of anion compositions used in batch 1 jar tests. The alkalinity and pH values were fixed at 120 mg/L as $CaCO_3$ and 7.5, respectively.

Percentage of desalinated water in the blend (%)	$[Cl^-]$ (mg/L)	$[SO_4^{2-}]$ (mg/L)
0	28	79.2
20	53.8	64.5
50	92.5	42.4
80	131.2	20.2
100	157	5.5

6.1.1 Iron release from corroding iron coupons

Soluble and total iron measurements are operationally defined by our jar test protocol and are useful primarily for comparison and determination of specific effects. ICP/MS measurements of iron release from coupons exposed to the synthetic water during eight weeks showed that total iron levels became stable after 5 weeks of exposure (Figure 6.1). The average iron concentrations from week 6 to week 8 were used in the discussion that follows to examine the impacts of water quality conditions.

Figure 6.2 (A) shows that soluble iron concentrations decreased as the percentage of desalinated water increased in the absence of DOC. However, in the presence of DOC, soluble iron concentrations increased dramatically, especially in waters blends with 80% and 100% desalinated water. In the extreme case of 100% of desalinated water, the presence of DOC present in the water caused a dramatic, up two-orders of magnitude higher levels of soluble iron.

In contrast of the behavior of soluble iron, total iron concentrations did not change significantly as the blending ratio increased. However, DOC still had a pronounced effect on total iron release, which increased with the concentration of NOM (Figure 6.2 (B)). The behavior of the fraction of soluble iron vs. the blending ration and DOC demonstrated that in the absence of DOC, the contribution of soluble to total iron decrease as the percentage of desalinated water increased. However, this behavior was reversed at DOC levels of 0.5 and 1.0 mg/L. At DOC concentration of 2 mg/L, the fraction of dissolved iron was between 60 to 80% for all blends of desalinated and conventionally treated water (Figure 6.2 (C)).

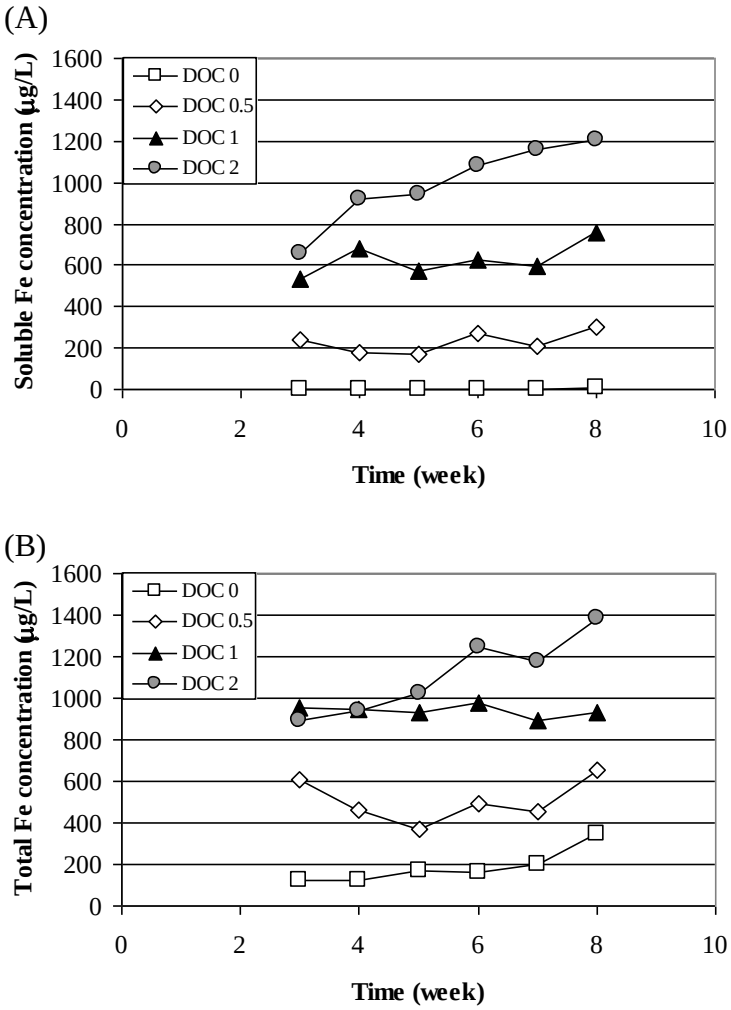

Figure 6.1 Typical profiles of (A) soluble and (B) total iron release from Fe coupons during the 8 week-long jar test. 100% desalinated water blend.

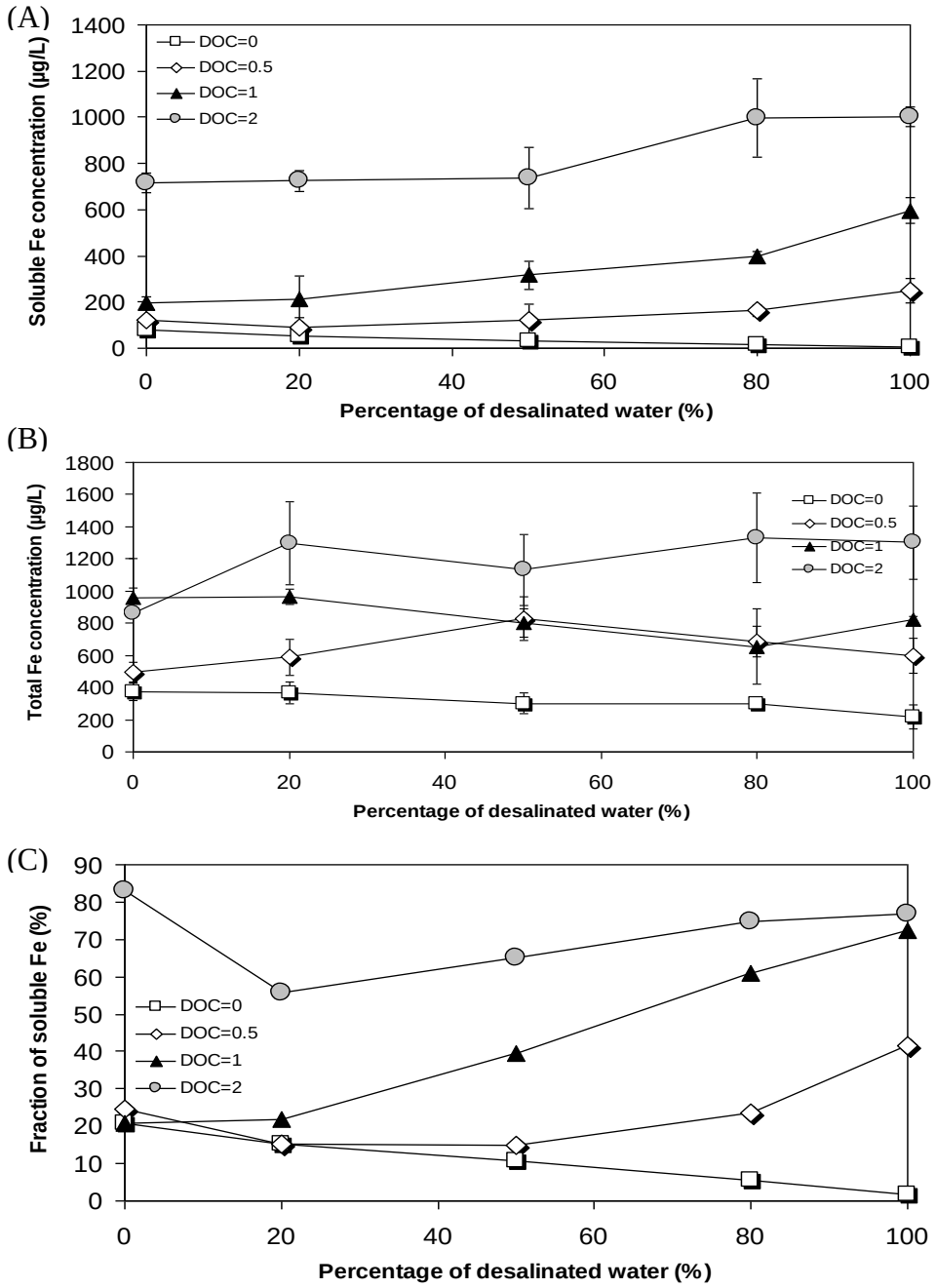

Figure 6.2 Impact of desalinated water blending ratios and DOC concentrations on the average (A) soluble, (B) total iron concentrations and (C) fraction of soluble iron released from iron coupons during exposure week 6 to 8. The error bars indicates ±1 standard deviation.

6.1.2 Impact of desalinated water and NOM on iron corrosion rates and scale retention factors

Iron corrosion rates in the blends were determined by weight loss measurement. Three measurements of coupon weight were carried out. The initial weight of a coupon (W_0) was determined before exposure. After 8 week exposure, its dry weight with corrosion scales still attached to the surface (W_1) and that after scales were removed (W_2) were measured. The overall weigh loss of an iron coupon's mass is defined as:

$$\Delta W_{loss} = W_0 - W_2$$

The weight of scales retained on the coupon's surface is expressed as:

$$W_{scale} = W_1 - W_2$$

Total weight loss (ΔW_{loss}) results and the formula derived based on the conventional theory of electrochemical corrosion were used to determine the apparent corrosion rates ($i_{corr}^{\Delta W}$).

$$i_{corr}^{\Delta W}\left(\mu A/cm^2\right) = \frac{1000 \cdot \Delta W_{loss}(mg) \cdot n \cdot F}{AW_{Fe} \cdot S \cdot t_{\exp}}$$

In this equation, ΔW_{loss} is the weight loss (in mg), n is the number of electrons (three for the oxidation of Fe^0 to Fe^{3+}), F is the Faraday constant (96500 A·sec/mol), AW_{Fe} is atomic weight of Fe, S is the surface area of iron coupons (3.3 cm^2), and t_{exp} is the overall exposure time (4,838,400 seconds, which is equivalent to 8 weeks of exposure in our experiments).

Dimensionless scale retention factors (SR) were determined using W_{scale} value. Based on results from our previous study (Liu et al., 2011), we assumed that the scales attached to the coupons' surface were mostly ferric hydroxide ($Fe(OH)_3$) for blends with <50%

desalinated water and lepidocrocite (γ-FeO(OH)) for blends with ≥50% desalinated water. The scale retention factor was therefore expressed as:

$$SR = \frac{\left(\frac{W_{scale}}{MW_{scales}}\right)}{\left(\frac{\Delta W_{loss}}{AW_{Fe}}\right)}$$

In the above equation, SR stands for the scale retention factor. MW_{scales} *is* 106.86 g/mol for blends with <50% desalinated water and is 88.85 g/mol for blends with ≥50% desalinated water, and AW_{Fe} is atomic weight of Fe.

The measurements of weight loss and SR values for the exposed coupons showed that as percentage of desalinated water in the blends increased, so did the corrosion rates (Figure 6.3 (A)). The data present in Figure 6.3 were the average values of the two coupons; the difference between two coupons had an average standard deviation of ±10% and ±25% for corrosion rates and SR, respectively. In the absence of NOM, the corrosion rate increased from 12 μA/cm^2 in unblended surface water to 18 μA/cm^2 in 100% desalinated water. The concentration of NOM also affected the corrosion rates, increasing them in general. For instance, in the absence of desalinated water, the increase of DOC from 0 to 2 mg/L was accompanied by the increase of the corrosion rates from 12 to 16 μA/cm^2. However, this effect of NOM was considerably more dominant in low blending ratios (less than 60% of desalinated water). In 100% desalinated water, effects of DOC on the corrosion rates were practically absent.

Measurements of the SR values (Figure 6.3 (B)) showed the increase of the overall corrosion rates associated with DOC was counterbalanced by much higher SR values observed in the presence of NOM. For instance, the SR values in the absence of NOM

were in the range 0.55 to 0.65 for water blends with the fraction of desalinated water < 60%. At higher desalinated water contributions, the SR values decreased to ca. 0.40.

In contrast with that, corrosion scales developed in the presence of DOC, even at concentration of 0.5 mg/L, were considerably less friable and tended to remain on the surface, In fact, the SR values determined for the range DOC 1 to 2 mg/L and fractions of desalinated water in the blend < 50% were between 0.8 to 0.9. However, increase of the fraction of desalinated water caused the SR values to decrease, but in the presence of NOM the SR values were always considerably higher than those in the absence of NOM.

6.1.3 Impact of desalinated water and NOM on structure and morphology of iron corrosion scales

Structural measurements indicated that the effects described in the preceding section were likely to be associated with effects of NOM and blending on the nature of the corrosion solids formed on the surface of iron.

XRD measurements demonstrated the dominant XRD-identifiable crystalline phases in the corrosion scales formed in surface water (Figure 6.4) or desalinated water (Figure 6.5) were lepidocrocite and magnetite. The relative contribution of lepidocrocite and the intensity of its XRD lines over the background (most likely caused by the highly amorphous phase of HFO) were higher in desalinated water, especially in the absence of NOM. Calcite was also detected in the scales, but only in those formed in surface water with its higher calcium concentration (23.4 mg/L).

Changes of the morphology of the surfaces of corroding iron are reflected in SEM images shown in Figure 6.6. It demonstrates that clusters of thin lath-like crystals were present in scales formed in the absence of NOM in both the surface water and desalinated water

(Figure 6.6 (A) and (C)). However, these crystals were more developed and exhibited more symmetry in 100% desalinated water. Based on XRD and previous studies, these formations are very likely to be lepidocrocite (Cornell and Schwertmann, 2003).

Prior literature (Cornell and Schwertmann, 2003) suggests that chloride tends to promote lepidocrocite formation. This is in accord with the SEM data showing that bigger and more symmetric clusters of lepidocrocite were formed in 100% desalinated water that had the highest chloride concentration. In addition, small rounded or octahedral crystals, most likely those of magnetite were present on the surface but the most dominant features in the tested samples were associated with lepidocrocite.

NOM caused the morphology of the corroding iron surfaces to change. In its presence, dispersed structures lacking discernible crystalline features were formed on the surface. The lack of phases with pronounced crystalline order was especially notable in surfaces exposed to the synthetic surface water (Figure 6.6 (B) and (D)).

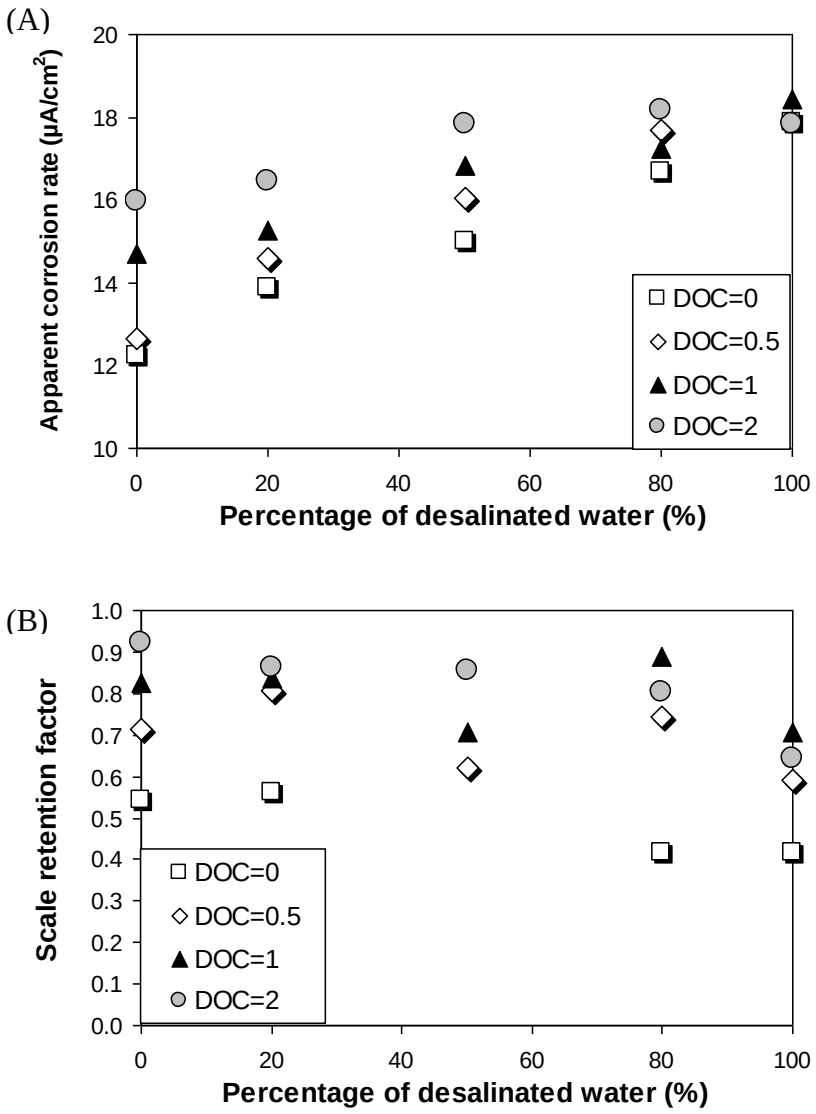

Figure 6.3 Impacts of blending of desalinated water and NOM concentration on (A) apparent corrosion rate and (B) scale retention factor based on weight loss measurements for iron coupons.

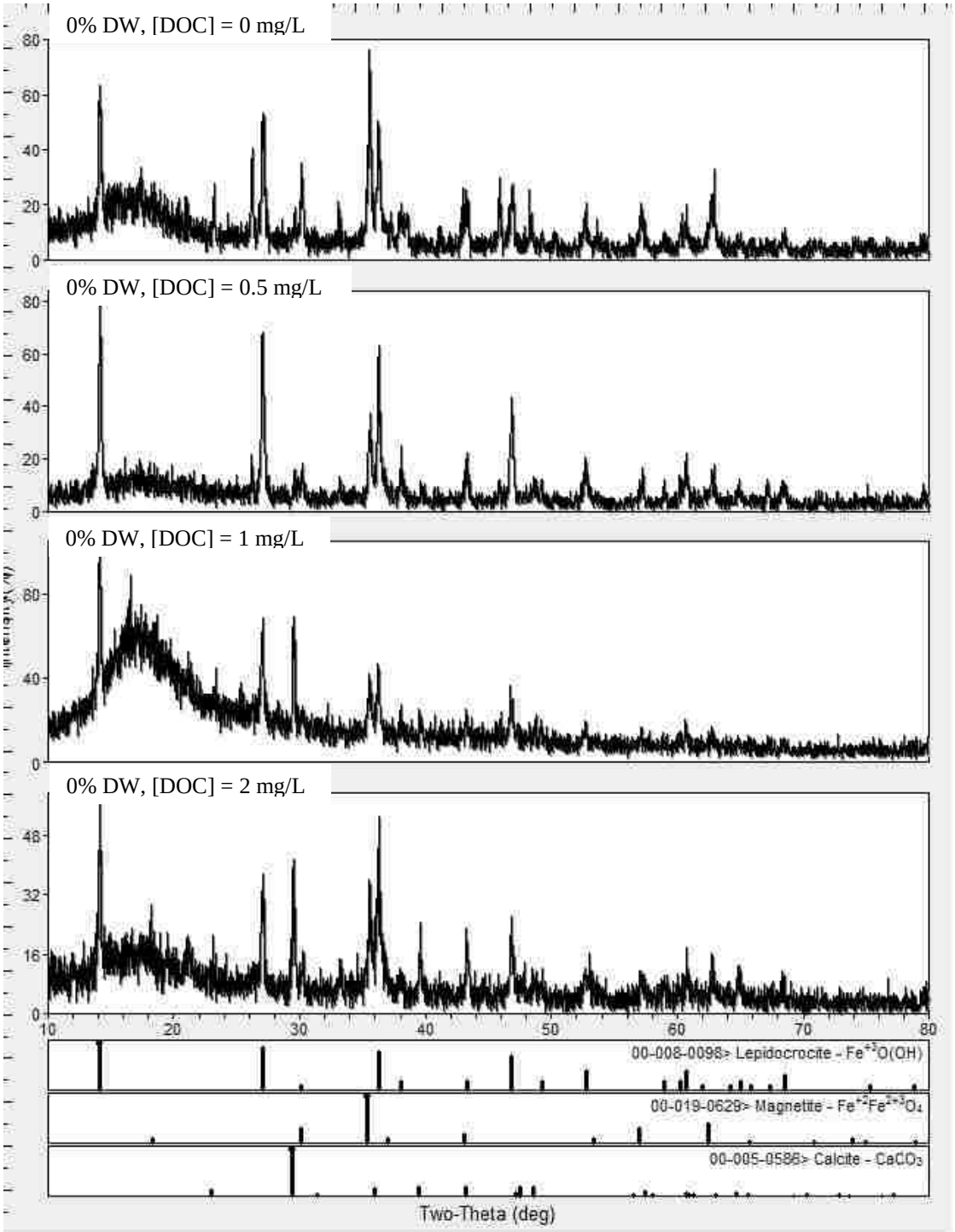

Figure 6.4 Effects of NOM on XRD data obtained for corrosion scales formed in synthetic surface water.

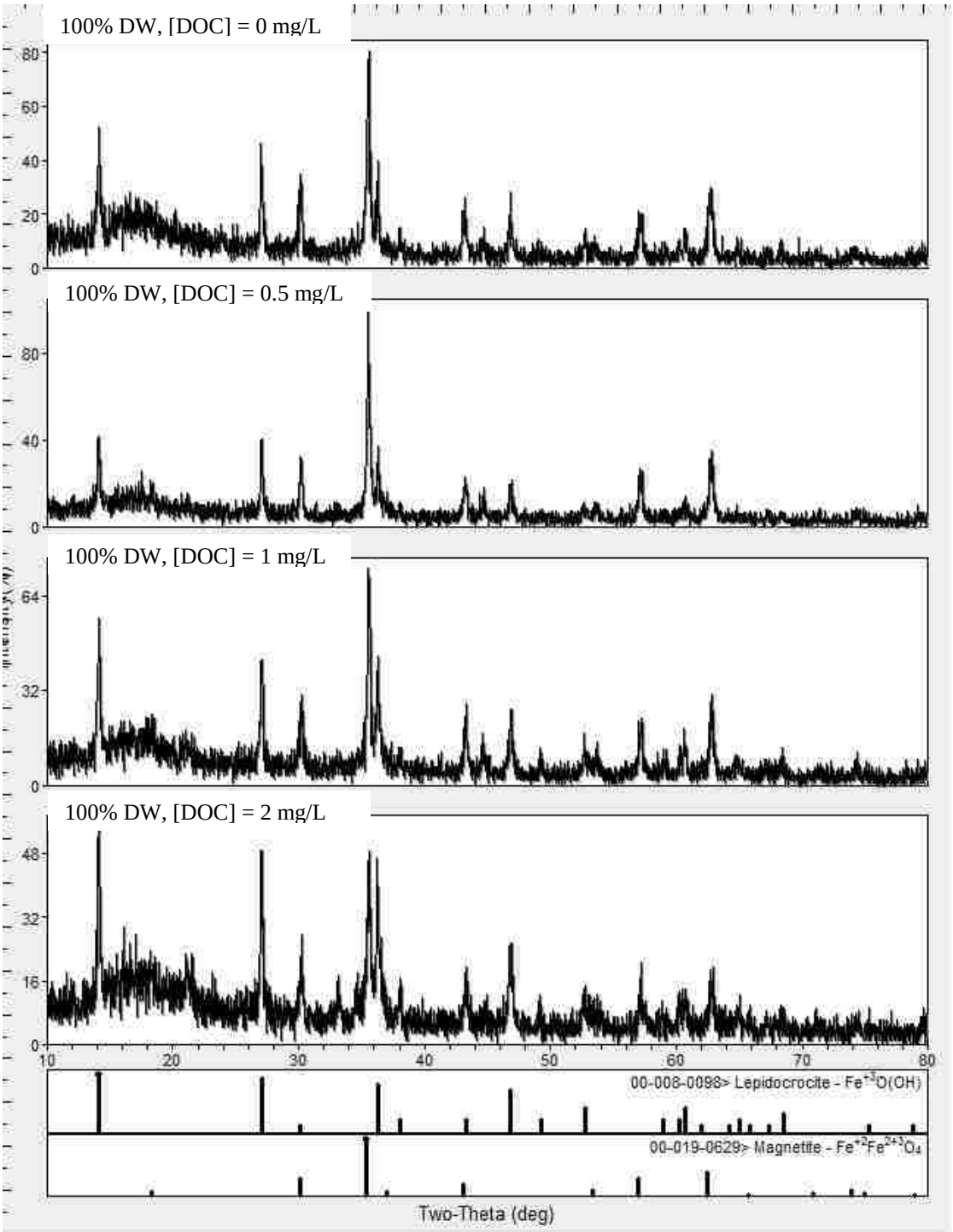

Figure 6.5 Effects of NOM on XRD data obtained for corrosion scales formed in desalinated water.

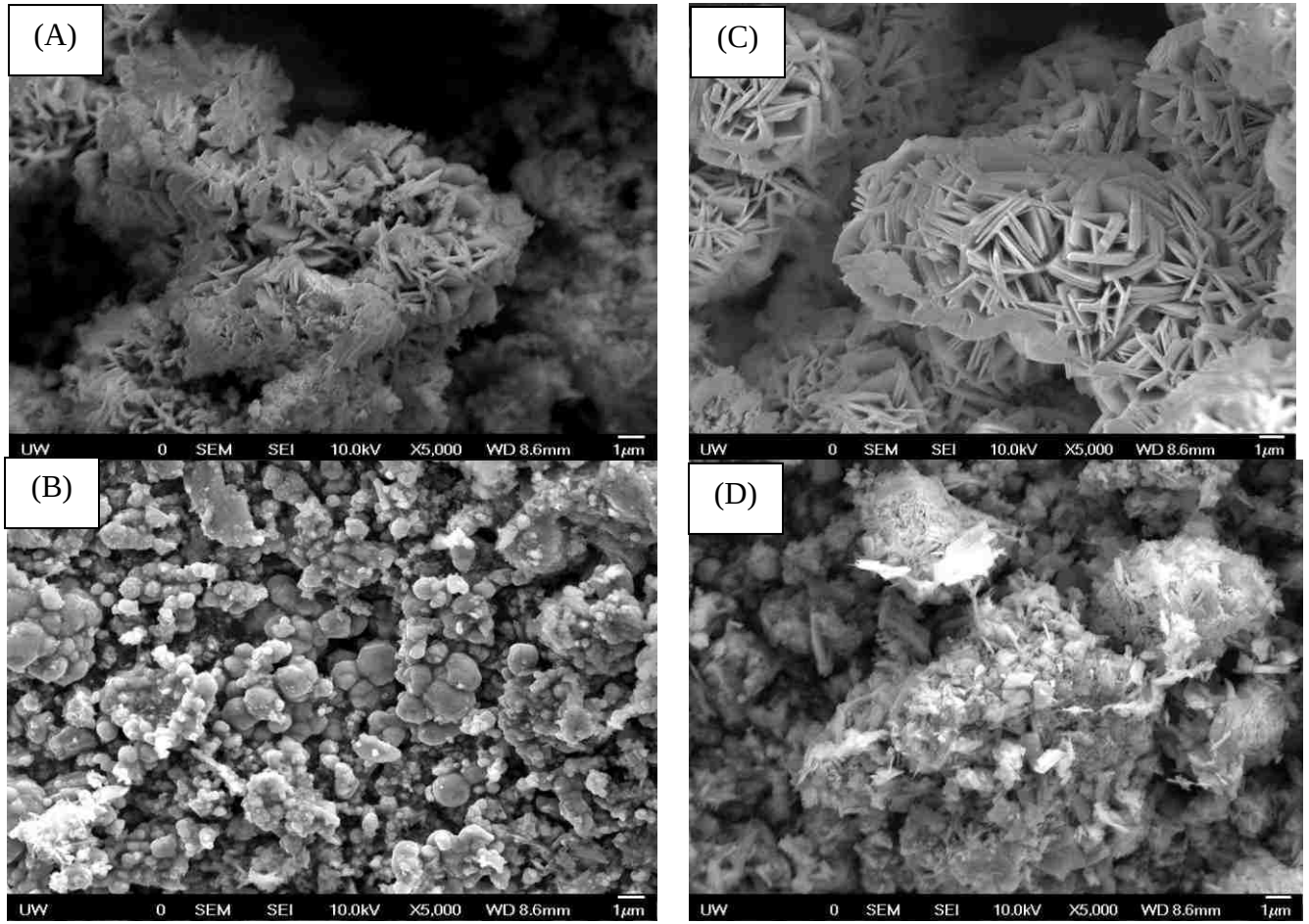

Figure 6.6 Morphological changes of corrosion scales formed in different blending of desalinated water and NOM. (A) 0% desalinated water, [DOC]= 0 mg/L; (B) 0% desalinated water, [DOC]= 1 mg/L; (C) 100% desalinated water, [DOC]= 0 mg/L; and (D) 100% desalinated water, [DOC]= 1 mg/L.

6.1.4 Initial comparison of relative importance of NOM and anionic effects on iron corrosion and release

Changes of iron corrosion rates and iron release discussed above can be associated with both changing concentrations of anions, notably sulfate and chloride, and NOM in the blends of desalinated/conventionally treated water. Prior research demonstrates that NOM can indeed induce complex, site-specific effects on iron corrosion. For instance, Benjamin et al. 1996 reported a suppression of corrosion rates of iron in the presence of humic substances from Lake Constance. Dick and Rodrigues 2006 observed that peat fulvic acid added to 0.01 M Na_2SO_4 caused the rate of electrochemical oxidation of iron and its pitting propensity to decrease, while humic acid caused it to increase. Strong adsorption of NOM and its influence on the morphology of corrosion products was also observed in experiments with zero-valent iron particles, with NOM promoting the formation of amorphous surface scales and dispersed particles (Tsang et al. 2009; Rao et al. 2009; Giasuddin et al. 2007). Effects of chloride and sulfate on the corrosion of iron in drinking water are also complex, with chloride tending to increase rates of corrosion and Fe release while sulfate tends to exert a moderate degree of suppression, with more adhering and uniform surface scales formed in its presence at least in some cases (e.g., Vatankhah et al. 1998a; Vatankhah et al. 1998b; Kwon et al. 2006; Taylor et al. 2006; Zhang and Edwards 2007; Shi and Taylor 2007).

Therefore, we examined the hypothesis that iron corrosion and release in the synthetic water blends were affected by (A) the anionic composition; (B) DOC concentration and (C) a cross-combination of these factors. The detailed list of anion compositions corresponding to blending ratios can be referred to Table 6.1. To quantify this hypothesis,

phenomenological expressions were developed to fit the data shown in Figure 6.2 and Figure 6.3. Optimizations of coefficients reflecting effects of f_{desal}, DOC and their combinations in these equations yielded the following expressions:

$$i\left(\mu A/cm^2\right)=12.2+5.5\left(f_{desal}\right)-1.5\left(f_{desal}\right)\cdot\left(DOC\right)+2\cdot DOC \quad (1)$$

$$TOTFe\left(mg/L\right)=378-150\left(f_{desal}\right)^{0.4}+360\left(f_{desal}\right)^{0.4}\cdot\left(DOC\right)^{0.4}+329\cdot DOC \quad (2)$$

$$Fe_{sol}\left(mg/L\right)=52-50\left(f_{desal}\right)^{2}+340\left(f_{desal}\right)^{2}\cdot\left(DOC\right)^{0.4}+160\cdot DOC^{2} \quad (3)$$

Results of fitting that employed this hypothesis demonstrate that the modeling carried out using the above expressions resulted in very good fits to the experimental data (Figure 6.7). Expressions 1, 2 and 3 allowed achieving high R^2 values (0.95, 0.89 and 0.99 for corrosion rates, total and soluble iron concentrations, respectively).

Equations 1, 2 and 3 quantify the extent of changes induced by variation of anionic composition of blended water, NOM concentration and synergistic (or antagonistic) effects of these components. In the case of Fe corrosion rates, the term reflecting joint effects of NOM and increasing chloride concentrations is negative thus showing that NOM tends to counteract to the acceleration of corrosion by chloride. In contrast with that, NOM acts synergistically with increasing chloride (and/or decreasing sulfate) in accelerating iron release.

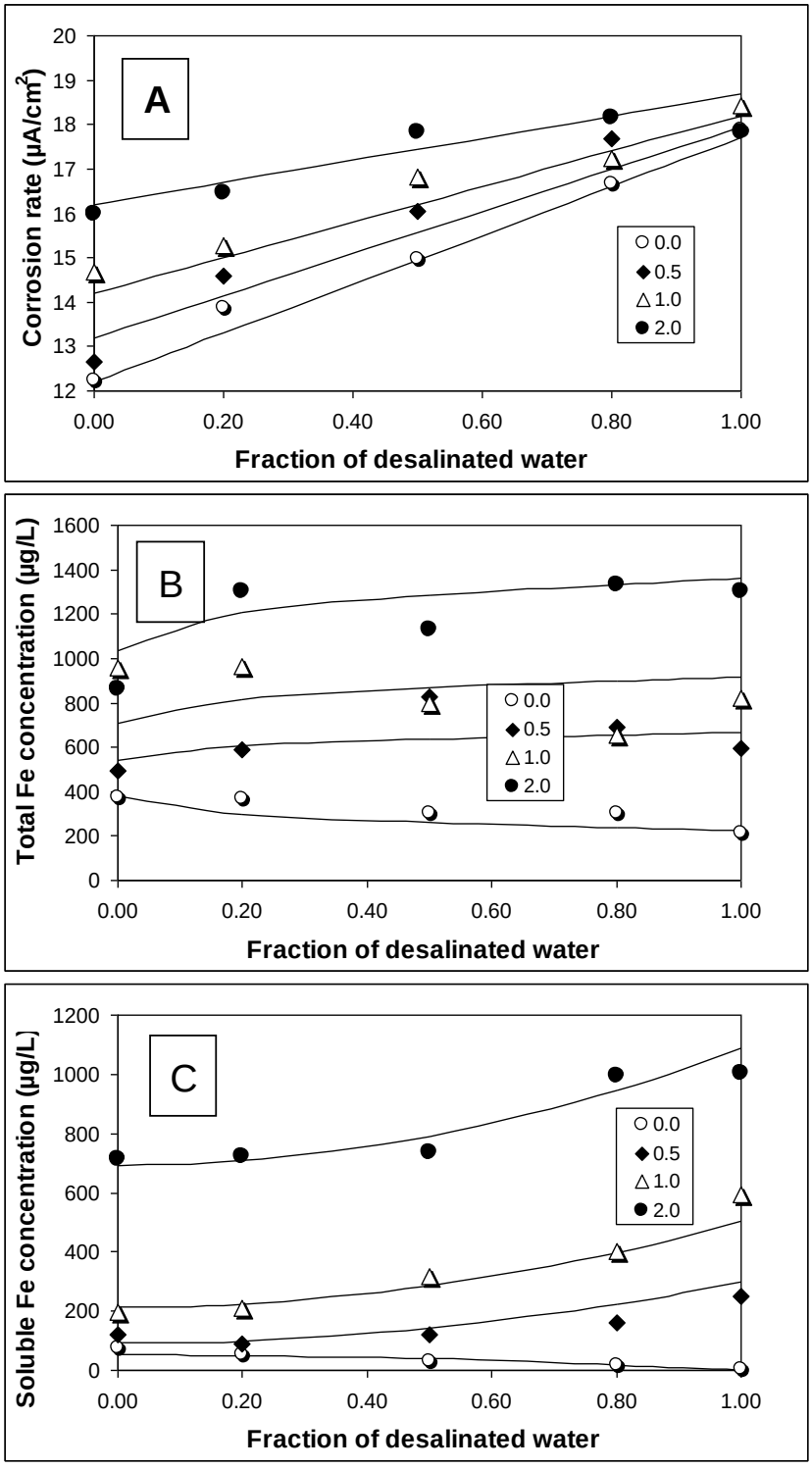

Figure 6.7 Effects of NOM concentration and anionic composition on the corrosion of iron in synthetic water. Alk. 120 mg/L, pH 7.5 (A) corrosion rates; (B) total iron release and (C) soluble iron release.

6.1.5 Retention of inorganic contaminants within/on iron corrosion scales

Impacts of blending of desalinated and surface water and also those of NOM on the retention of trace-level inorganic contaminants by corrosion scales are shown in Figure 6.8 and Figure 6.9. Retention ratios were determined the normalized (by its initial amount) difference between the initial spiked concentration (15 μg/L in this batch) and the final concentration of any specified analyte remaining in the solution over one week. The data presented in Figure 6.8 and Figure 6.9 are averaged values from week 6 to week 8.

These data demonstrate that in all cases the retention of lead, vanadium, chromium, copper and arsenic was consistently higher than that of zinc, cadmium, nickel and uranium.

The blending of desalinated and surface water did not have a pronounced impact on retention of these contaminants; although in some cases, for instance at DOC concentration of 1 mg/L, the retention of these elements decreases as the blending ratio increases. A similar but less pronounced effect can be seen at the DOC concentration of 0.5 mg/L.

In contrast with that, the influence of NOM on the retention of these elements is more significant, with NOM causing a prominent decrease of these elements' retention. In the absence of NOM, more than 90% of Pb, V, Cr, and Cu were accumulated within/on iron corrosion scales; while about 70-80% of Zn, Cd, and Ni were retained. Uranium behaved very differently from other inorganic contaminants. It was the least retained element (about 40-50%) and effects of blending ratio and NOM did not change its behavior significantly.

With increasing DOC, the retention ratio measured for many of the examined elements, expect uranium, decreased to less than 60% in 2 mg/L DOC water. The lower rate of retention of the examined inorganic contaminants in the presence of higher NOM levels indicates that the accumulation of metals in corrosion scales is likely to be higher at lower DOC concentrations that are expected for blended waters having high proportions of desalinated water, in comparison to typical surface waters.

6.2 Separation of effects of chloride, sulfate and NOM on metal corrosion, accumulation and release of inorganic contaminants with/from corroded metals

This part of the study was carried out in an attempt to separate effects of chloride and sulfate on the corrosion of iron. The concentrations of these ions did not change independently in the previous phase of experiments. Prior research shows that complex phenomena and yet insufficiently explored phenomena can be expected in this system. For instance, Imran et al. (2005) demonstrated that increases in red water occurrence with increases in chloride and sulfate concentrations. Lytle et al. (2003) also observed that total iron release increased in the presence of 100 mg/L of chloride. While these studies demonstrated that chloride and sulfate are aggressive anions with regards to iron release, they did not address NOM effect in the presence of these ions.

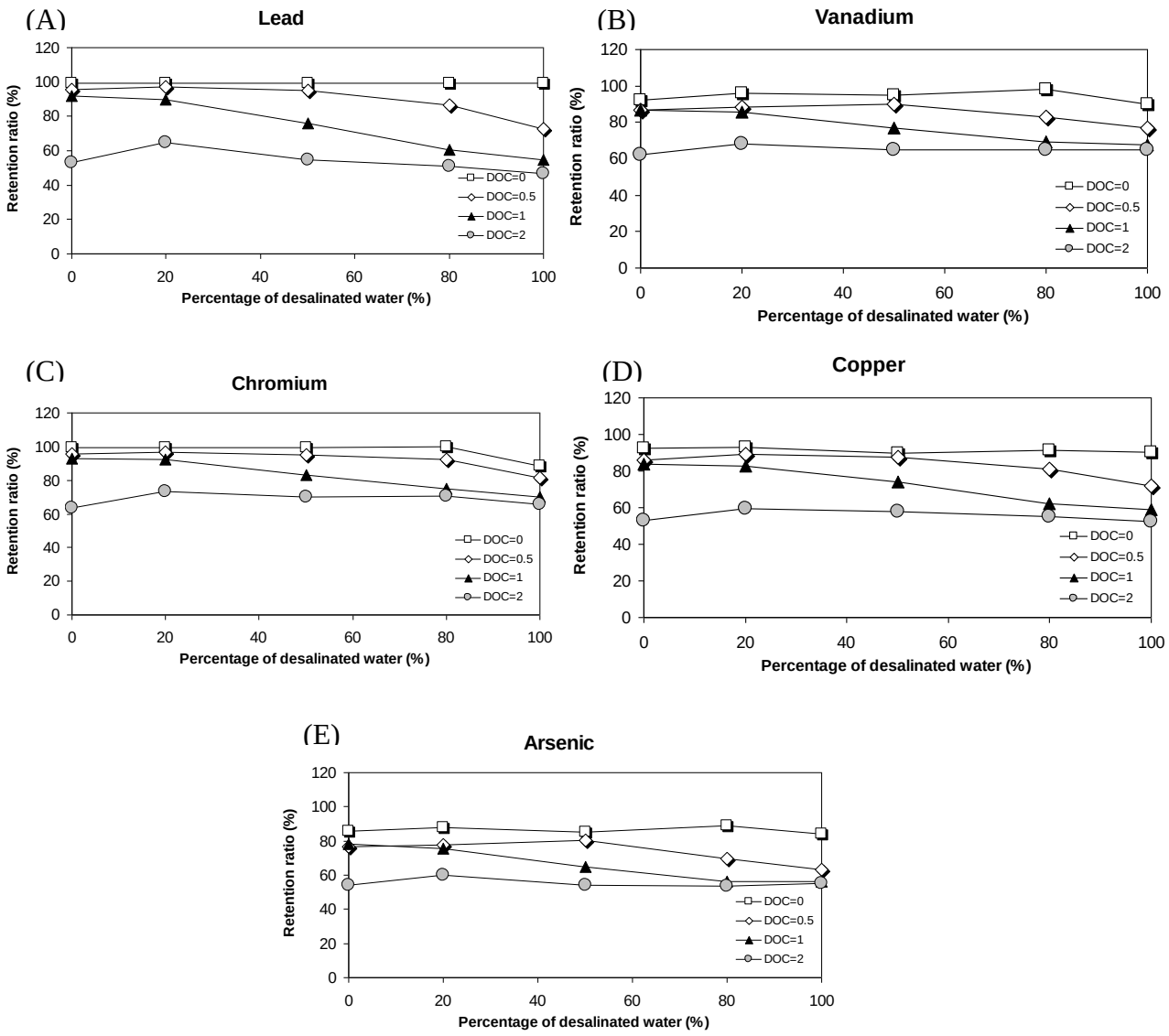

Figure 6.8 Impacts of blending of desalinated/surface water and NOM on the retention by corrosion scales of (A) lead; (B) vanadium; (C) chromium; (D) copper; and (E) arsenic. Initial concentrations of the heavy metals are 15 µg/L in all cases.

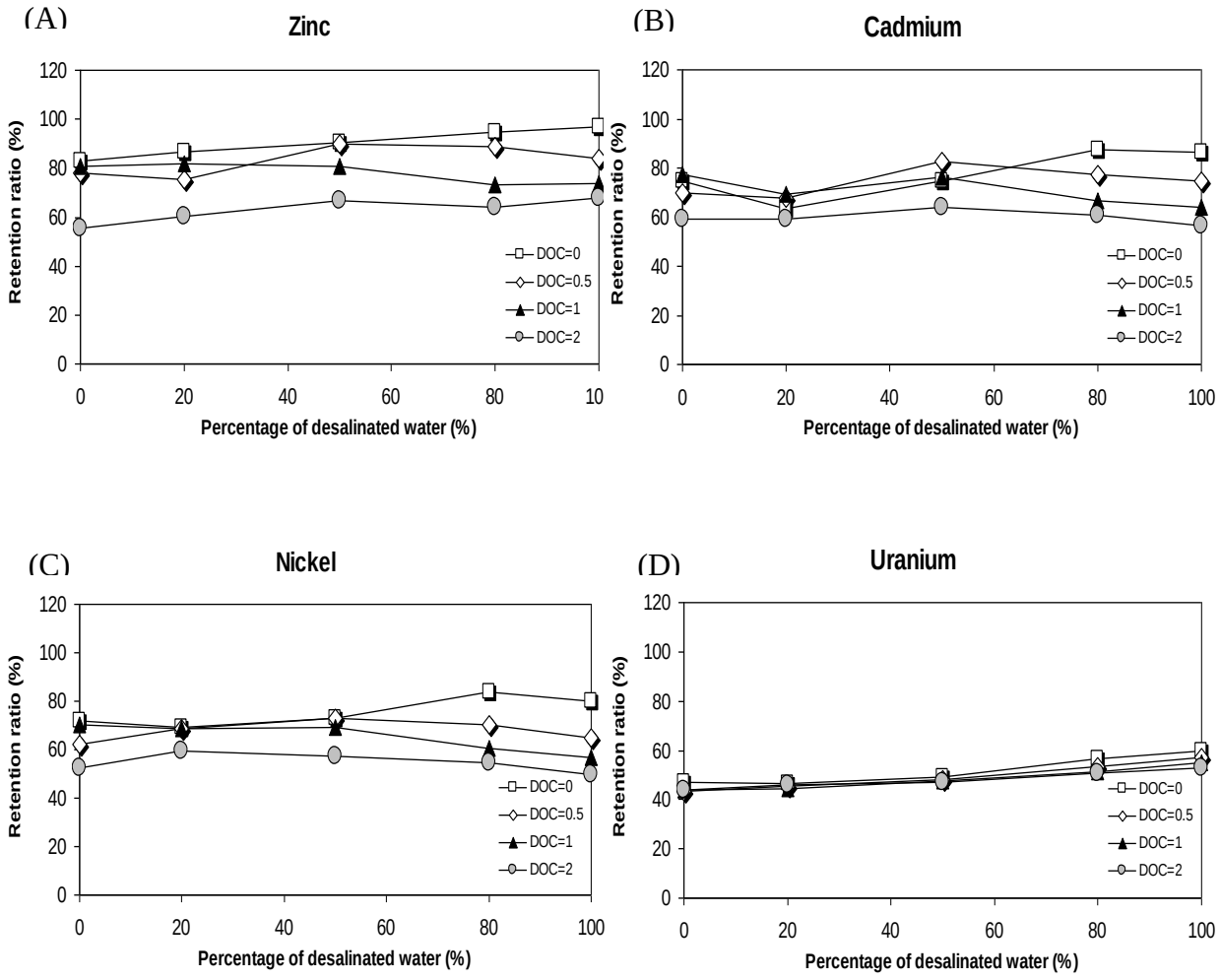

Figure 6.9 Impacts of blending of desalinated/surface water and NOM on the retention by corrosion scales of (A) zinc; (B) cadmium; (C) nickel; and (D) uranium. Initial concentrations of the heavy metals are 15 µg/L in all cases.

Our results presented above show that the influence of NOM can be significant. Accordingly, effects of anions (chloride or sulfate) and NOM on metal release, retention and release of inorganic contaminants were studied based on jar tests that employed iron, copper, lead/tin coupons and varying compositions of synthetic waters. Four levels of chloride (30, 80, 160, and 250 mg/L) or sulfate concentrations (0, 40, 80, and 120 mg/L) and two NOM concentrations (0 and 1 mg/L prepared from Suwannee River Fulvic Acid) were tested in this study. Details of these jar tests are described in the previous Materials and Methods chapter. Detailed water composition are shown in Table 3.3.3.

6.2.1 Iron release from iron coupons corroding in water containing varying levels of chloride and sulfate

Impacts of anions and NOM concentrations on iron release are shown in Figure 6.10 and Figure 6.11. Chloride effect on iron release was not pronounced until chloride concentration increased to as high as 250 mg/L; more iron was released at this high level of chloride. Compared with the influence of chloride, DOC significantly affected iron release. In the presence of DOC, soluble and total iron concentrations were four and two times, respectively, higher than those in the absence of DOC (Figure 6.10 (A) and (B)).

Changes of the fraction of soluble iron vs. chloride concentration and DOC indicated that the contribution of soluble to total iron increased as DOC increased (Figure 6.10 (C)). In the case of DOC 1 mg/L, more than 50% to 70% of released iron was in the operationally defined soluble iron fraction. In the absence of DOC, soluble iron accounted for less than 20% of the released iron.

Examination of sulfate effects (Figure 6.11) demonstrated that both soluble and total iron release increased as level of sulfate increased, especially in the presence of NOM. Effects

of DOC on iron release were more pronounced than those of sulfate. Similarly to what was observed for combined chloride and DOC effects, soluble and total iron released in water with varying sulfate levels increased four and two times more than those in the absence of DOC (Figure 6.11 (A) and (B)).

However, the behavior of the fraction of soluble iron was somewhat different from that in the case of the chloride/DOC. That is, in the presence of DOC the contribution of soluble iron decreased as the sulfate concentration increased (Figure 6.11 (C)). In the case of DOC 1 mg/L, fraction of soluble iron decreased from about 60% to 35% as sulfate level increased from 0 to 120 mg/L.

6.2.2 Impact of anions and NOM on iron corrosion rates and scale retention factors

Iron corrosion rates and scale retention levels were determined by weight loss measurements. The formulas of the apparent corrosion rate ($i_{corr}^{\Delta W}$) and scale retention factor (SR) were described in detail in previous section 6.1.2. The data present in Figure 6.12 were the average values of the two coupons; the difference between two coupons had an average standard deviation of ±10% and ±25% for corrosion rates and SR, respectively. The apparent corrosion rate (Figure 6.12 (A)) showed that as the chloride level increased, so did the corrosion rate. In contrast to chloride, the effect of sulfate on corrosion rate in the absence of DOC was not prominent. In general, NOM slightly increased corrosion rates only slightly. Although a dramatic increase was observed at the highest sulfate level, this may be an artifact.

Measurements of SR values (Figure 6.12 (B)) indicated that, in the absence of NOM, increases of chloride concentrations to 160 mg/L caused the SR values to increase but they decreased at higher chloride concentration. However, in the presence of NOM, SR

values were always higher (in the range 0.90 to 0.95) and decreased slightly with the increasing chloride level.

Increase of sulfate concentrations level always resulted in lower SR values. Similarly to the chloride/NOM system, SR values in the presence of NOM were in the range 0.80 to 0.95 and always considerably higher than those in the absence of NOM.

In prior research, NOM was observed to decrease corrosion rates of galvanized steel and cast iron (Sontheimer et al., 1981; Benjamin et al., 1996). However, Suwannee River fulvic acid added in our study slightly increased the iron corrosion rate. NOM was also observed to promote the formation of more protective scales (McNeill and Edwards, 2001; Benjamin et al., 1996). In accord with these observations, we also found that scale retention factors in the presence of NOM were consistently higher than those without NOM. This suggests the formation of more stable scales on the surface of corroding iron. This indeed agrees strongly with the results of our SEM, XRD and EXAFS examination of scales formed in blends of desalinated and conventionally treated water (Liu et al., 2011). This also means that variations of NOM concentrations rather than sulfate and/or chloride levels in the blends are likely to be major cause of the observed effects.

6.2.3 Retention and release of inorganic contaminants within/from iron corrosion scales

Retention of heavy elements within iron corrosion scales

Impacts of chloride and NOM at a constant sulfate level (80 mg/L) on the retention of inorganic contaminants by iron corrosion scales are demonstrated in Figure 6.13 and

Figure 6.14. These effects were very different for systems with and without organic carbon.

In the absence of NOM, the retention percent of tested elements decreased in the following order: lead > vanadium > chromium > copper > arsenic > zinc > cadmium > nickel > uranium. The retention of lead was highest and reached almost 100% of that initially present in the water. On the other hand, the retention rate determined for uranium was between 20 to 35%.

Higher levels of chloride did not significantly affect the retention of most elements, except copper and, in a more complicated fashion, cadmium and nickel. The retention of copper decreased almost linearly with the concentration of chloride from ca. 85% to 55% for chloride concentration of 30 and 250 mg/L respectively.

NOM had a considerably more prominent effect on the retention of these contaminants. When the DOC concentration was increased from 0 to 1 mg/L, the retention of lead, vanadium and chromium dropped from more than 80% to 30%. The influence of NOM on copper retention was even more pronounced, and almost no copper was retained by the corrosion scales in the presence of NOM and the highest chloride concentration. The effect of NOM on the retention of zinc, cadmium, and nickel was lesser, and the retention of uranium did not exhibit consistent changes caused by variation of chloride or NOM concentrations.

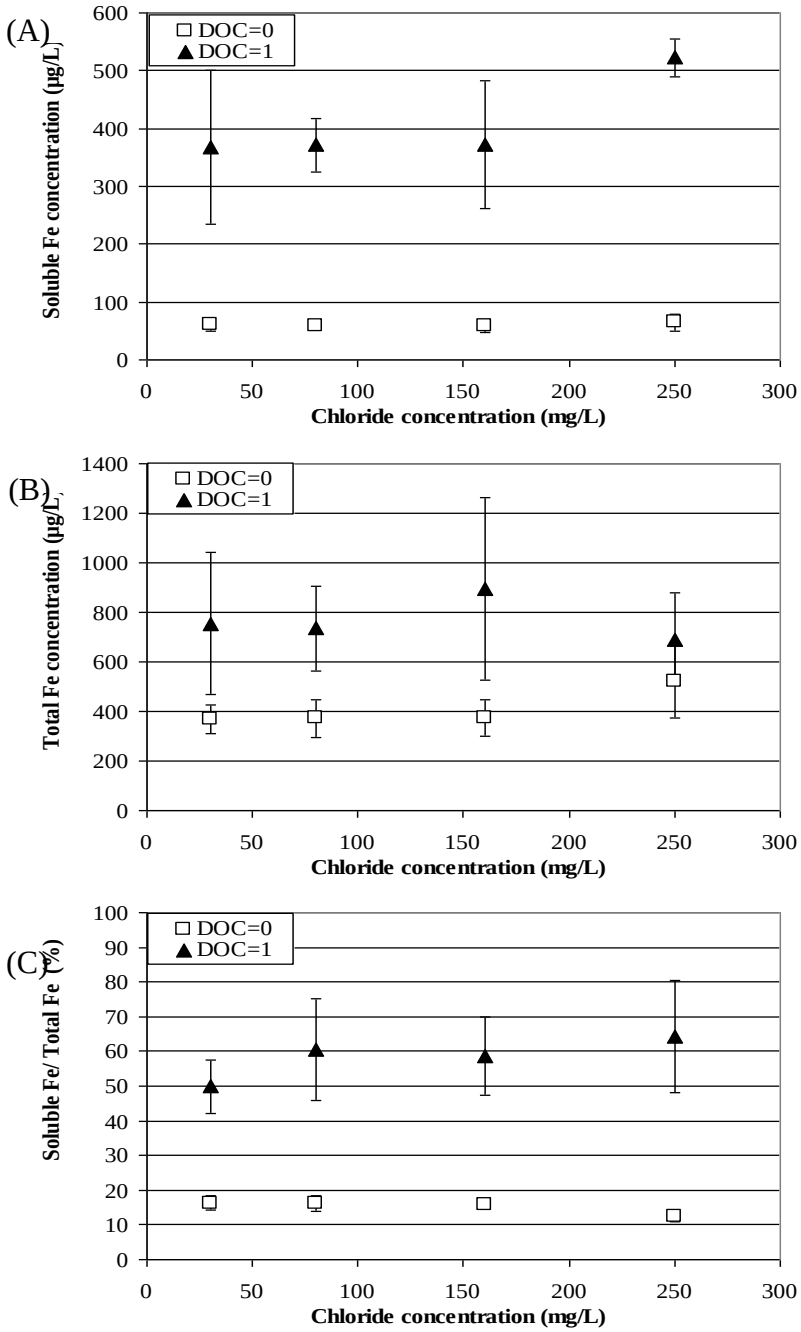

Figure 6.10 Effects of chloride and DOC concentrations on the average (A) soluble, (B) total iron concentrations and (C) fraction of soluble iron released from iron coupons during exposure week 6 to 8. The error bar corresponds to ±1 standard deviation. Calcium, magnesium and sulfate concentrations were fixed at 20, 10, and 80 mg/L, respectively.

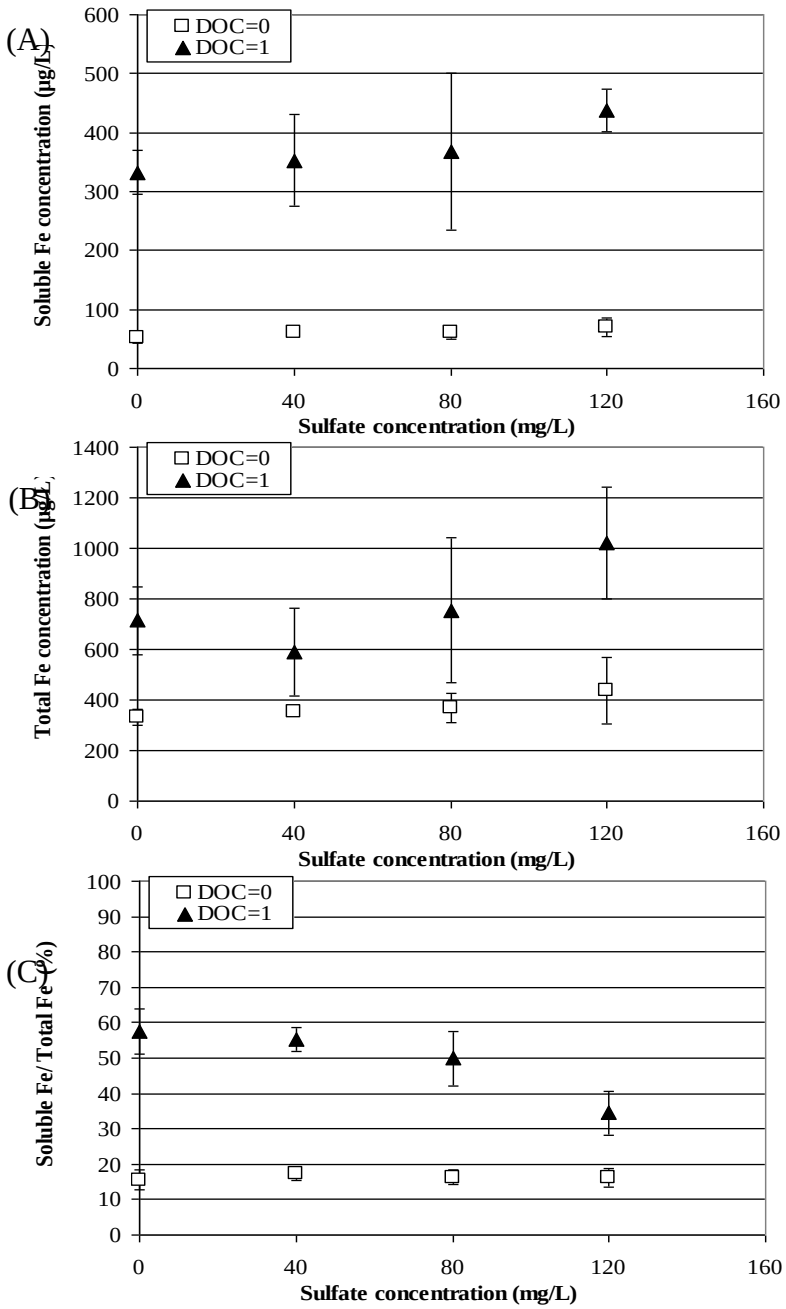

Figure 6.11 Effects of sulfate and DOC concentrations on the average (A) soluble, (B) total iron concentrations and (C) fraction of soluble iron released from iron coupons during exposure week 6 to 8. The error bar corresponds to ±1 standard deviation. Calcium, magnesium and chloride concentrations were fixed at 20, 10, and 30 mg/L, respectively.

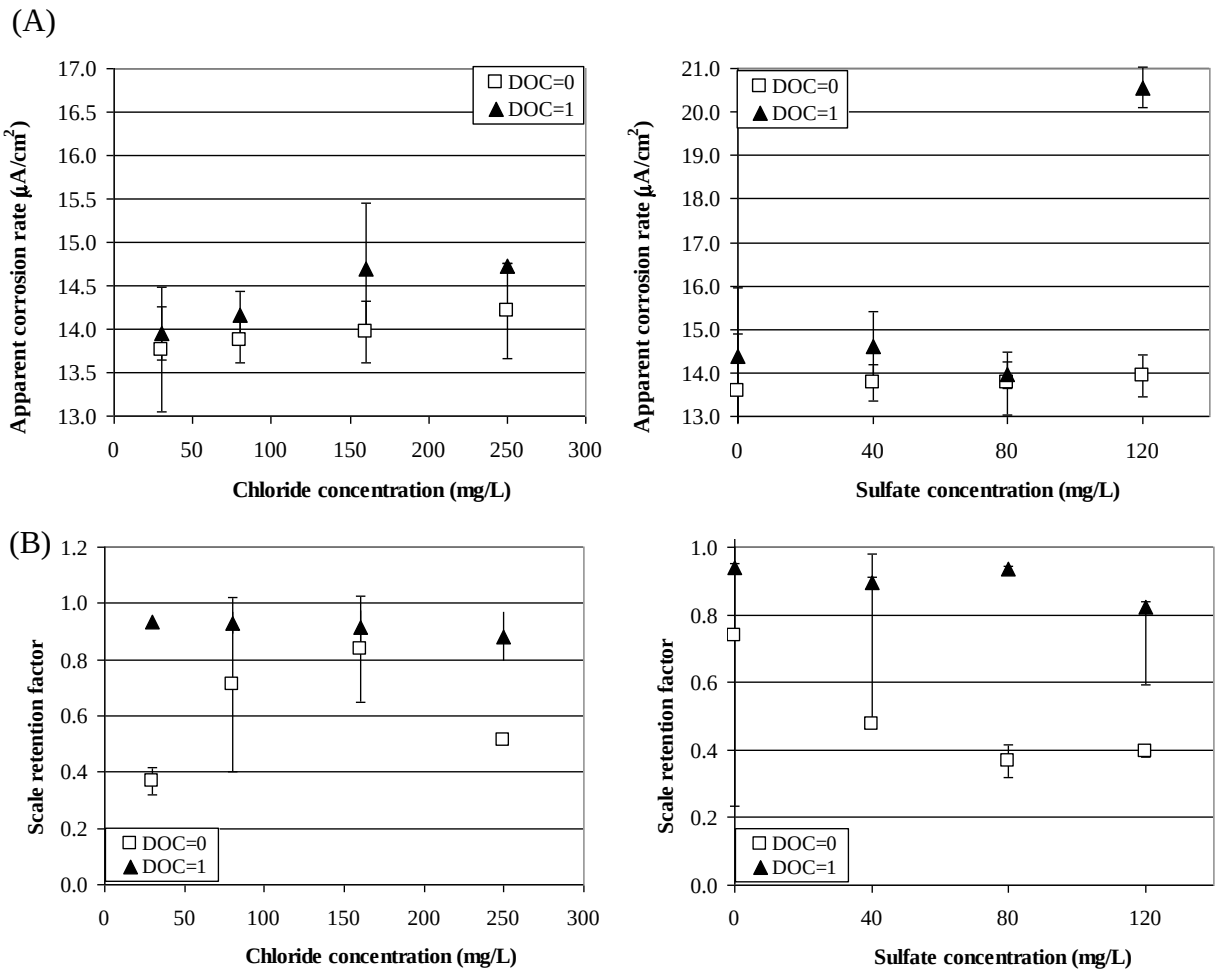

Figure 6.12 Impacts of chloride/sulfate and NOM concentrations on (A) apparent corrosion rates and (B) scale retention factors based on weight loss measurements for iron coupons.

Impacts of sulfate and those of NOM at a fixed chloride level (30 mg/L) on the retention of inorganic contaminants by iron corrosion scales are demonstrated in Figure 6.15 and Figure 6.16. The general trend of retention of these elements was similar to those in waters containing chloride and NOM. In the absence of NOM, higher levels of sulfate led to somewhat lower retention of the tested elements although this effect was not very consistent.

In the presence of NOM, variations of sulfate in the range below 80 mg/L generally did not affect the retention of the heavy metals. However, the retention of all elements increased at the highest level of sulfate (120 mg/L). The presence of NOM invariably reduced the retention of all tested elements. The impacts of NOM on retention of lead, vanadium, chromium, copper, and arsenic were more significant than those on zinc, cadmium, nickel, and uranium. Even in the case of uranium whose retention by iron scales was only marginally affected by variations of chloride and NOM, the introduction of NOM in the sulfate/NOM system resulted in a slight but consistent decrease of the retention of this element.

Release of heavy elements from iron corrosion scales

Following the eight-weeks exposures designed to determine the extent of retention of the selected inorganic contaminants by iron scales formed in varying water chemistries, one of the coupons present in the selected jars was exposed to a different water composition. This was done to test the effect of DOC, chloride and combined effect of DOC and chloride on the release of accumulated inorganic contaminants. The logistics of these experiments is described in detail in Material and Methods section 3.3.2.4. Detailed experimental conditions for release of inorganic contaminants can refer to Table 3.3.4.

These experiments demonstrated that among the accumulated contaminants, copper, chromium, zinc and nickel were the most mobile elements. Figure 6.17 demonstrates the cumulative percent (%) of copper, chromium, zinc and nickel that was released over eight weeks in the experiment designed to examine the mobility of the retained metals. The cumulative release percentage was determined by summing up soluble concentrations released from coupon over eight weeks divided by accumulated amount within coupon.

Effect of changing the DOC concentration while maintaining the same anionic composition of the ambient water is shown in the first group of the data (Fe11-W1 and Fe1-W11).

When the coupon had been exposed in water containing 1 mg/L DOC and switched to water having 0 mg/L of NOM, 34.4%, 14.9%, and 5% of the retained copper, chromium, and zinc were released during eight weeks, respectively. On the other hand, when the coupon had been exposed to organic-free water and switched to that with a 1 mg/L DOC level, only 10.8%, 4.4%, and 4% of retained copper, chromium, and zinc were released during eight weeks, respectively. However, it needs to be kept in mind that the amounts of inorganic contaminants accumulated on or within corrosion scales on coupons that had corroded in the presence of DOC waters were less than those formed in the absence of DOC water.

The extent of chloride effects on the release of the retained contaminants is shown in Group 2 of the data (Fe7-W3 and Fe3-W7). This demonstrates that variations of chloride in water did not significantly affect release of these contaminants. Both for water that had corroded at low chloride concentration and switched to that with high chloride, and vice versa, 20%, 5%, 4%, and 4% of copper, chromium, nickel, and zinc were released during

the eight weeks of exposures carried out to determine the mobility of the heavy metals. As for combined effects of chloride and NOM (group 3: Fe17-W2 and Fe2-W17), about 50% and 28% of retained copper were released when coupons switched to opposite water qualities.

The cumulative eight-week releases of all the other accumulated elements including vanadium, arsenic, cadmium, lead, and uranium were less than 3% of the amount accumulated during the initial exposures. It indicated that once retained within the scales these elements became stable and largely not susceptible to changes of water compositions.

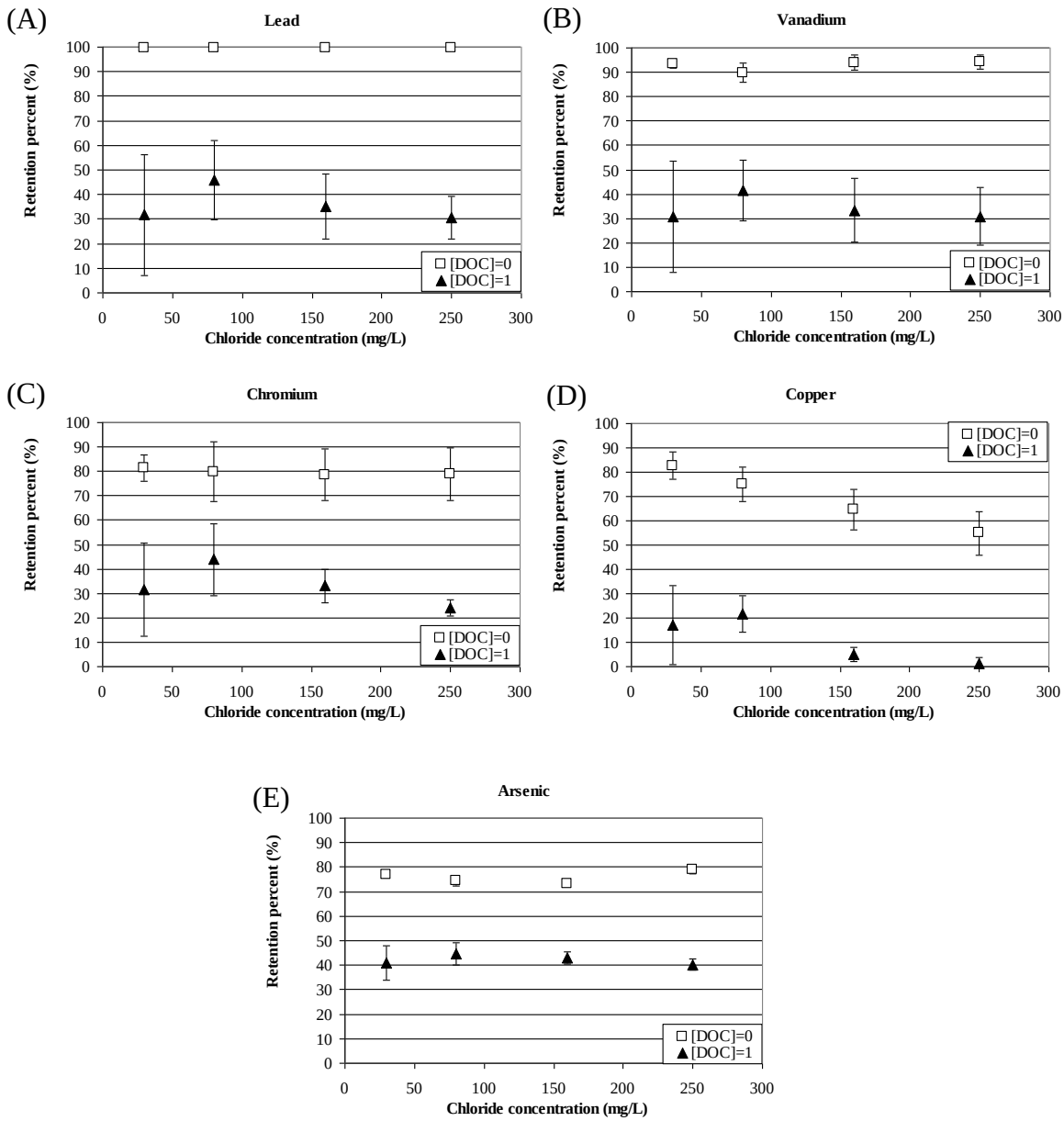

Figure 6.13 Impacts of chloride and NOM on the retention by corrosion scales of (A) lead; (B) vanadium; (C) chromium; (D) copper; and (E) arsenic. Initial concentrations of the heavy metals are 5 μg/L in all cases.

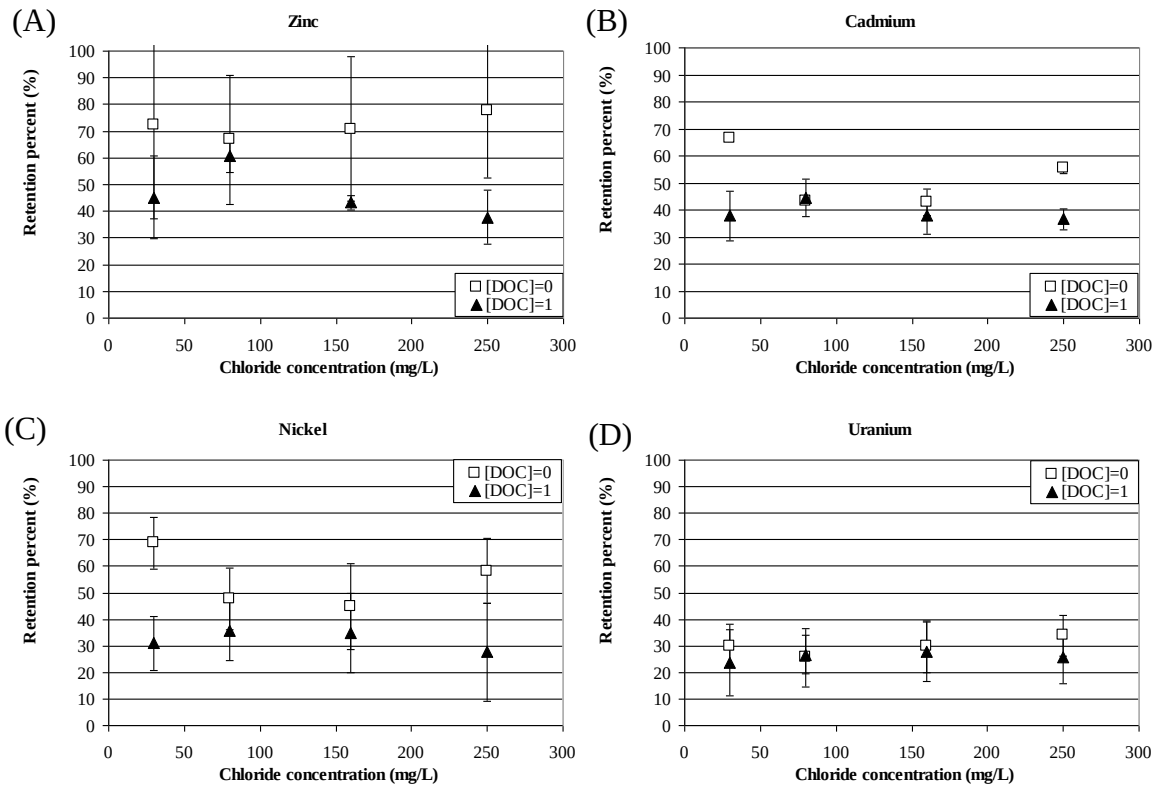

Figure 6.14 Impacts of chloride and NOM on the retention by corrosion scales of (A) zinc; (B) cadmium; (C) nickel; and (D) uranium. Initial concentrations of the heavy metals are 5 μg/L in all cases.

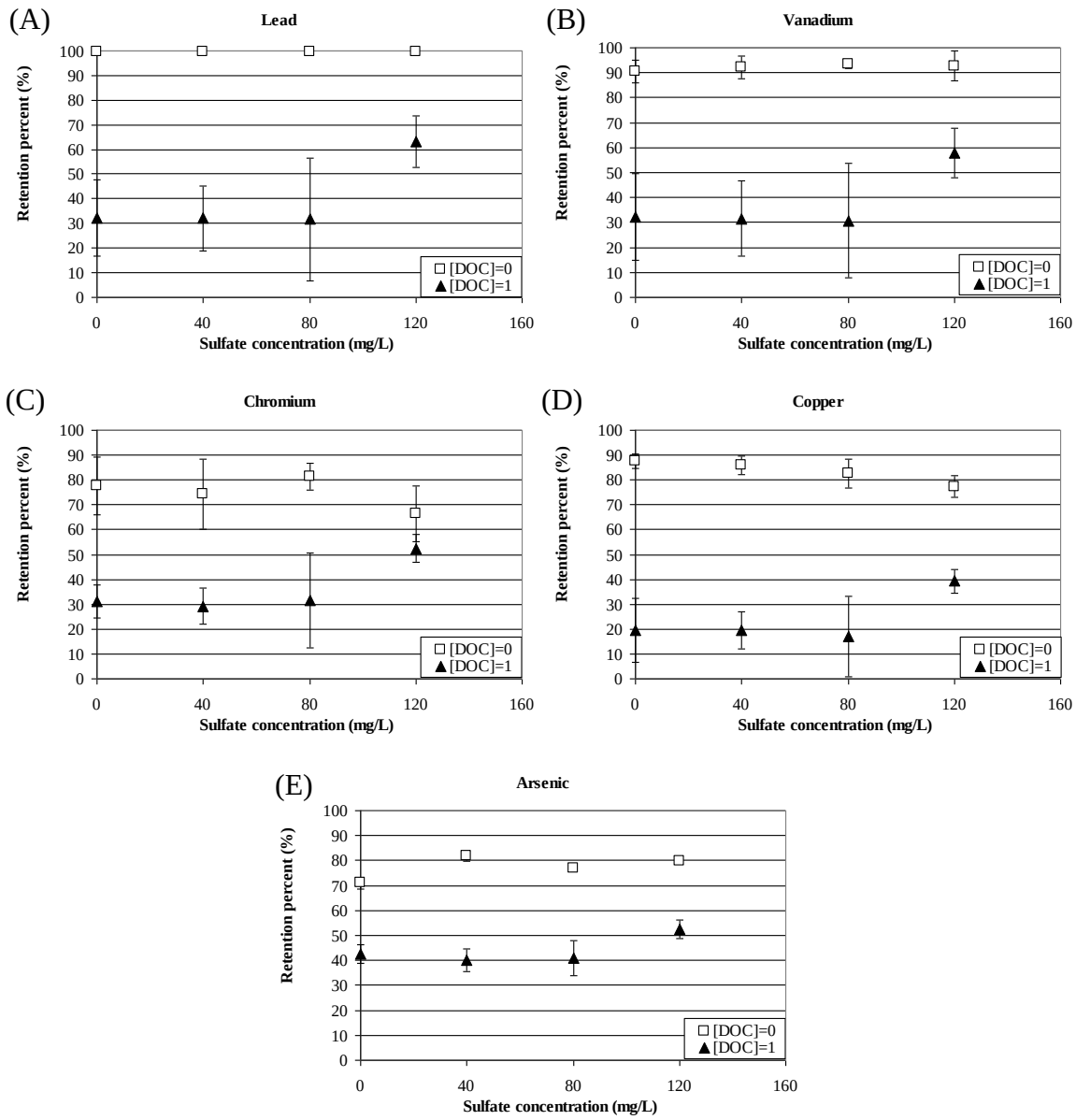

Figure 6.15 Impacts of sulfate and NOM on the retention by corrosion scales of (A) lead; (B) vanadium; (C) chromium; (D) copper; and (E) arsenic. Initial concentrations of the heavy metals are 5 μg/L in all cases.

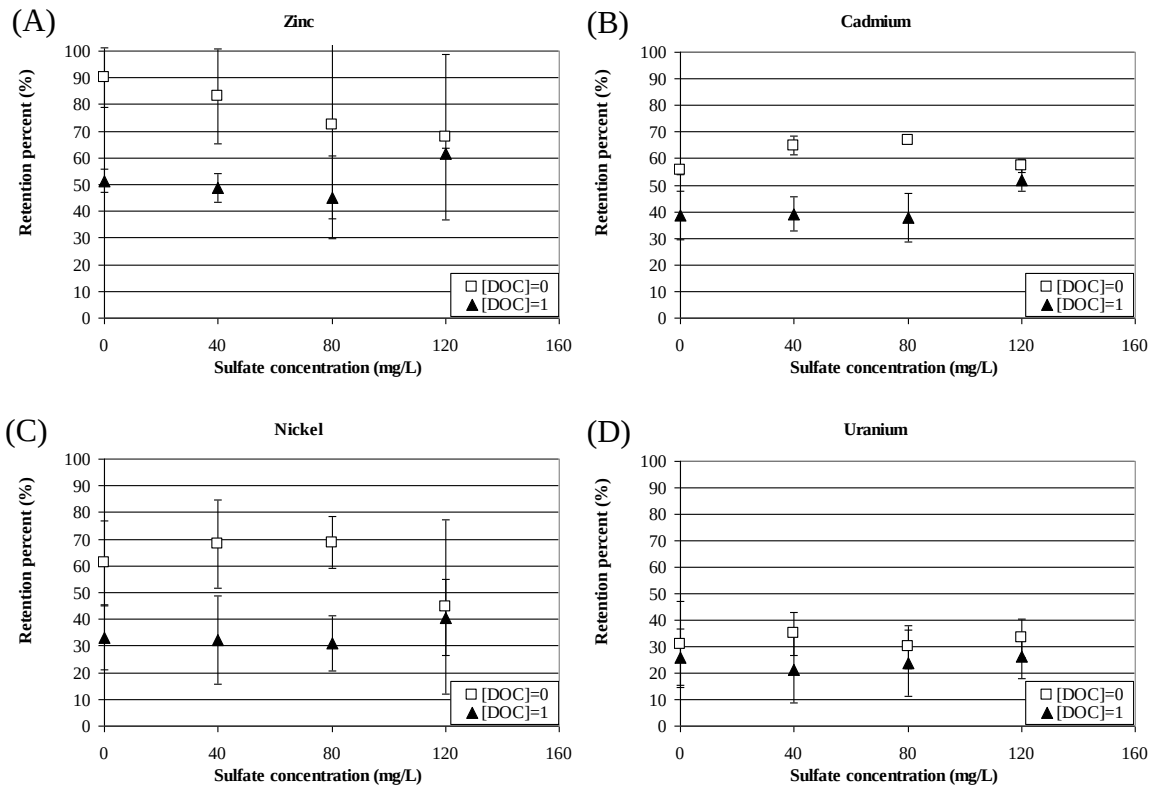

Figure 6.16 Impacts of sulfate and NOM on the retention by corrosion scales of (A) zinc; (B) cadmium; (C) nickel; and (D) uranium. Initial concentrations of the heavy metals are 5 μg/L in all cases.

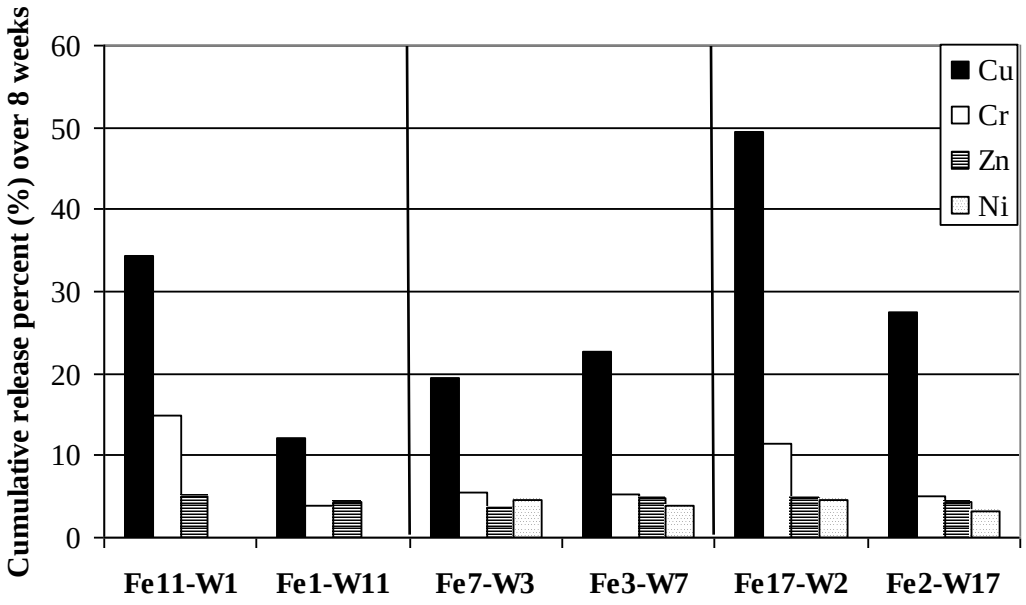

Figure 6.17 Cumulative release percent (%) of copper, chromium, zinc and nickel in the release experiment over eight weeks. Experimental conditions for release study can refer to Table 3.3.4.

6.2.4 Copper or lead release from corroding copper or lead/tin coupons

In the case of exposures of copper and lead/tin solder coupons, almost all released copper and lead were found to exist in soluble form. Accordingly, only soluble copper and lead concentrations were used to describe relevant impacts of water chemistry in the following discussion.

Figure 6.18 shows effects of chloride, sulfate, and NOM on the average of copper and lead concentrations from the corroding copper and lead/tin coupons. In the absence of NOM, Cu concentrations slightly decreased as chloride or sulfate increased (Figure 6.18 (A)). For example, at DOC 0 mg/L, soluble Cu decreased from 225 to 175 μg/L as chloride changed from 30 to 250 mg/L. The presence of NOM promoted the soluble Cu release at least 1.5 to 2.5 times higher than those without NOM. The increasing anion levels only slightly increased soluble Cu concentrations. For instance, soluble Cu

increased from 225 to 383 μg/L as DOC increased from 0 to 1 mg/L. With increasing chloride concentrations at DOC 1 mg/L, soluble Cu only increased from 383 to 430 μg/L as chloride changed from 30 to 250 mg/L.

The magnitude of lead release was much smaller than copper release (Figure 6.18 (B)). Less than 100 μg/L of lead was found in the tested conditions. In the case of Pb release, impacts of anions were very different from those observed for copper. Higher chloride levels enhanced Pb release but higher sulfate levels reduced it. The presence of NOM still promoted lead release, especially at high DOC and chloride concentrations. For example, at a chloride concentration of 250 mg/L, lead concentration increased from 21 to 83 μg/L as DOC increased from 0 to 1 mg/L. Sulfate effect on lead release was totally different from that of chloride effect. Specifically, increasing sulfate levels caused Pb release to decrease. This was especially notable in water containing 1 mg/L DOC. In that case, on the absence of sulfate, lead concentration was 91 μg/L but it dropped to 21 μg/L as sulfate increased to 120 mg/L.

The observed pronounced effects NOM on copper and lead release are comparable with those reported in previous studies (Schock et al., 1996; Korshin et al., 2005; Burlingame et al., 2006). They are likely to have been caused by the formation of Cu- or Pb-NOM complexes and also surface charges effects of NOM but these aspects of NOM effects were not examined in this study.

6.2.5 Retention and release of inorganic contaminants within/from copper or lead/tin coupons

Retention of inorganic contaminants within copper or lead/tin coupons

Figure 6.19 and Figure 6.20 demonstrate the impacts of chloride, sulfate and NOM on the retention of inorganic contaminants by copper coupons. The retention levels of almost all the tested elements were less than 20%, except chromium which had more than 50% retention on the copper coupons in the absence of NOM.

Interactions of the inorganic contaminants with corroding copper surfaces did not undergo significant changes with increasing chloride or sulfate levels. NOM effects were more pronounced, especially for chromium. As was seen in the case of iron corrosion, the retention of the heavy metals in the presence of NOM was lower than that without NOM. For instance, in the case of chromium, more than 50% of the Cr initially present in the ambient water was retained by copper coupons in the absence of NOM. The retention of Cr decreased to less than 20% in the presence of NOM.

Figure 6.21 and Figure 6.22 show the impacts of chloride, sulfate and NOM on the retention of inorganic contaminants by lead/tin coupons. Six of the eight tested elements had retention rates < 20% in these experiments. Only chromium and copper had higher retentions in the absence of NOM.

In the absence of NOM, the retention of these elements increased as the chloride concentration increased from 30 to 160 mg/L and decreased at higher chloride levels. As was uniformly the case for the other studied metals, the retention of the heavy metals on lead/tin solder decreased in the presence of NOM.

The effect of sulfate on the retention of the heavy elements was different from that of chloride. In general, the retention of elements, except copper, decreased as sulfate concentration increased from 0 to 80 mg/L, and then slightly increased as sulfate concentration increased further from 80 to 120 mg/L. The behavior of copper was somewhat different because its retention sharply decreased from more than 50% to 4% as sulfate concentration increased form 40 to 120 mg/L in the absence of NOM.

Release of inorganic contaminants from copper or lead/tin coupons

Similarly to how it was done with the iron coupons, after eight weeks of exposures in the presence of the inorganic contaminants in the ambient water, selected copper or lead/tin coupons were exposed to different water compositions. This was done to test the effect of DOC, chloride and combined effect of DOC and chloride on the release of accumulated inorganic contaminants. Detailed information concerning these release experiment is presented in Material and Methods section 3.3.2.4. Detailed experimental conditions are shown in Table 3.3.4.

Figure 6.23 (A) shows the cumulative release (in % units) of pre-accumulated inorganic contaminants from copper coupons. The data show that zinc, lead, chromium, vanadium, and nickel were relatively easily desorbed from the copper coupons due to water chemistry changes. For instance, when the selected copper coupons were switched from water that initially contained 1 mg/L DOC to that without NOM (group 1:Cu11-W1 and Cu1-W11), 88.9%, 66.8%, 62.3% and 31.2% of the retained Zn, V, Cr and Pb were released, respectively. In contrast, when copper coupons switched from water whose initial DOC was 0 to that with a 1 mg/L DOC level, only 24.4%, 7.8%, 6.5%, and 6.3% of retained Zn, Pb, V, and Cr were released, respectively. This appears to indicate that

metals retained on the surface of copper coupons in the presence of DOC retain their mobility, possibly because of the formation of strong NOM-metal complexes.

The effect of chloride variations on the mobility of the heavy elements retained on copper surface was largely insignificant, as was the case in the experiments with iron coupons. Combinations of chloride and NOM variations caused effects (group 3: Cu17-W2 and Cu2-W17) similar to those caused by chloride variations only (Cu7-W3 and Cu3-W7).

Figure 6.23 (B) shows the cumulative release of inorganic contaminants pre-accumulated on the lead/tin coupons. Zinc, copper, chromium, vanadium, nickel were more sensitive to changes of water qualities than the other contaminants, and most of them were relatively easily mobilized. Pre-retained zinc, copper, chromium, and vanadium were somewhat sensitive to changes of DOC. In contrast with the results for copper coupons, chloride exerted a significant effect on the release of the inorganic contaminants from lead/tin coupons. When lead/tin coupons were switched from a low (30 mg/L) to a high (250 mg/L) chloride level, more than 80% of the pre-retained Zn, Cu, V, Ni, and Cd were released during the 8 weeks of exposures in water without these contaminants. (Group 2: Pb3-W7). In the case of combined effects of chloride and DOC, almost all the retained Zn and V were released back to water as chloride and DOC both increased from low to high level (Group 3: Pb2-W17).

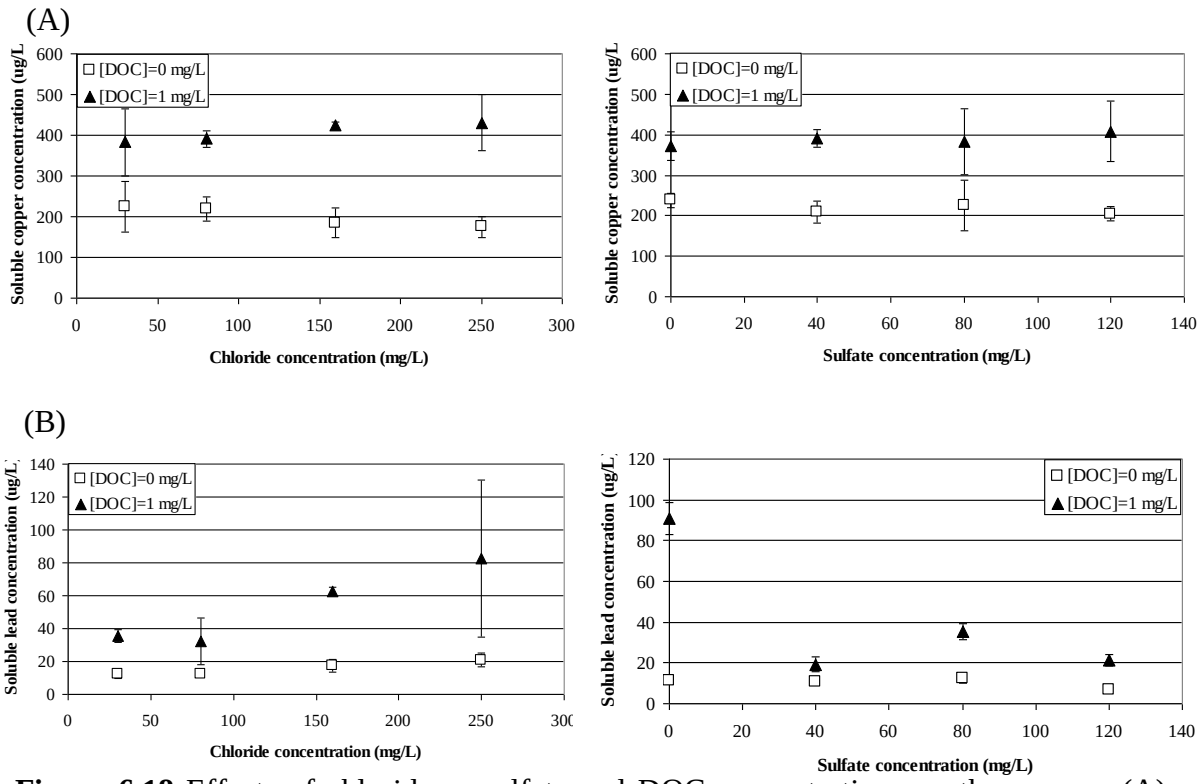

Figure 6.18 Effects of chloride or sulfate and DOC concentrations on the average (A) soluble copper, and (B) soluble lead concentrations released from copper or lead/tin coupons during exposure week 6 to 8. The error bar indicated ±1 standard deviation.

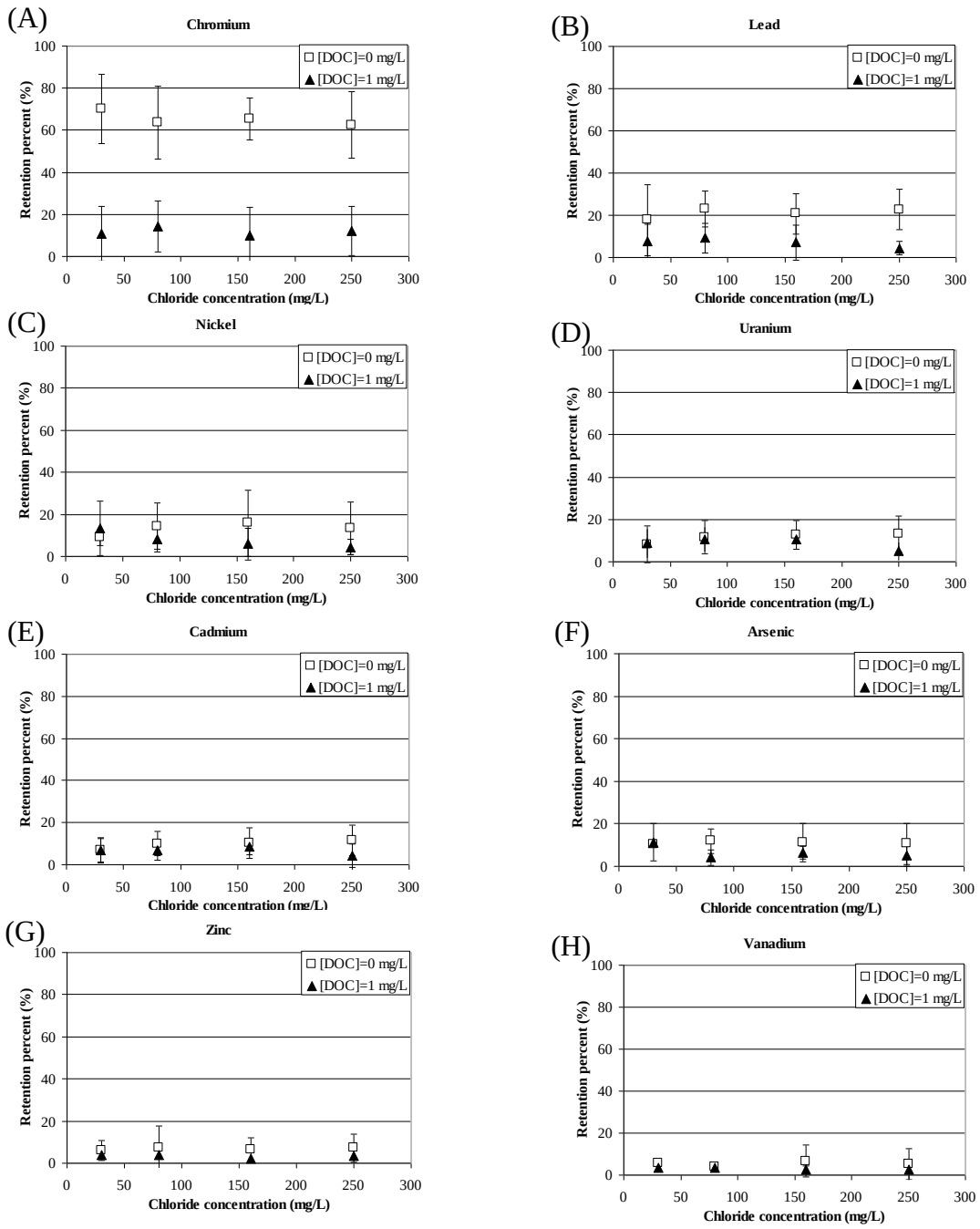

Figure 6.19 Impacts of chloride and NOM on the retention by copper coupons of (A) chromium; (B) lead; (C) nickel; (D) uranium; (E) cadmium; (F) arsenic; (G) zinc; and (H) vanadium. Initial concentrations of the heavy metals are 5 μg/L in all cases.

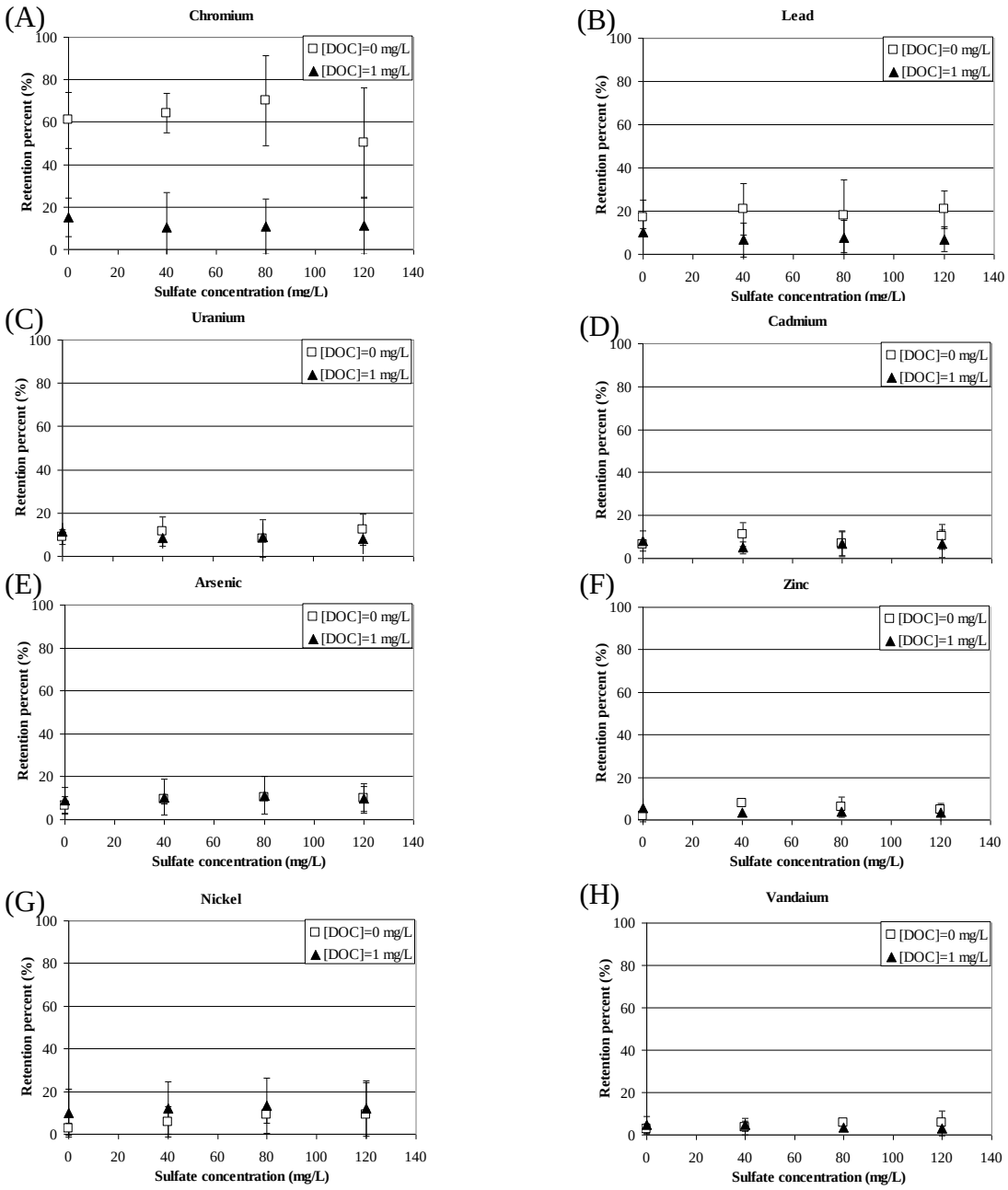

Figure 6.20 Impacts of sulfate and NOM on the retention by copper coupons of (A) chromium; (B) lead; (C) uranium; (D) cadmium; (E) arsenic; (F) zinc; (G) nickel; and (H) vanadium. Initial concentrations of the heavy metals are 5 μg/L in all cases.

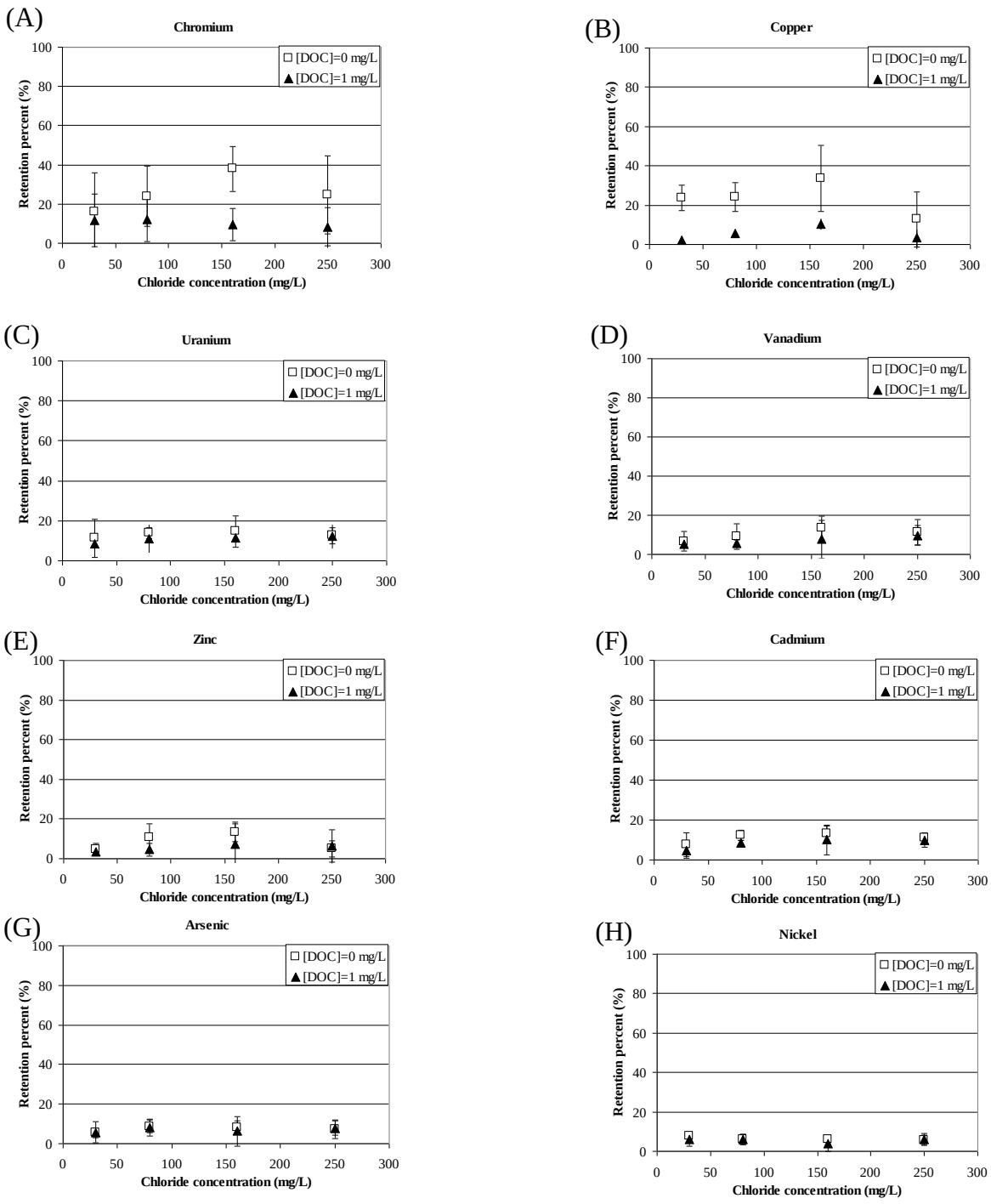

Figure 6.21 Impacts of chloride and NOM on the retention by lead/tin coupons of (A) chromium; (B) copper; (C) uranium; (D) vanadium; (E) zinc; (F) cadmium; (G) arsenic; and (H) nickel. Initial concentrations of the heavy metals are 5 μg/L in all cases.

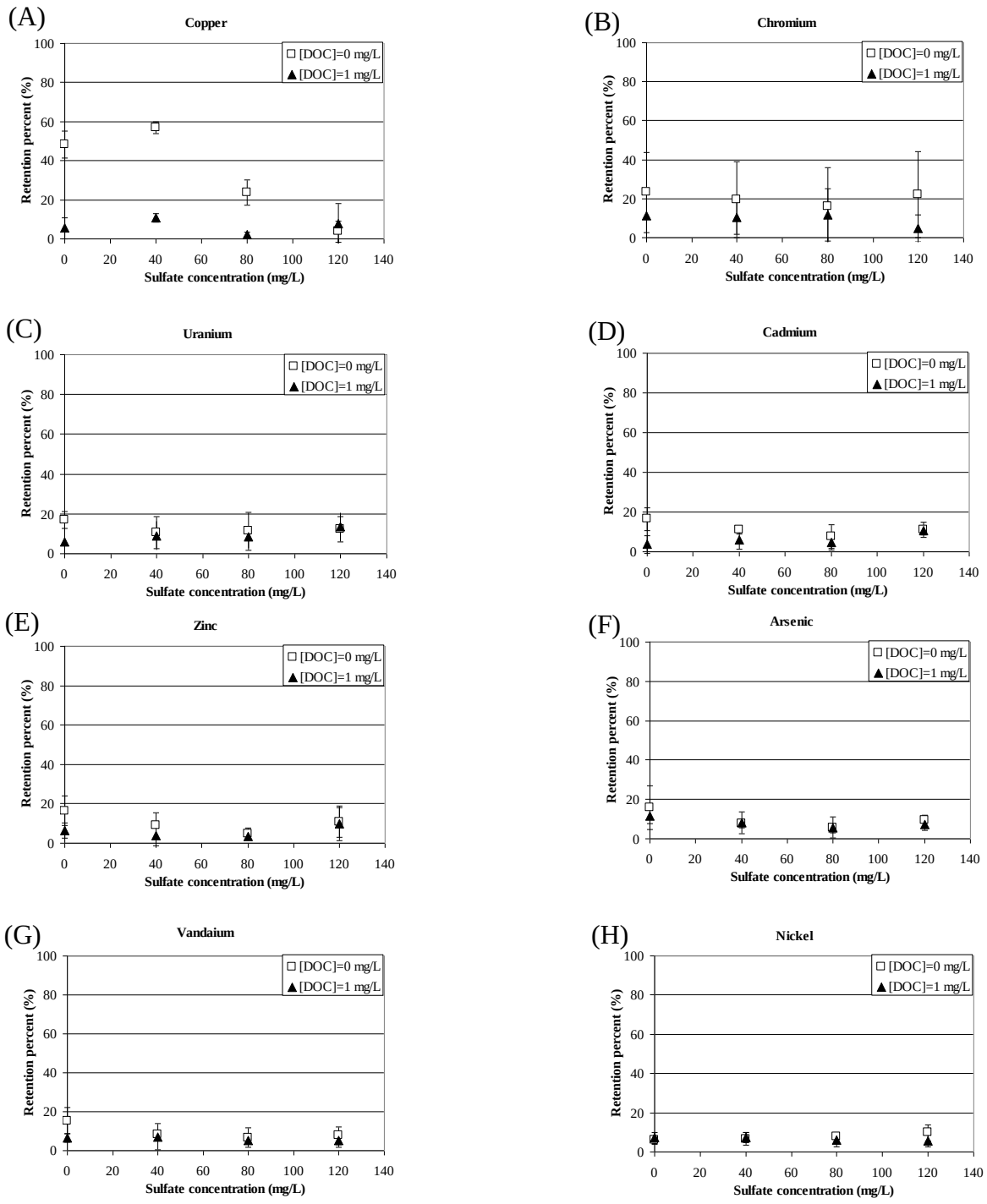

Figure 6.22 Impacts of sulfate and NOM on the retention by lead/tin coupons of (A) copper; (B) chromium; (C) uranium; (D) cadmium; (E) zinc; (F) arsenic; (G) vanadium; and (H) nickel. Initial concentrations of the heavy metals are 5 μg/L in all cases.

(A)

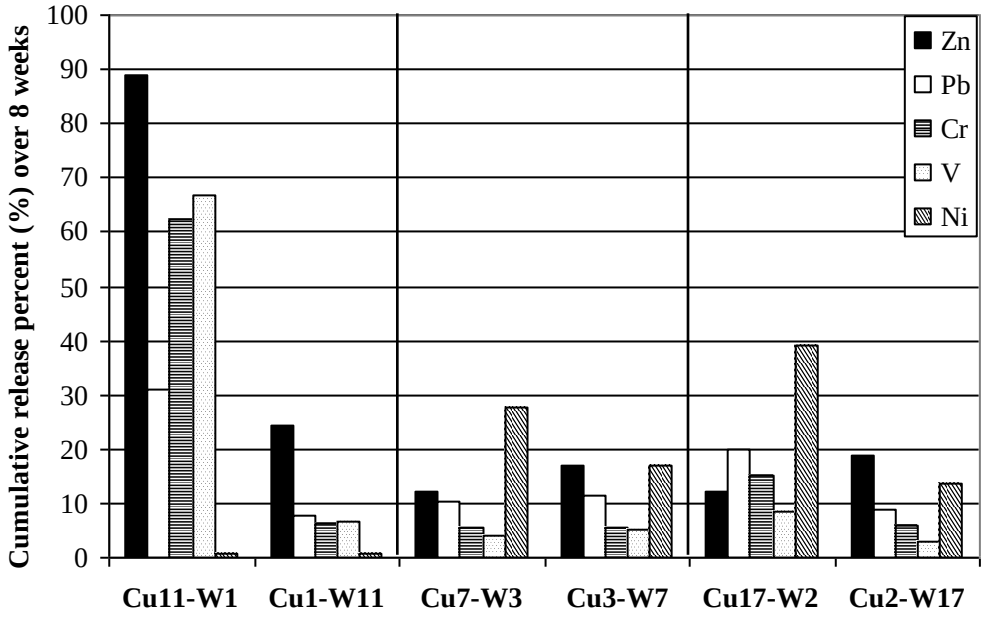

(B)

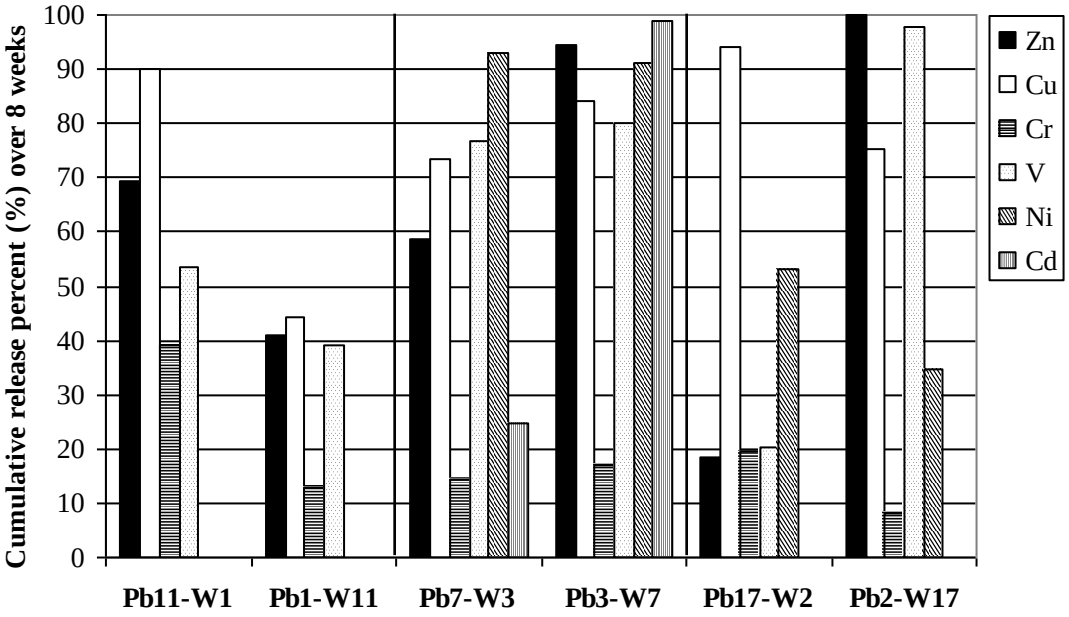

Figure 6.23 Cumulative release percent (%) of accumulated inorganic contaminants from (A) copper coupons (B) lead/tin coupons in the release experiment over eight weeks. Experimental conditions for release study can refer to Table 3.3.4.

6.3 Conclusions

Impacts of blending of surface water and desalinated water on iron corrosion and retention of inorganic contaminants

Experiments with water chemistries mimicking those of blended desalinated/conventionally treated water showed that NOM was a very important player in this system. The presence of NOM caused soluble and total iron concentrations to increase. Iron corrosion rate were also affected by both NOM and blending ratio but less prominently than iron released. An important finding made in these experiments was that both NOM and blending ratio influenced the scale retention factors and higher DOC levels resulted in considerably higher SR values.

These phenomena appear to be associated with changes iron minerals predominating on corroding iron surfaces. XRD measurements show that lepidocrocite and magnetite tended to be present in most cases, while calcite was detected only in the scales formed in surface water. Higher chloride concentrations resulted in the deposition of bigger and more symmetric clusters of lepidocrocite while NOM promoted the formation of dispersed structures lacking discernible crystalline features.

The retention of lead, vanadium, chromium, copper and arsenic by these scales was in all cases consistently higher than that of zinc, cadmium, nickel and uranium. Changes of anionic concentrations per se in varying blending ratios did not have pronounced impact on retention of these contaminants, but NOM did decrease their retention.

Separation of effects of chloride, sulfate and NOM on metal corrosion, accumulation and release of inorganic contaminants with/from corroded metals

Experiments with the blends in which concentrations of chloride and sulfate changes simultaneously were followed by those designed to estimate effects of these solution components per se. These experiments confirmed that in general, NOM influence on metal release was much more pronounced than that of anions. For all three tested metals (Fe, Cu and Pb), NOM tended to increase metal release. However, the factor of scale retention on the surface of iron was much higher in the presence of NOM.

In contrast with NOM effects, those of the examined anions were more metal-specific. For iron, chloride did not impact on iron release, unless the exposures were carried out in the presence of high level of chloride. Increasing sulfate levels resulted in increases of both soluble and total iron concentrations. For copper, increasing chloride or sulfate concentrations only slightly increased copper release. Increased chloride concentrations also enhanced lead release while sulfate had an opposite effect.

Retention of inorganic contaminants within/on iron corrosion scales was much more prominent compared with that within/on copper or lead/tin coupons. It is not surprising since considerably more voluminous corrosion scales were formed on the surface of irons and the identified iron corrosion products (such as lepidocrocite, magnetite) are known to have strong affinities to sorb heavy metals. The retention percent of tested elements within/on iron corrosion scales decreased in the following order: lead > vanadium > chromium > copper > arsenic > zinc > cadmium > nickel > uranium. For copper and lead/tin coupons, the retention of most elements was less than 20%, except chromium. NOM impacts on retention of inorganic contaminants were much pronounced than those

of anions. With elevated DOC levels, retention of inorganic contaminants was significantly reduced. Anions did not significantly affect the retention of these elements, except in cases of Fe and Pb/Sn coupons where increasing sulfate levels slightly decreased the retention percent of tested elements.

Results from the release experiments that employed selected coupons switched to water chemistries different from those employed in the initial exposures indicated that Cu, Cr, Zn, Ni, V, Pb were the most mobile elements that could be remobilized due to changes of water chemistry. NOM effect on release of the pre-retained elements from iron and copper coupons was much prominent than that of chloride effect. It may be suggested that metals retained on the surface of iron or copper coupons in the presence of DOC retain their mobility, possibly because of the formation of strong NOM-metal complexes. However, release of inorganic contaminants from lead/tin coupons showed somewhat different behavior with chloride exerting a more significant influence on the release of the pre-retained heavy elements than NOM.

Chapter 7 Assessment of Effects of NOM and Anions on Iron Corrosion

Impacts of NOM and anions (chloride and sulfate) on soluble/total iron release and iron corrosion rates were assessed based on jar tests that used iron coupons and different compositions of synthetic waters. Altered NOM (Suwannee River NOM ozonated with different ratio of O_3/DOC) was used to explore the influence of different types of NOM on iron corrosion. Six anion concentrations (0, 40, 80, 120, 160, and 200 mg/L of chloride or sulfate), three NOM concentrations (0, 1 and 2 mg/L), and three O_3/DOC ratios (0, 1 and 2 for altered NOM) were tested in this study. Detailed information on these exposures is given in the Materials and Methods chapter of this dissertation. Detailed water compositions are referred to Table 3.4.1.

7.1 Characterization of altered NOM

Suwannee River NOM ozonated using varying O_3/DOC ratios was characterized by high performance size exclusion chromatography (HPSEC). HPSEC chromatograms for the altered NOM are presented in Figure 7.1. Organics with higher molecular weight are first eluted from the column and those with low molecular weight are eluted later. The intensity of UV absorbance of the samples was detected by a UV detector at 254 nm. Therefore, these HPSEC profiles primarily represent the presence of aromatic or double bond organic compounds.

Major peaks in the HPSEC profiles appeared at elution times 13.57, 13.77, 14.65, and 15.85 min. These peaks correspond to high, intermediate, medium, and low apparent

molecular weight (AMW) components in the HPSEC profiles of original Suwannee River NOM (O_3/DOC = 0).

Ozone treatment significantly decreased the absorbance of the high and intermediate AMW fractions at O_3/DOC = 1 and 2, respectively. Only a slight decrease was observed for the medium AMW peaks. Ozonation did not affect the low AMW fraction.

Previous research (e.g., Amy et al., 1992; Owen et al., 1995) have found that ozone treatment tends to decrease the higher AMW fractions of NOM with a concomitant increase in the lower AMW fractions. However, an absolute increase in the lower AMW fractions of NOM was not observed in our study although the integration of the observed HPSEC profiles would result in increases of the relative contributions of the low AMW fraction.

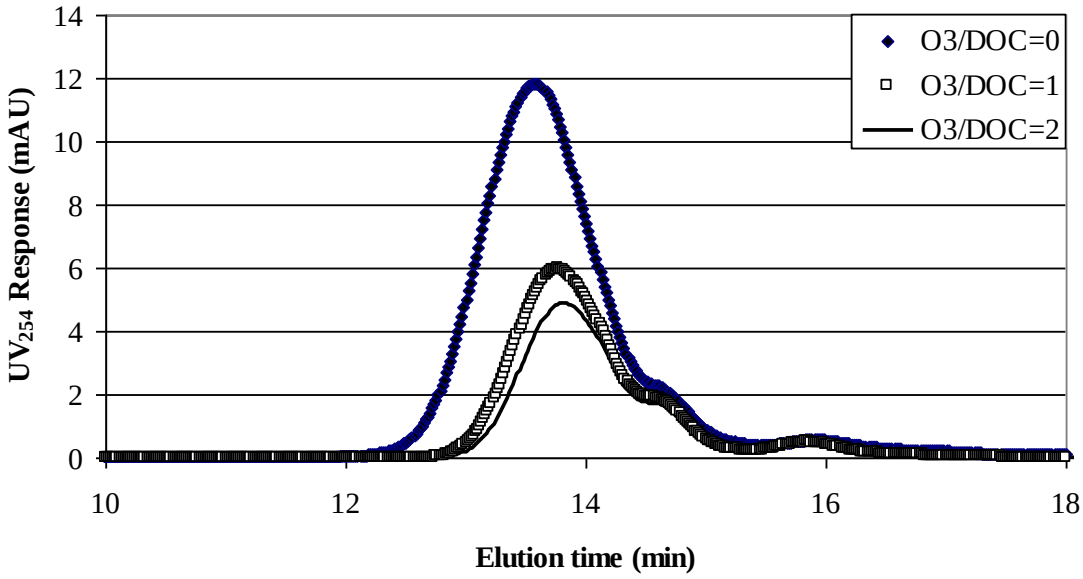

Figure 7.1 High performance size exclusion chromatography (HPSEC) chromatograms of Suwannee River NOM at three O_3/DOC ratios.

7.2 Iron release from iron coupons corroding in the presence of altered NOM

Figure 7.2 shows the NOM impacts on iron release. Detailed water compositions can be referred to Table 3.4.1 (jar number 1 to 3). In the absence of NOM, the soluble iron concentration was extremely low (4.4 µg/L). Its levels increased dramatically as DOC concentration increased (from 4.4 µg/L to 541 or 777 µg/L in the presence of 1 or 2 mg/L DOC, respectively). Total iron concentrations also increased with that of DOC, but in a lesser extent compared to those of soluble iron concentrations (from 618 µg/L in the absence of DOC to 835 or 1160 µg/L in DOC 1 or 2 mg/L, respectively).

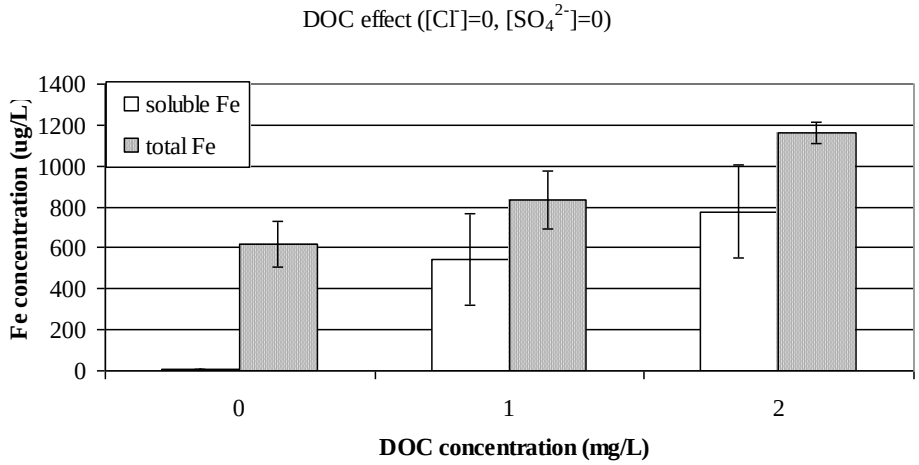

Figure 7.2 Effects of concentrations of unaltered NOM on average soluble and total iron concentrations released from corroding iron coupons during exposure week 7 to 9. The error bar indicated ±1 standard deviation.

The combined effects of anions and NOM on iron release are shown in Figure 7.3. In the absence of DOC, the influence of chloride on soluble iron was largely insignificant and the soluble iron concentrations were extremely low. However, total iron release increased significantly by the presence of chloride. For example, the total iron concentration was 618 µg/L at a chloride concentration of 0 mg/L. At the highest chloride level of 200

mg/L, the total iron concentration increased by 5.6 times higher (3463 μg/L) (Figure 7.3 (A)).

In the presence of NOM, soluble iron concentrations increased but the chloride effect on them was not monotonic. At a 1 mg/L DOC level, soluble iron increased notably as chloride concentration was changed from 0 to 40 mg/L, but soluble iron levels experienced a slight decrease as chloride concentration increased further. For a 2 mg/L DOC level, increasing chloride levels had only a marginal effect on soluble iron concentrations.

As for total iron release, higher DOC concentrations did not result in higher total iron release. In fact, at chloride concentrations equal or higher than 80 mg/L, much less total iron was released compared to that seen in the absence of DOC. Higher chloride levels contributed to higher total iron concentration at a fixed DOC level.

Figure 7.3 (B) shows impacts of sulfate and NOM on iron release. The results demonstrate that both sulfate and NOM increased the soluble and total iron concentration. The combined effect of sulfate and NOM on iron release was simpler and monotonic compared with that seen in the chloride/NOM system. It should be noted that both soluble and total iron concentrations affected by sulfate and NOM were higher than those affected by chloride and NOM.

In comparison with data presented in Figure 6.1, iron concentrations were much higher in this test. The major difference of these two batches was probably the hardness cations. The absence of cations (calcium and magnesium) in the previously discussed exposures may have resulted in higher iron release.

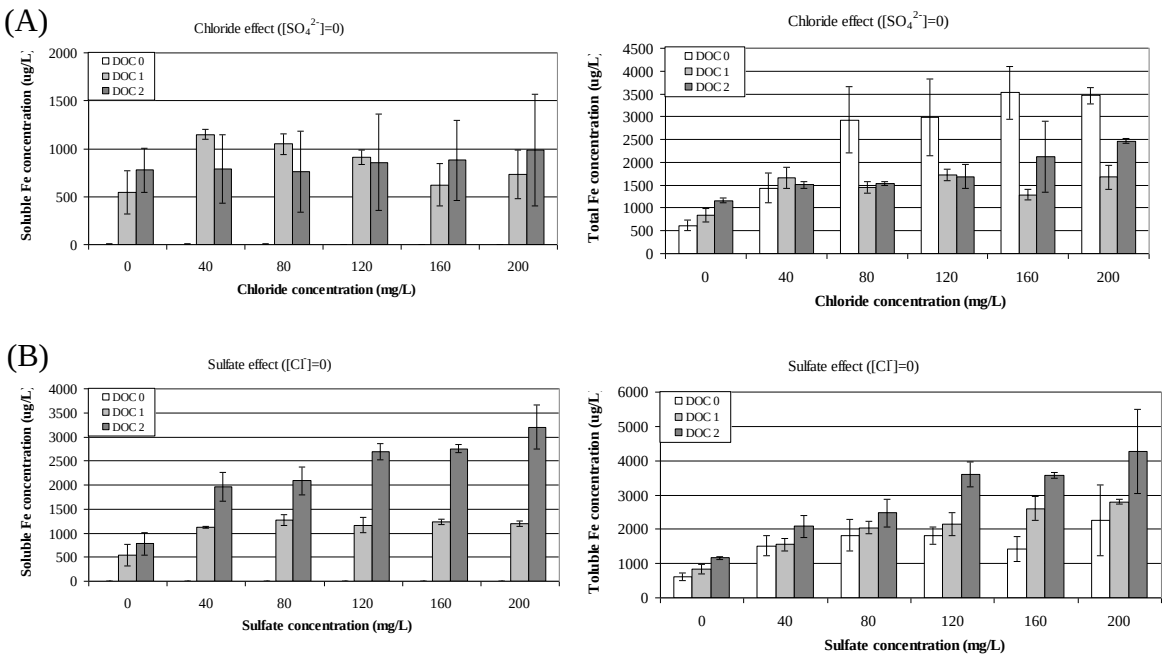

Figure 7.3 Effects of (A) chloride or (B) sulfate and concentrations of unaltered NOM on average soluble and total iron concentrations released from iron coupons during exposure week 7 to 9. The error bar indicated ±1 standard deviation.

Figure 7.4 shows effects of O_3/DOC ratios on iron release. At both DOC levels (DOC 1 or 2 mg/L), oxidation of NOM by ozone resulted in comparatively lower soluble and total iron concentrations. For example, at DOC level of 1 mg/L and O_3/DOC ratio of 0 (i.e., original Suwannee River NOM), soluble and total iron concentrations were 541 and 835 µg/L, respectively. Soluble and total iron concentrations decreased to 416 and 545 µg/L, respectively for the same concentration of NOM treated with a 2 O_3/DOC ratio. This is likely to be associated with a less pronounced complexation and surface activity of NOM altered by O_3/DOC oxidation.

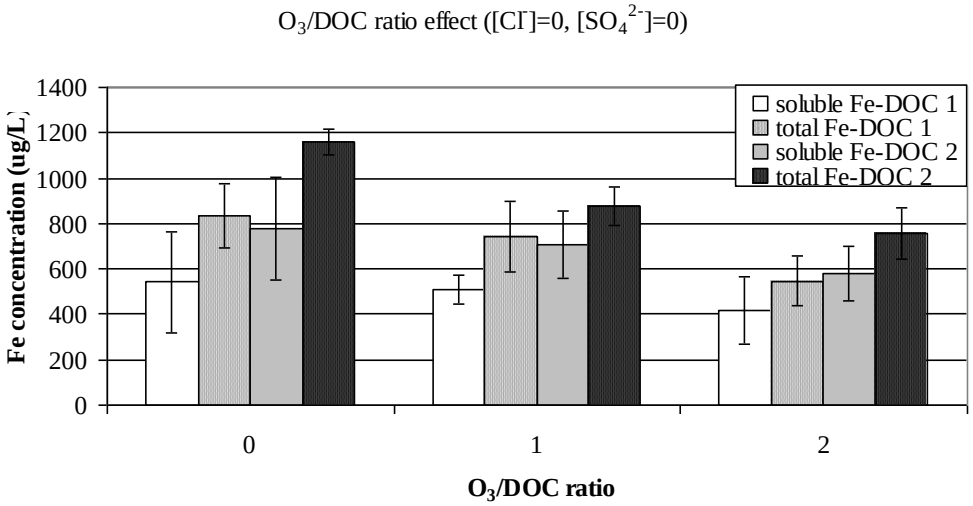

Figure 7.4 Effect of NOM oxidized using different O_3/DOC ratios on average soluble and total iron concentrations from corroding iron coupons during exposure week 7 to 9. The error bar indicated ±1 standard deviation.

Effects of chloride and O_3/DOC ratios at two DOC levels (1 mg/L and 2 mg/L) on the average soluble and total iron concentrations released from iron coupons are shown in Figure 7.5. At DOC concentration of 1 mg/L (Figure 7.5 (A)), soluble iron concentrations decreased as chloride level increased at O_3/DOC ratio of 1 or 2. In contrast, total iron concentrations increased as chloride level increased at three O_3/DOC ratios. For total iron concentrations, significant increases of total iron concentrations were observed as chloride increased from 0 to 40 mg/L. Further increases of chloride levels did not contribute to appreciably higher total iron concentrations and total iron concentrations leveled off as chloride changed from 40 to 200 mg/L.

At DOC level of 2 mg/L (Figure 7.5 (B)), the behavior of soluble iron concentrations was not monotonic. It increased as chloride level changed from 0 to 120 mg/L and then slightly decreased as chloride changed from 120 to 200 mg/L at O_3/DOC ratio of 1 or 2.

In contrast, total iron concentrations increased as chloride level increased at three O_3/DOC ratios.

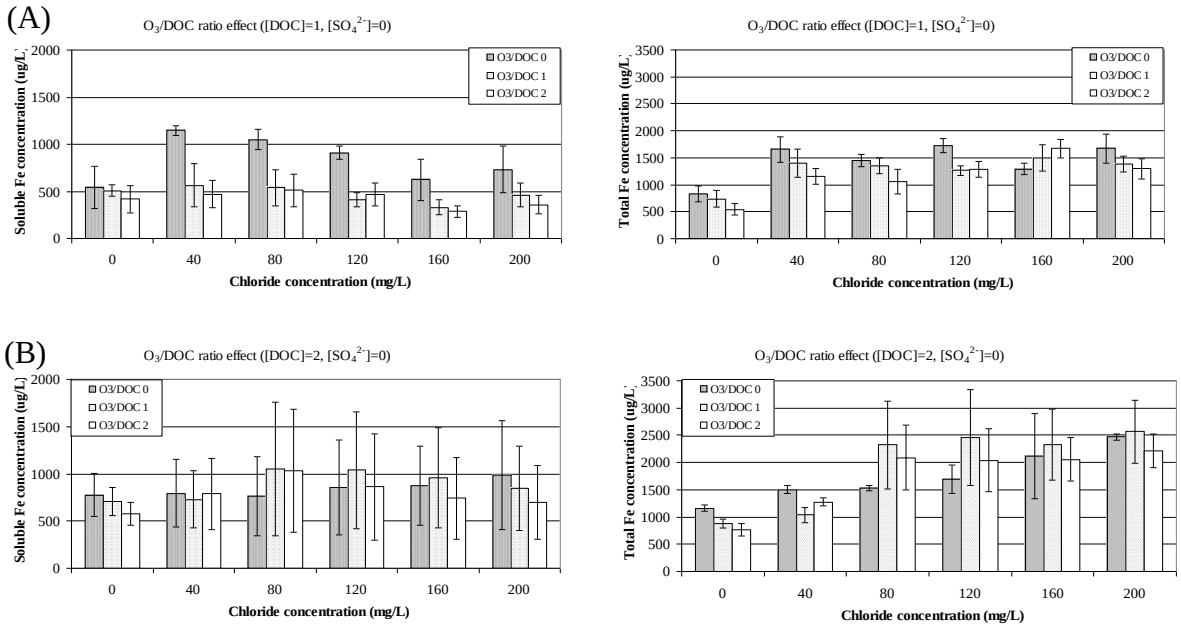

Figure 7.5 Effects of chloride and NOM altered using varying O_3/DOC ratios on average soluble and total iron concentrations released from iron coupons during exposure week 7 to 9 (A) DOC 1 mg/L and (B) DOC 2 mg/L. The error bar corresponds to ±1 standard deviation.

Figure 7.6 shows the effects of sulfate and O_3/DOC ratios at two DOC concentrations (1 and 2 mg/L) on averaged soluble and total iron concentrations released from iron coupons. At a fixed sulfate level, higher O_3/DOC ratios resulted in lesser extent of soluble and total iron concentrations. At a fixed O_3/DOC ratio, the effect of sulfate on soluble iron release was non-monotonic. For example, at DOC level of 1 mg/L and O_3/DOC ratio of 1 (Figure 7.6 (A)), soluble iron concentration increased as sulfate increased from 0 to 40 mg/L and then it decreased as sulfate changed from 40 to 200 mg/L. At DOC level of 2 mg/L, it was observed that the maximum soluble iron

concentrations appeared at sulfate level of 120 mg/L at O_3/DOC ratio of 1 or 2. As for total iron concentrations, they increased as sulfate level increased at both DOC levels and three O_3/DOC ratios. Both soluble and total iron concentrations in the presence of sulfate tended to be higher than those in the presence of chloride. For instance, at chloride or sulfate level of 200 mg/L, DOC level of 2 mg/L and O_3/DOC ratio of 1, total iron concentrations affected by sulfate or chloride were 3026 or 2570 μg/L, respectively.

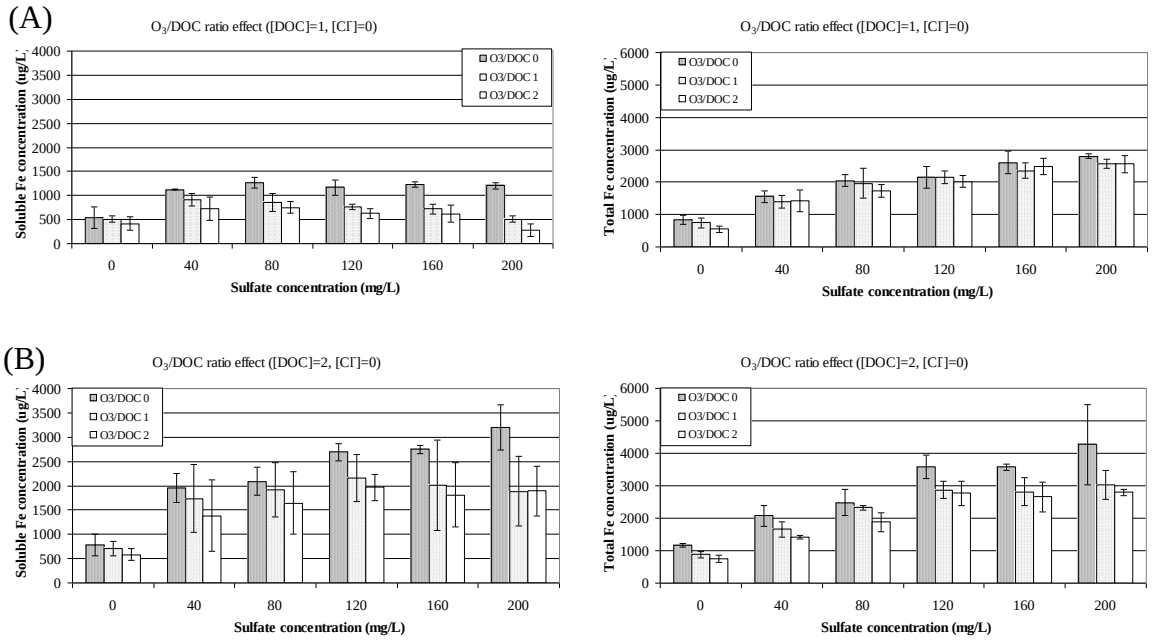

Figure 7.6 Effects of sulfate and NOM altered using varying O_3/DOC ratios on average soluble and total iron concentrations released from iron coupons during exposure week 7 to 9 (A) DOC 1 mg/L and (B) DOC 2 mg/L. The error bar corresponds to ±1 standard deviation.

7.3 Impacts of NOM and anions on iron corrosion rate and scale retention factor

The NOM impacts on iron corrosion rate and scale retention factor are presented in Figure 7.7. Iron corrosion and scale retention factors were determined based on weight loss measurements. Details of calculation of the apparent corrosion rate ($i_{corr}^{\Delta W}$) and scale retention factor (SR) were described in section 6.1.2 of this thesis. The data presented in Figure 7.7 were the average values of the two coupons; the difference between two coupons had an average standard deviation of ±10% and ±25% for corrosion rates and SR, respectively. The results demonstrate that both the apparent corrosion and scale retention factors increased with increasing DOC concentrations at O_3/DOC ratio of 0 (i.e., unaltered Suwannee River NOM). After altering NOM by ozonation, apparent corrosion rate also increased with increasing O_3/DOC ratios at DOC level of 1 mg/L. But, at DOC level of 2 mg/L, the behavior of the corrosion rates was reversed. It decreased with increasing O_3/DOC ratios (Figure 7.7 (A)). On the other hand, scale retention factors did not undergo significant changes with O_3/DOC ratios (Figure 7.7 (B)). It suggested that the apparent corrosion rate not only affected by NOM concentrations but also the compositions of NOM. However, given the scatter of corrosion rates' determinations, this effect is small. Scale retention factors, however, were markedly influenced by NOM concentrations but not by its alteration.

Figure 7.8 shows the effects of anions and concentrations of unaltered NOM on the corrosion and scale retention factors. As was seen before, higher chloride and DOC levels resulted in slightly higher corrosion rates (Figure 7.8 (A)). For example, at chloride level of 0 mg/L, apparent corrosion rates were 24.9 and 26.9 μA/cm^2 for DOC concentrations of 0 and 2 mg/L, respectively. As chloride level increased to 200 mg/L, apparent

corrosion rates increased to 28.3 and 30 μA/cm^2 for DOC concentrations of 0 and 2 mg/L, respectively. Higher chloride level also caused the scale retention factors to decrease slightly but this effect is weak especially at high DOC concentrations.

(A)

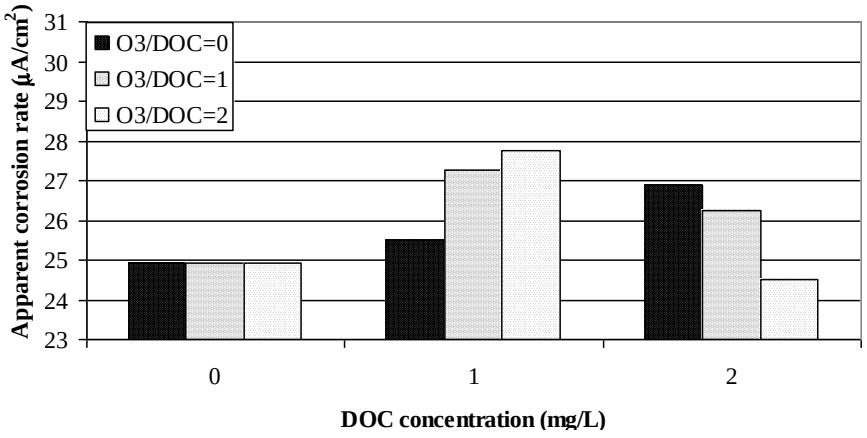

(B)

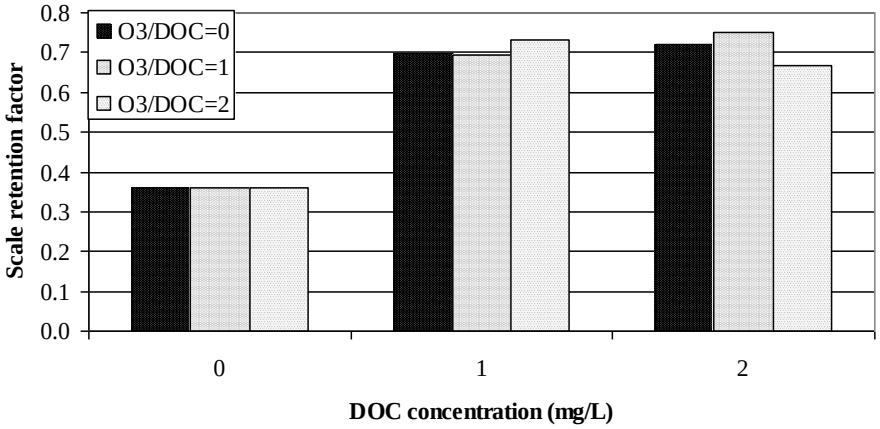

Figure 7.7 Impacts of NOM concentrations and its alteration by oxidation using varying O_3/DOC ratios on (A) apparent corrosion rates and (B) scale retention factors determined based on weight loss measurements for iron coupons exposed to the baseline water chemistry.

Impact of sulfate on apparent corrosion rates was more pronounced than that of chloride (Figure 7.8 (B)). In the absence of NOM, apparent corrosion rates increased from 24.9 to 28.1 μA/cm^2 as sulfate concentration increased from 0 to 40 mg/L. Further increments of

sulfate concentrations did not contribute to higher corrosion rates, which were largely stable for sulfate levels 80 to 200 mg/L.

In general, the corrosion rates measured in the presence of sulfate were somewhat higher than those in the presence of chloride. Higher sulfate concentrations also resulted in lower scale retention factors, which was especially significant for a 1 mg/L DOC level. Indeed, the scale retention factor decreased from 0.7 to 0.29 as sulfate concentration increased from 0 to 200 mg/L. This effect was counteracted at a higher DOC concentration of 2 mg/L. In that case, the scale retention rate decreased from 0.72 to 0.5~0.6 as sulfate concentrations increased from 0 to 40~200 mg/L.

Combined effects of chloride and O_3/DOC ratios on apparent corrosion and scale retention factors are presented in Figure 7.9. For any particular O_3/DOC ratio, higher chloride contributed to higher corrosion rates, except at DOC level of 2 mg/L with O_3/DOC ratio of 1, the apparent corrosion rate varied between 26 and 29 $\mu A/cm^2$ as the concentration of chloride increased from 0 to 200 mg/L.

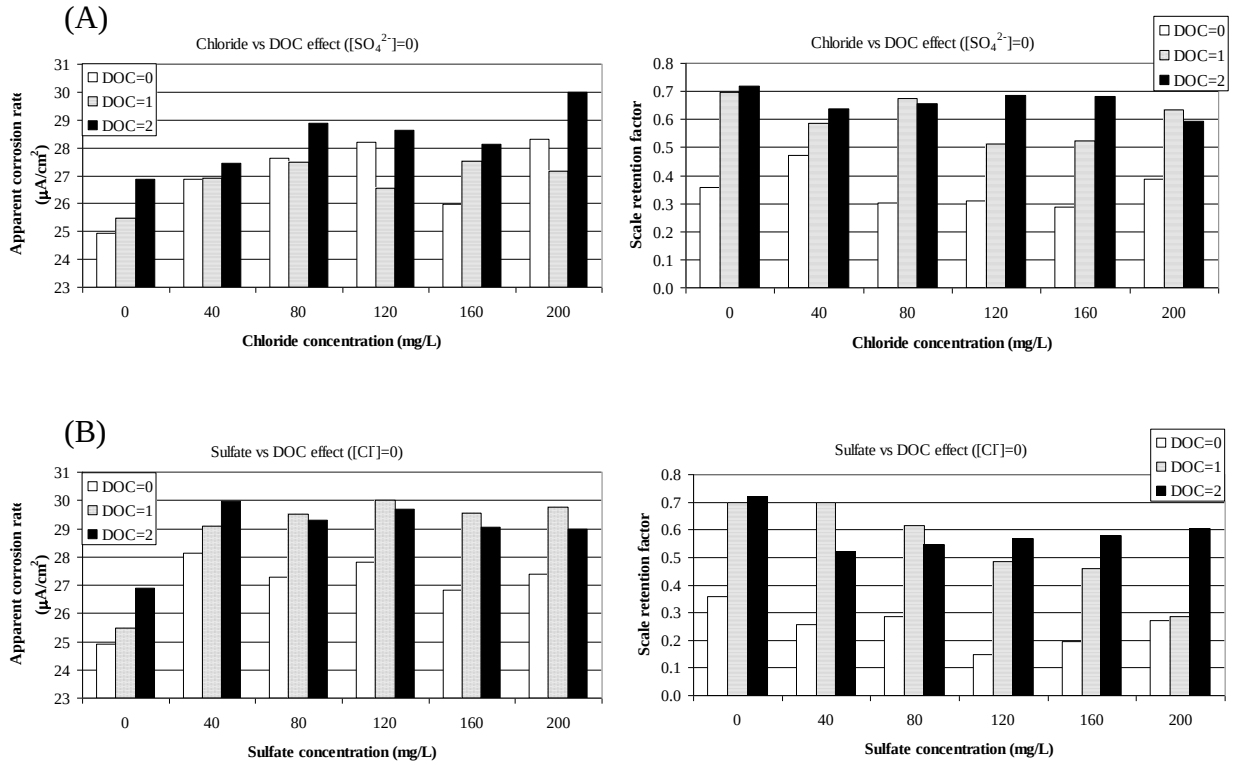

Figure 7.8 Effects of (A) chloride or (B) sulfate and concentrations of unaltered NOM on apparent corrosion and scale retention factors estimated based on weight loss measurements for iron coupons.

At DOC level of 1 mg/L, higher O_3/DOC ratios resulted in higher corrosion rates (Figure 7.9 (A)). In most cases, corrosion rates were highest at a 1.0 O_3/DOC, although these values obtained for O_3/DOC ratios of 1 or 2 did not have significant differences. Corrosion rate determined for the O_3/DOC ratio of 2 were generally lower than those at O_3/DOC ratio of 0 or 1 (Figure 7.9 (B)). For example, at chloride concentration of 200 mg/L, apparent corrosion rates were 30, 28.3, and 27.8 µA/cm^2, respectively, at O_3/DOC ratios of 0, 1, and 2.

Impact of chloride on scale retention factors for a 1 mg/L DOC level was more pronounced than that at the DOC concentration of 2 mg/L. Higher chloride

concentrations reduced the scale retention factor more significantly at DOC level of 1 mg/L but considerably less so measurements carried out for a 2 mg/l DOC level. For instance, at DOC 1 mg/L and O_3/DOC ratio of 2, scale retention factors decreased from 0.73 to 0.36 as chloride level increased from 0 to 200 mg/L. In contrast, at a 2 mg/L DOC and O_3/DOC ratio of 2, scale retention factor decreased from 0.67 to 0.57 as the chloride level changed from 0 to 200 mg/L.

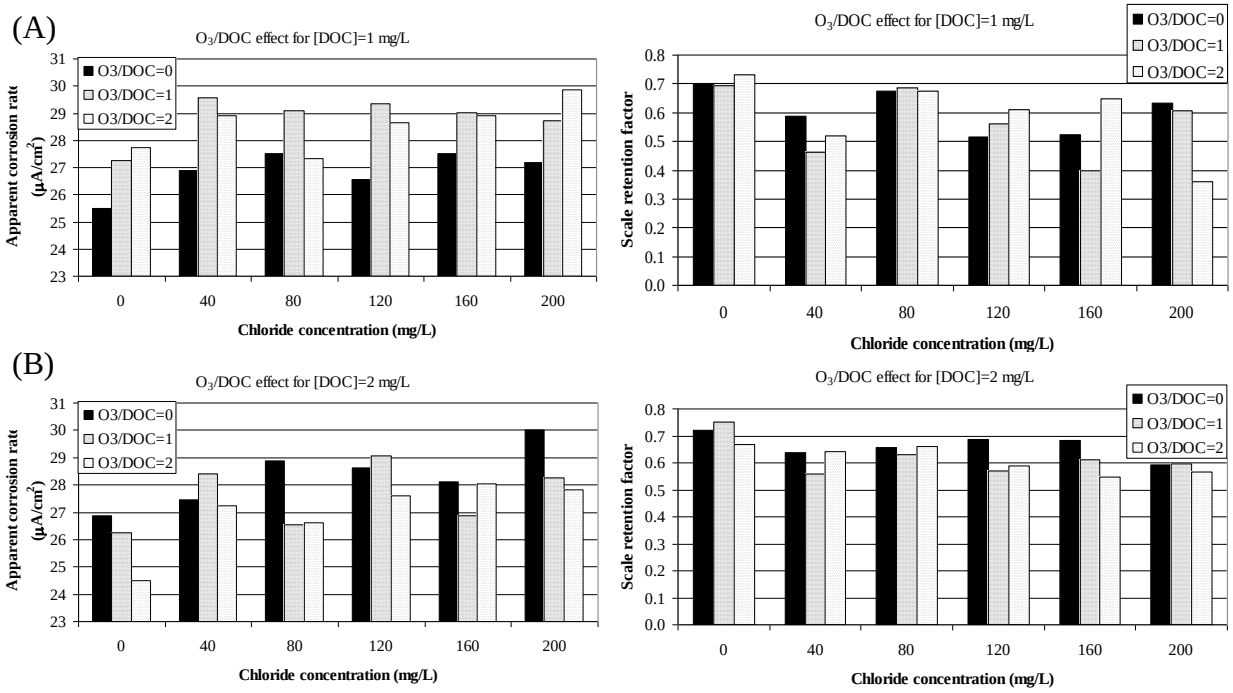

Figure 7.9 Effects of chloride and NOM altered by oxidation using varying O_3/DOC ratios at DOC concentrations of (A) 1 mg/L and (B) 2 mg/L on apparent corrosion and scale retention factors.

Figure 7.10 shows combined effects of sulfate and O_3/DOC ratios on corrosion and scale retention factors. At DOC level of 1 mg/L, increasing sulfate concentrations resulted in increasing apparent corrosion rate at O_3/DOC ratio of 0. However, for NOM altered using O_3/DOC ratio of 1 or 2, corrosion rates first increased as sulfate increased from 0 to 40 mg/L. They were relatively stable as sulfate changed from 40 to 160 mg/L, and then

decreased at sulfate concentration of 200 mg/L (Figure 7.10 (A)). For a 2 mg/L DOC, the impact of sulfate on corrosion rates was also O_3/DOC ratio dependent (Figure 7.10 (B)). At O_3/DOC ratio of 0, its behavior was similar to that at DOC level of 1 mg/L. That is, increasing sulfate concentrations resulted in increasing corrosion rate. At O_3/DOC ratio of 1, no clear trend was found as sulfate level changed; apparent corrosion rate varied in a wide range of 24~29 $\mu A/cm^2$. At O_3/DOC ratio of 2, higher sulfate levels contributed to higher apparent corrosion rate. Sulfate effect on scale retention factor was more significant at DOC level of 1 mg/L compared to that at DOC level of 2 mg/L. For instance, at O_3/DOC ratio of 2, scale retention factor decreased from 0.73 to 0.35 as sulfate level increased from 0 to 200 mg/L at DOC level of 1 mg/L. However, it only decreased from 0.67 to 0.51 at DOC level of 2 mg/L.

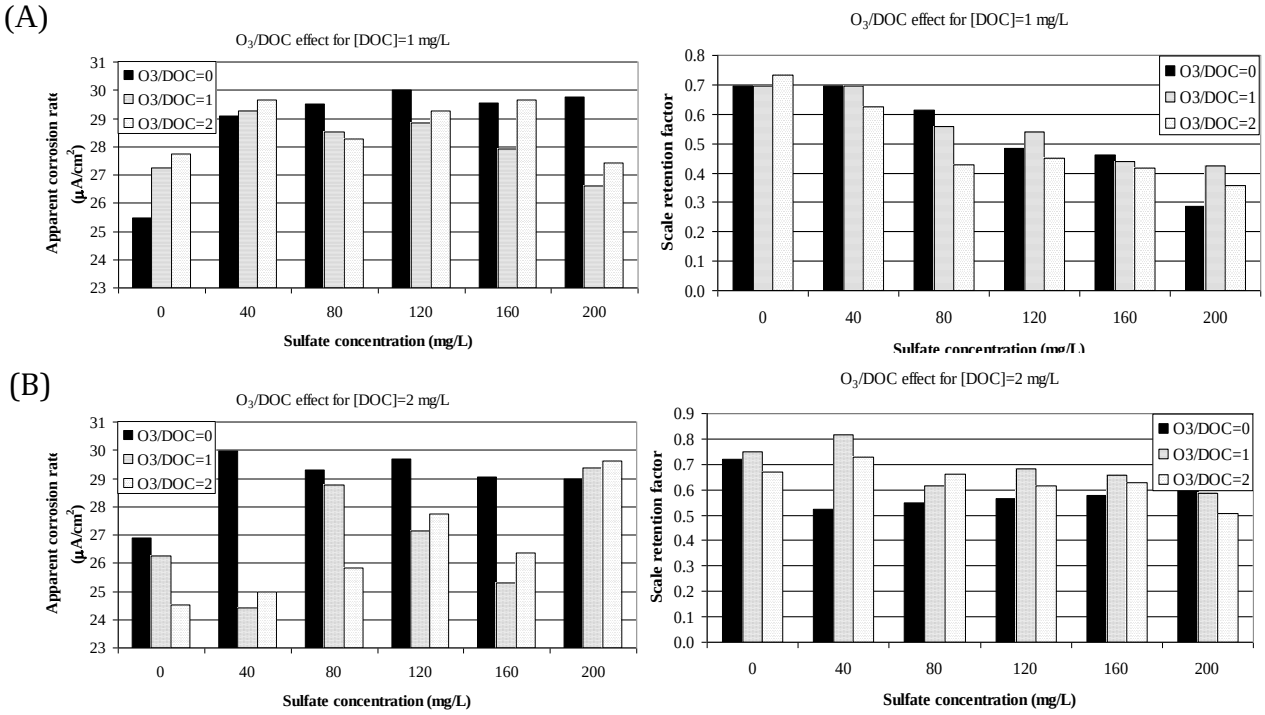

Figure 7.10 Effects of sulfate and NOM altered by oxidation using varying O_3/DOC ratios at DOC concentrations of (A) 1 mg/L and (B) 2 mg/L on apparent corrosion and scale retention factors.

7.4 Conclusions

Examination of NOM effects on iron release demonstrated that increasing concentrations of unaltered NOM resulted in prominent increases of both soluble and total iron concentrations but the effect were somewhat different with sulfate and chloride. In the chloride/NOM system, increasing chloride levels increased both soluble and total iron concentrations but the behavior was not monotonic. In contrast with that, the sulfate/NOM system had a simpler and monotonic behavior, with higher sulfate levels and/or NOM concentrations contributing to higher soluble and total iron release.

NOM alteration by ozone oxidation suppressed somewhat, but not completely NOM effects. NOM oxidation using higher O_3/DOC ratios caused both soluble and total iron release to decrease. In the chloride/altered NOM system, higher chloride concentrations resulted in higher total iron concentrations, but soluble iron release was non-monotonic. In the sulfate/altered NOM system examined at a fixed sulfate concentration, higher O_3/DOC ratio resulted in lower soluble and total iron release. At a fixed O_3/DOC ratio and varying sulfate, increasing sulfate levels caused total iron release to increase, but the behavior of soluble iron was not monotonic.

The corrosion rates and scale retention were primarily affected by NOM concentrations and less so by whether NOM was altered by ozonation or not. Examination of the effects of anions with either unaltered or altered NOM showed that in general higher chloride or sulfate levels increased apparent corrosion rate and at the same time decreased scale retention. One exception from that trend was observed for the sulfate/altered NOM system in which changes of corrosion rates depended on O_3/DOC ratio.

In all, the data show that NOM plays a prominent role in the corrosion behavior of iron in drinking water. Our data provide a new insight into its effects but further studies are necessary to determine its influence in a wider range of pHs, alkalinities and other water chemistry parameters.

Chapter 8 Conclusions and Future Research

This research investigated the occurrence, accumulation, and release of inorganic contaminants in the drinking water distribution systems. Impacts of water quality changes on iron corrosion, retention and release of inorganic contaminants within/from the corrosion scales were also addressed based on jar tests carried out at varying anionic concentrations, NOM levels and alteration. This chapter summarizes the key findings of this research and also suggests research directions for future work.

8.1 Conclusions

Elemental and structural composition of corrosion scales formed in drinking water distribution systems predominated by unlined cast iron pipes and also of deposits mobilized during hydrant flushing events were characterized. Goethite (α-FeOOH), magnetite (Fe_3O_4) and siderite ($FeCO_3$) were the primary crystalline phases identified in most of the tested samples. Among the major constituent elements of the scales, iron was most prevalent by a considerable margin, followed, in the order of decreasing prevalence, by sulfur, organic carbon, calcium, inorganic carbon, phosphorus, manganese, magnesium, aluminum and zinc.

Among the trace inorganic contaminants found in the scales, barium had the highest concentrations, followed by, in the decreasing order, lead, nickel, vanadium, arsenic, chromium, uranium, cadmium, antimony, selenium, and thallium. For TOC, TIC, Mg, Pb, Ni, Cr, and Sb, the cumulative occurrence profiles showed that hydrant flush solids have consistently higher levels of these components compared with pipe specimens. It suggests that these elements are more accessible to hydrant disturbances or changes of water qualities.

Examination of the speciation of heavy elements found in the corrosion scales via sequential extractions and measurements of soluble and particulate metal fractions released from suspended corrosion solids demonstrated that arsenic, chromium and vanadium are primarily associated with the mobilization-resistant fraction. On the other hand, nickel and manganese are much more mobile than all the other inorganic contaminants examined in this study. X-ray absorbance measurements confirmed that the arsenic in the sample with the highest As concentration was dominated by As(V) bound by iron oxides.

Experiments with water chemistries mimicking those of blended desalinated/conventionally treated water showed that NOM had a more pronounced effect on iron corrosion and retention of inorganic contaminants than the blending ratio. The presence of NOM caused total iron concentrations and corrosion rates to increase somewhat, while the retention of inorganic contaminants decreased. These phenomena are associated with changes in iron minerals predominating on corroding iron surfaces, especially the formation of more crystalline but less adhering to the surface solids in the absence of NOM.

Experiments that addressed separate effects of chloride, sulfate and NOM again confirmed that in general, NOM influence on metal release was much more pronounced than that of anions and NOM tended to increase metal release and corrosion rates and reduce the retention of inorganic contaminants. Results from the release experiments that employed selected coupons switched to water chemistries different from those employed in the initial exposures indicated that Cu, Cr, Zn, Ni, V, Pb were the most mobile elements that could be remobilized due to changes of water chemistry.

NOM alteration by ozonation suppressed somewhat, but not completely effects seen for unaltered NOM (Suwannee River NOM). NOM oxidation using higher O_3/DOC ratios caused both soluble and total iron release to decrease. The corrosion rates and scale retention were also primarily affected by NOM concentrations and less so by whether NOM was altered by ozonation or not. Examination of the effects of anions with either unaltered or altered NOM showed that in general higher chloride or sulfate levels increased apparent corrosion rate and at the same time decreased scale retention.

8.2 Future research

While this study established the occurrence and typical levels of the representative inorganic contaminants in corrosion scales formed in drinking water, more research is needed to confirm the existence of consistent differences between levels of selected trace inorganic contaminants occurring in corrosion scales and hydraulically mobile phases (e.g., hydrant flush solids and colloidal particles) originating from the same systems. The impact of flow pattern, for instance maximal flows and their durations, in a hydrant flush event also needs to be studied.

Well-designed pipe-loop studies with different water qualities are also needed to identify the factors which can cause the release of such accumulated contaminants back into waters. A need also exists to determine the potential for public health impacts associated with the accumulation and release of trace inorganic contaminants.

Effects of NOM and anions (chloride and sulfate) on iron corrosion, accumulation and release of inorganic contaminants have been assessed in some extent in this study. They demonstrated that NOM plays a prominent role in the corrosion behavior of iron in drinking water. Further research is necessary to determine NOM influence in a wider

range of pHs, alkalinities and other water chemistry parameters, such as presence of cations (calcium or magnesium) or corrosion inhibitors. It is also necessary to address effects of NOM site-specificity and its alteration by processes (e.g., coagulation, chlorination) other than ozonation which was employed in this study.

Finally, it is necessary to carry out experiments designed to examine in more detail effects of NOM concentration and properties, in combination with other applicable water quality parameters, on the corrosion rates and properties of surface solids formed during prolonged exposures similar to those in drinking water distribution systems.

LIST OF REFERENCES

Ali, M.A., Dzombak, D.A., 1996. Effects of simple organic acids on sorption of Cu^{2+} and Ca^{2+} on goethite. Geochimica et Cosmochimica Acta 60(2), 291-304.

American Water Works Association Research Foundation and DVGW-Technologiezentrum Wasser (AwwaRF and TZW). 1996. Internal Corrosion of Water Distribution Systems, 2nd ed. Denver, CO.

Amy, G.L., Sierka, R.A. Bedessem, J., Price, D., Tan, L., 1992. Molecular size distributions of dissolved organic matter. Journal of American Water Works Association, 84(6), 67-75.

Barkatt, A., Pulvirenti, A.L., Adel-Hadadi, M.A., Viragh, C., Senftle, F.E., Thorpe, A.N., Grant, G.R., 2009. Composition and particle size of superparamagnetic corrosion products in tap water. Water Research 43(13), 3319-3325.

Bednar, A.J., Medina, V.F., Ulmer-Scholle, D.S., Frey, B.A., Johnson, B.L., Brostoff, W.N., Larson, S.L., 2007. Effects of organic matter on the distribution of uranium in soil and plant matrices. Chemosphere 70(2), 237-247.

Benjamin, M.M., Sontheimer, H., Leroy, P., 1996. Corrosion of iron and steel. In Internal Corrosion of Water Distribution Systems. Cooperative Research Report, AWWA Research Foundation, Denver, CO, 29-70.

Blackmore, D.P.T., Ellis, J., Riley, P.J., 1996. Treatment of a vanadium-containing effluent by adsorption/coprecipitation with iron oxyhydroxide. Water Research, 30(10), 2512-2516.

Borch, T., Camper, A.K., Biederman, J.A., Butterfield, P.W., Gerlach, R., Amonette, J.E., 2008. Evaluation of characterization techniques for iron pipe corrosion products and iron oxide thin films. Journal of Environmental Engineering-ASCE 134(10), 835-844.

Burlingame, G.A., Lytle, D.A., Snoeyink, V.L., 2006. Why red water? Understanding iron release in distribution systems. Opflow 32(12), 12-16.

Cancès, B., Juillot, F., Morin, G., Laperche, V., Polya, D., Vaughan, D.J., Hazemann, J.-L., Proux, O., Brown Jr., G.E., Calas, G., 2008. Changes in arsenic speciation through a contaminated soil profile: a XAS based study. Science of the Total Environment 397(1-3), 178-189.

Cancès, B., Juillot, F., Morin, G., Laperche, V., Alvarez, L., Proux, O., Hazemann, J.-L., Brown Jr.G.E., Calas, G., 2005. XAS evidence of As(V) association with iron oxyhydroxides in a contaminated soil at a former arsenical pesticide processing plant. Environmental Science & Technology 39(24), 9398-9405.

Cornell, R.M.; Schwertmann, U. 2003. The iron oxides: structure, properties, reactions, occurrence and uses. Wiley-VCH Publishing, Weinheim.

Copeland, R.C., Lytle, D.A., Dionysiou D.D., 2007. Desorption of arsenic from drinking water distribution system solids. Environmental Monitoring and Assessment 127(3), 523-535.

Dick, L.F.P., Rodrigues, L.M., 2006. Influence of humic substances on the corrosion of the API 5LX65 steel. Corrosion 62(1), 35-43.

Dixit, S., Hering, J.G., 2003. Comparison of arsenic(V) and arsenic(III) sorption onto iron oxide minerals: Implications for arsenic mobility. Environmental Science & Technology 37(18), 4182-4189.

Dodge, D.J., Francis, A.J., Gillow, J.B., Halada, G.P., Clayton, C.R., 2002. Association of uranium with iron oxides typically formed on corroding steel surfaces. Environmental Science & Technology 36(16), 3504-3511.

Dong, D., Derry, L.A., Lion, L.W. 2003. Pb scavenging from a freshwater lake by Mn oxides in heterogeneous surface coating materials. Water Research 37(7), 1662-1666.

EPA. **2002b**. *Health Risks from Microbial Growth and Biofilms in the Distribution System*. EPA, Office of Water. Washington, D.C. http://www.epa.gov/safewater/disinfection/tcr/pdfs/whitepaper_tcr_biofilms.pdf

Fendorf, S., Eick, M.J., Grossl, P., Sparks, D.L., 1997. Arsenate and chromate retention on goethite: I. Surface structure. Environmental Science & Technology 31(2), 315-320.

Fisher, E.L., Fuortes, L.J., Valentine, R.L., Mehrhoff, M., Field, R.W., 2000. Dissolution of ^{226}Radium from pipe-scale deposits in a public water supply. Environment International 26(1), 69-73.

Flemming, H.C., 1995. Sorption Sites in Biofilms. Water Science and Technology 32(8), 27-33.

Flemming, H.C., Neu, T.R., Wozniak, D.J., 2007. The EPS Matrix: the "House of Biofilm Cells". Journal of Bateriology. 189(22), 7945-7947.

Frau, F., Biddau, R., Fanfani, L., 2008. Effect of Major Anions on Arsenate Desorption from Ferrihydrite- Bearing Natural Samples. Applied Geochemistry 23(6), 1451-1466.

Friedman, M.J.; Hill, A.S.; Martel, K.D.; Holt, D.; Smith, S.; Ta, T.; Sherwin, C.; Hiltebrand, D., Pommerenk, P., Hinedi, Z., Camper, A., 2003. Establishing Site-Specific Flushing Velocities. AwwaRF. Denver, CO.

Friedman, M.J., Hill, A.S., Reiber, S.H., Valentine, R.L., Larsen, G., Young, A., Korshin, G.V., Peng, C.-Y., 2010. Assessment of inorganics accumulation in drinking water systems scales and sediments. Water Research Foundation, Denver, CO.

Fuller, C.C., Bargar, J.R., Davis, J.A., Piana, M.J., 2002. Mechanisms of uranium interactions with hydroxyapatite: implications for ground water remediation. Environmental Science & Technology 36(2), 158-165.

Gauthier, V., Barbeau, B., Tremblay, G., Millette R., Nernier A.-M., 2003. Impact of Raw Water Turbidity Fluctuations on Drinking Water Quality in a Distribution System. Journal of Environmental Engineering and Science 2(4), 281-291.

Gauglitz, R., Holterdorf, M., Franke, W., Merx, G., 1992. Immobilization of heavy metals by hydroxylapatite. Radiochimica Acta. 58(59),253-257.

Gerke, T.L., Maynard, J.B., Schock, M.R., Lytle D.L., 2008. Physiochemical characterization of five iron tubercles from a single drinking water distribution system: possible new insights on their formation and growth. Corrosion Science 50(7), 2030-2039.

Gerke, T.L.; Scheckel, K.G.; & Schock, M.R., 2009. Identification and distribution of vanadinite ($Pb_5(V^{5+}O_4)_3Cl$) in lead pipe corrosion by-products. Environmental Science & Technology 43(12), 4412-4418.

Gerke, T.L., Scheckel, K.G., Maynard, J.B., 2010. Speciation and distribution of vanadium in drinking water iron pipe corrosion by-products. Science of the Total Environment 408(23), 5845-5853.

Giasuddin, A.B.M., Kanel, S.R., Choi, H., 2007. Adsoprtion of humic acid unto nanoscale zerovalent iron and its effect on arsenic removal. Environmental Science & Technology 41(6), 2022-2027.

Green-Pedersen, H., Jensesn, B.T., Pind, N., 1997. Nickel adsorption on MnO_2, $Fe(OH)_3$, montmorillonite, humic Acid and calcite: a comparative study. Environmental Technology, 18(8), 807-815.

Guidelines for Drinking-Water Quality. 3rd edition. World Health Organization, Geneva, 2008.

Hangjangsit, L., Beech, I., Edyvean, R., Hammond, C. 1994. Biofilm Development on Stainless Steel in a Potable Water System. European Federation of Corrosion. 15, 323-327.

Hill, A.S., Friedman, M.J., Reiber, S.H., Korshin, G.V., Valentine, R.L., 2010. Behavior of trace inorganic contaminants in drinking water distribution systems. Journal of the American Water Works Association 102(7), 107-118.

Hill, C.P., 2010. Overview of internal corrosion impacts in drinking water distribution systems. In Internal Corrosion Control in Water Distribution Systems, AWWA Research Foundation, Denver, CO, pp. 1-11.

Hitchcock, A.P., Dynes, J.J., Lawrence, J.R., Obst, M., Swerhone, G.D.W., Korber, D.R. Leppard, G.G., 2009. Soft X-ray spectromicroscopy of nickel sorption in a natural river biofilm. Geobiology 7(4), 432-453.

Imran, S.A., Dietz, J.D., Mutoti, G., Taylor, J.S., Randall, A.A., Copper, C.D., 2005. Red water release in drinking water distribution systems. Journal of the American Water Works Association 97(9), 93-100.

Jain, A., Loeppert, R.H., 2000. Effect of competing anions on the adsorption of arsenate and arsenite by ferrihydrite. Journal of Environmental Quality 29(5), 1422-1430.

Khaokaew, S., Chaney, R.L., Landrot, G., Ginder-Vogel, M., Sparks, D.L., 2011. Speciation and release kinetics of cadmium in an alkaline paddy soil under various flooding periods and draining conditions. Environmental Science & Technology 45(10), 4249-4255.

Kim, E.J., Herrera, J.E., 2010. Characteristics of lead corrosion scales formed during drinking water distribution and their potential influence on the release of lead and other contaminants. Environmental Science & Technology 44(16), 6054-6061.

Korshin, G.V., Ferguson, J.F., Perry, S. 1996. Influence of natural organic matter on corrosion of copper in potable waters. Journal of the American Water Works Association 88(7), 36-47.

Korshin, G.V., Ferguson, J.F., Lancaster, A.N., 2005. Influence of natural organic matter on the morphology of corroding lead surfaces and behavior of lead-containing particles. Water Research 39(5), 811-818.

Krishnamurti, G.S.R., Huang, P.M., Van Rees, K.C.J., Kozak, L.M., Rostad, H.P.W., 1995. Speciation of particulate-bound cadmium of soils and its bioavailability. Analyst 120(3), 659-665.

Krishnamurti, G.S.R., Naidu R., 2002. Solid-solution speciation and phytoavailability of copper and zinc in soils. Environmental Science & Technology 36(12), 2645-2651.

Kwon, S.K., Suzuki, S., Saito, M., Waseda, Y., 2006. Atomic-scale structure and morphology of ferric oxyhydroxides formed by corrosion of iron in various aqueous media. Corrosion Science 48 (11), 3675-3691.

Lalonde, S.V., Amskold, L.A., Warren, L.A., Konhauser, K.O., 2007. Surface chemical reactivity and metal adsorptive properties of natural cyanobacterial mats from an alkaline hydrothermal spring, Yellowstone National Park. Chemical Geology 243(1), 36-52.

Linge, K.L., 2008. Methods for investigating trace element binding in sediments. Critical Review in Environmental Science and Technology 38(3), 165-196.

Liu, H, Schonberger, K.D., Korshin, G.V., Ferguson, J.F., Meyerhofer, P., Desormeaux, E., Luckenbach, H., 2010. Effects of blending of desalinated water with treated surface drinking water on copper and lead release. Water Research 44(14), 4057-4066.

Lytle, D.A., Sarin, P., Snoeyink, V.L., 2003. The effect of chloride and orthophosphate on the release of iron from drinking water distribution system cast iron pipe. In Proc. Of the AWWA Water Quality Technology Conference. Denver, Colo.

Lytle, D.A.; Sorg, T.J.; & Frietch, C., 2004. Accumulation of arsenic in drinking water distribution systems. Environmental Science & Technology 38(20), 5365-5372.

Lytle, D.A., Schock M.R., 2005. Formation of Pb(IV) oxides in chlorinated water. Journal of the American Water Works Association 97(11), 102-114.

Lytle, D.A., Sorg, T.J., Muhlen, C., Wang, L., 2010. Particulate arsenic release in a drinking water distribution system. Journal of the American Water Works Association 102(3), 87-98.

Manning, B.A., Hunt, M.L., Amrhein, C., Yarmoff, J.A., 2002. Arsenic(III) and arsenic(V) reactions with zerovalent iron corrosion products. Environmental Science & Technology 36(24), 5455-5461.

McFadden, M., Reiber, S.H., Kwan, P.K., Giani, R., 2009. Investigation of sorption and desorption processes between lead and iron corrosion scales in plumbing materials. Water Quality Technology Conference and Exposition, Seattle.

McNeill, L.S., Edwards, M., 2001. Iron pipe corrosion in distribution systems. Journal of American Water Works Association 93(7), 88-100.

Meng, X., Korfiatis, G.P., Bang, S., Bang, K.W., 2002. Combined effects of anions on arsenic removal by iron hydroxides. Toxicology letters 133(1), 103-111.

Munk, L., Faure, G., 2004. Effects of pH Fluctuations on Potentially Toxic Metals in the Water and Sediment of the Dillon Reservoir, Summit County, Colorado. Applied Geochemistry 19(7), 1065-1074.

Murray, J. 1975. The interaction of metal ions at the manganese dioxide-solution interface. Geochimica et Cosmochimica Acta , 39(4), 505-519.

Naeem, A., Westerhoff, P., Mustafa, S., 2007. Vanadium removal by metal (hydr)oxide adsrobents. Water Research 41(7), 1596-1602.

Nelson, Y.M., Lo, W., Lion, L.W., Shuler, M.L., Ghiorse, W.C., 1995. Lead Distribution in a Simulated Aquatic Environment: Effects of Bacterial Biofilms and Iron Oxide. Water Research 29(8), 1934-1944.

O'Reilly, S.E., Strawn, D.G., Sparks, D.L., 2004. Residence time effects on arsenate adsorption/desorption mechanisms on goethite. Soil Science Society of America Journal 65(1), 67-77.

Ouvrard, S., Simmonnot, M.O., Sardin, M., 2002. Reactive behavior of natural manganese oxides towards the adsorption of phosphate and arsenate. Industrial & Engineering Chemistry Research 41(11), 2785-2791.

Owen, D.M., Amy, G.L., Chowdhury, Z.K., Paode, R., McCoy, G., Viscosil, K., 1995. NOM characterization and treatability. Journal of American Water Works Association, 87(1), 46-63.

Park, S.-K., Kim, Y.-K., Choi, S.-C., 2008. Response of Microbial Growth to Orthophosphate and Organic Carbon Influx in Copper and Plastic Based Plumbing Water Systems. Chemosphere 72(7), 1027-1034.

Peng, C.-Y., Korshin, G.V., Valentine, R.L., Hill, A.S., Friedman, M.J., Reiber, S.H., 2010. Characterization of elemental and structural composition of corrosion scales and deposits formed in drinking water distribution systems. Water Research 44(15), 4570-4580.

Percival, S., Beech, I., Knapp, B., Edyvean, R.G., Wales, D.S., 1997. Biofilm Development on Stainless Steel 304 and 316 in a Potable Water System. Journal CIWEM 11, 289-294.

Radu, T., Subacz, J.L., Phillippi, J.M., Barnett, M.O., 2005. Effects of Dissolved Carbonate on Arsenic Adsorption and Mobility. Environmental Science & Technology 39(20), 7875-7882.

Rao, P.H., Mak, M.S.H., Liu, T.Z., Lai, K.C.K., Lo, I.M.C., 2009. Effects of humic acid on arsenic(V) removal by zero-valent iron from groundwater with special references to corrosion products analyses. Chemosphere. 75(2), 156-162.

Reiber, S., Dostal, G., 2000. Well Water Disinfection Sparks Surprises. Opflow 26(3), 3-6.

Rihs, S., Sturchio, N.C., Orlandini, K., Cheng, L., Teng, H., Fenter, P., Bedzyk, M.J., 2004. Interaction of uranyl with calcite in the presence of EDTA. Environmental Science & Technology 38(19), 5078-5086.

Roccaro, P., Barone, C., Mancini, G., Vagliasindi, F.G.A., 2007. Removal of manganese from water supplies intended for human consumption: a case study. Desalination 210(1), 205-214.

Sarin, P., Snoeyink, V.L., Bebee, J., Kriven, W.M., Clement. J.A., 2001. Physico-chemical characteristics of corrosion scales in old iron pipes. Water Research 35(12), 2961-2969.

Sarin, P., Snoeyink, V.L., Lytle, D.A., Kriven, W.M., 2004. Iron corrosion scales: model for scale growth, iron release, and colored water formation. Journal of Environmental Engineering 130(4), 364-373.

Schock, M.R., Wagner, I., Oliphant, R.J., 1996. Corrosion and solubility of lead in drinking water. In Internal Corrosion of Water Distribution Systems. Cooperative Research Report, AWWA Research Foundation, Denver, CO.

Schock, M.R. 2005. Distribution Systems and Reservoirs and Reactors for Inorganic Contaminants (Chapter 6). In: *Distribution System Water Quality Challenges in the 21st Century*. AWWA. Denver, CO.

Schock, M.R., Holm, T.R., 2003. Are we monitoring in the right places for inorganics and radionuclides? Journal of New England Water Work Association 7(2), 102-116.

Schock, M.R., Hyland, R., Welch, M., 2008. Occurrence of contaminant accumulation in lead pipe scales from domestic drinking water distribution systems. Environmental Science & Technology 42(12), 4285-4291.

Schwertmann, U, Cornell, R., 1991. Iron Oxides in the Laboratory, VHC Publishers: New York.

Sherman D.M., Randall S.R., 2003. Surface complexation of arsenic(V) to iron(III) (hydr)oxides: Structural mechanism from ab initio molecular geometries and EXAFS spectroscopy. Geochimica et Cosmochimica Acta 67(22), 4223-4230.

Shi, B., Taylor, J., 2007. Iron and copper release in drinking-water distribution systems. Journal of Environmental Health-A 70(2), 29-36.

Shuman, L.M., 1985. Fractionation method for soil microelements. Soil Science 140(1), 11-22.

Sly, L.I., Hodgkinson, M. C., Arunpairojana, V., 1990. Deposition of Manganese in a Drinking Water Distribution System. Applied and Environmental Microbiology 56(3), 628-639.

Smith, E., Ghiassi, K., 2006. Chromate removal by an iron sorbent: mechanism and modeling. Water Environment Research 78(1), 84-93.

Snoeyink, V.L., Schock, M., Sarin, P., Wang, L., Chen, A.S.C., Harmon, S., 2003. Aluminum-Containing Scales in Water Distribution Systems: Prevalence and Composition. Journal of Water Supply: Research and Technology. 52(7), 455.

Sontheimer, H., Kolle, W., Snoeyink, V.L., 1981. The siderite model of the formation of corrosion-resistant scales. Journal of American Water Works Association 73(11), 572-579.

Stewart, B.D., Mayes, M.A., Fendorf, S., 2010. Impact of uranyl-calcium-carbonato complexes on uranium(VI) adsorption to synthetic and nature sediments. Environmental Science & Technology 44(3), 928-934.

Su, C., Suarez, D., 2000. Selenate and selenite sorption on iron oxides: an infrared and electrophoretic study. Soil Science Society of America Journal 64(1), 101-111.

Sugiyama, M.; Hori, T.; Kihara, S.; & Matsui, M., 1992. A geochemical study on the specific distribution of barium in lake Biwa, Japan. Geochimica et Cosmochimica Acta 56(2), 597-605.

Tamura, H., Katayama, N., Furuichi, R., 1996. Modeling of ion-exchange reactions on metal oxides with the Frumkin isotherm. 1. acid-base and charge characteristics of MnO_2, TiO_2, Fe_3O_4, and Al_2O_3 surface and adsorption affinity of alkali metal ions. Environmental Science & Technology 30(4), 1198-1204.

Teng, F., Guan, Y.T., Zhu, W.P., 2008. Effect of Biofilm on Cast Iron Pipe Corrosion in Drinking Water Distribution System: Corrosion Scales Characterization and Microbial Community Structure Investigation. Corrosion Science 50(10), 2816-2823.

Terzano, R.; Spagnuolo, M.; Vekemans, B.; Nolf, W.D.; Janssens, K.; Falkenberg, G.; Fiore, S., Ruggiero, P., 2007. Assessing the origin and fate of Cr, Ni, Cu, Zn, Pb, and V in industrial polluted soil by combined microspectroscopic techniques and bulk extraction methods Environmental Science & Technology 41(19), 6762-6769.

Tessier, A., Campbell, P.G.C., Bisson, M., 1979. Sequential extraction procedure for the speciation of particulate trace metals. Analytical Chemistry 51(7), 844-851.

Trived, P., Axe, L., 2001. Predicting divalent metal sorption to hydrous Al, Fe, and Mn oxides. Environmental Science & Technology 35(9), 1779-1784.

Trived, P., Axe, L., Tyson, T.A., 2001. XAS studies of Ni and Zn sorbed to hydrous manganese oxide. Environmental Science & Technology 35(22), 4515-4521.

Tsang, D.C.W., Graham, N.J.D., Lo, I.M.C., 2009. Humic acid aggregation in zero-valent iron systems and its effects on trichloroethylene removal. Chemosphere 75(10), 1338-1343.

Tuovinen, O.H., Button, K.S., Vuorinen, A., Carlson, L., Mair, D.M., Yut, L.A., 1980. Bacterial, chemical, and mineralogical characteristics of tubercles in distribution system pipelines. Journal of the American Water Works Association 72(11), 626-635.

U. S. Environmental Protection Agency. 2009a. National Primary Drinking Water Standards and National Secondary Drinking Water Standards. EPA 816-F-09-004. U.S. EPA, Office of Water, Washington DC.

U. S. Environmental Protection Agency. 2009b. Final Third Contaminant Candidate List 3. EPA 815-F-09-001. U.S. EPA, Office of Water, Washington DC.

Valentine, R.L., Spangler, K.M., Meyer, J., 1990. Removing radium by adding preformed hydrous manganese oxides. Journal of the American Water Works Association, 82(2), 66-71.

Vatankhah, G.; Menard, H.; Brossard, L. 1998A. Effect of sulfate and chloride ions on the electrochemical behavior of iron in aqueous phosphate solutions. Journal of Applied Electrochemistry 28 (9), 999-1004.

Vatankhah, G., Drogowska, M., Menard, H., Brossard, L., 1998B. Electrodissolution of iron in sodium sulfate and sodium bicarbonate solutions at pH 8. J. Appl. Electrochem. 28 (2), 173-183.

Vazquez, F.A., Heaviside, R., Tang, Z., Taylor, J.S., 2006. Effect of free chlorine and chloramines on lead release in a distribution system. Journal of the American Water Works Association 98(2), 144-154.

Verberk, J.Q.J.C., Vreeburg, J.H.G., Rietveld, L., Dijk, J.C.V., 2009. Particulate Fingerprinting of Water Quality in the Distribution System. Water SA. 35(2), 192-199.

Vreeburg, J.H.G., Schippers, D., Verberk, J.Q.J.C., and Dijk, J.C.V., 2008. Impact of Particles on Sediment accumulation in a Drinking Water Distribution System. Water Reserach 42(16), 4233-4242.

Waychunas, G.A., Rea, B.A., Fuller, C.C., Davis, J.A., 1993. Surface chemistry of ferrihydrite: Part 1. EXAFS studies of the geometry of coprecipitated and adsorbed arsenate. Geochimica et Cosmochimica Acta 57(10), 2251-2269.

Weng, L.P., Koopal, L.K., Hiemstra, T., Meeussen, J.C.L., Van Riemsdijk, W.H., 2005. Interactions of calcium and fulvic acid at the goethite-water interface. Geochimica et Cosmochimica Acta 69(2), 325-339.

Wilkie, J., Hering, J.G., 1996. Adsorption of arsenic onto hydrous ferric oxide: Effects of adsorbate/adsorbent ratios and co-occurring solutes. Colloids and Surfaces A 107, 97-110.

Zhang, Y., Edwards, M., 2007. Anticipating effects of water quality changes on iron corrosion and red water. Journal of Water Supply Research and Technology-AQUA 56 (1), 55-68.

Zhou, P., Gu, B., 2005. Extraction of oxidized and reduced forms of uranium from contaminated soils: effects of carbonate concentration and pH. Environmental Science & Technology 39(12), 4435-4440.

VITA

Ching-Yu Peng is originally from Kaohsiung, Taiwan. She earned her B.S. and M.S. in Environmental Engineering at the National Cheng Kung University, Taiwan in 1999 and 2001, respectively. After graduation, she worked at Chung Shan Industrial and Commercial High School, Taiwan as intern and was a research assistant at National Health Research Institutes and Environmental Resource and Management Research Center, Taiwan. In 2006, she received the Paul B. Liao Endowed Regental Fellowship for three years to study in the University of Washington. In 2012, she earned a Doctor of Philosophy at the University of Washington in Civil and Environmental Engineering.